A STUDY ON BUCKLING ANALYSIS OF FUNCTIONALLY GRADED MATERIAL BEAMS

Thesis Submitted in Partial Fulfillment of the

Requirements for the Degree of

Master of Mechanical Engineering

By

ARITRA MAJUMDAR

[Examination Roll No: M4MEC1616]

[University Registration No: 129393 of 2014-2015]

Under the Guidance of

Dr. DEBABRATA DAS

DEPARTMENT OF MECHANICAL ENGINEERING

FACULTY OF ENGINEERING & TECHNOLOGY

JADAVPUR UNIVERSITY

KOLKATA – 700032

MAY 2016

FACULTY OF ENGINEERING AND TECHNOLOGY

JADAVPUR UNIVERSITY

CERTIFICATE OF APPROVAL*

This foregoing thesis is hereby approved as a credible study of an engineering subject carried out and presented in a manner satisfactory to warrant its acceptance as a prerequisite to the degree for which it has been submitted. It is understood that by this approval the undersigned do not endorse or approve any statement made, opinion expressed or conclusion drawn therein but approve the thesis only for the purpose for which it has been submitted.

COMMITTEE ----------

ON FINAL EXAMINATION FOR

EVALUATION OF THE THESIS ----------

***Only in case the thesis is approved**

FACULTY OF ENGINEERING AND TECHNOLOGY

JADAVPUR UNIVERSITY

CERTIFICATE OF RECOMMENDATION

We hereby recommend that the thesis presented under our supervision by ***Mr. ARITRA MAJUMDAR*** *entitled "****A STUDY ON BUCKLING ANALYSIS OF FUNCTIONALLY GRADED MATERIAL BEAMS****" be accepted in partial fulfillment of the requirements for the degree of* ***Master of Mechanical Engineering****.*

Countersigned

Thesis Supervisor

Head of the Department

Department of Mechanical Engineering

Dean,

Faculty of Engineering and Technology

DECLARATION OF ORIGINALITY AND COMPLIANCE OF ACADEMIC ETHICS

I hereby declare that the thesis contains literature survey and original research work by the undersigned candidate, as a part of his *MASTER OF MECHANICAL ENGINEERING* studies. All information in this document have been obtained and presented in accordance with the academic rules and ethical conduct.

I also declare that, as required by these rules of conduct, I have fully cited and referenced all the material and results that are not original to this work.

Name: ARITRA MAJUMDAR

Examination Roll Number: M4MEC1616

Class Roll Number: 001411202021

University Registration No: 129393 of 2014-2015

Thesis Title: ***A STUDY ON BUCKLING ANALYSIS OF FUNCTIONALLY GRADED MATERIAL BEAMS***

Signature with Date:

ACKNOWLEDGEMENT

Walking by the sands of time we meet some people who touch our lives leaving an everlasting impression which would never fade; changing our world as we see it and helping us grow through the thick and thin… and THANK YOU becomes a very small word to acknowledge their contribution.

First and foremost, I would like to express my deepest gratitude to my supervisor- Dr. Debabrata Das, Assistant Professor, Department of Mechanical Engineering, Jadavpur University for being the guiding light from the inception to the completion of the thesis. *'There are two kinds of teachers- one kind who fills your stomach with so much quail shot that you can't move and the kind that just gives you a little prod behind and you jump to the skies'*- Robert Frost . Thank you sir for being the second kind; teaching me how to fly with a free spirit and yet work with equal ease. You have been the most amazing teacher and guide that I could ever imagine. You deserve much more than that.

'I think if I've learned anything about friendship, it's to hang in, stay connected, fight for them, and let them fight for you. Don't walk away, don't be distracted, don't be too busy or tired, don't take them for granted. Friends are part of the glue that holds life and faith together' - Jon Katz

Amlan Paul, Dipankar Das, Bablu Sikder, Tanmoy Bhattacharya and Mrityunjoy Routh - thanks for constantly inspiring me to follow my heart and pursue whatever I wanted to do. Being a friend in times of need and a scientific advisor whenever my ideas got blurred with confusion-thanking you would be just the wrong thing to do. The wonderful years of growing up together in pursuit of one's search for the unknown will always be cherished.

Last but certainly not the least, I would like to express my heartfelt love for my parents- my first teachers and my inspiration. It is from you that I got the ultimate inspiration of thinking beyond the horizon, walking past the normal boundaries of life.

It is you who taught me to question everything and thus kindled within me the joy of science. I hope that someday I'll make you proud. Thank you for letting me be 'me'.

Date: May 2016

(Aritra Majumdar)

Contents

List of Symbols

b	Width of the beam
$\{b\}$	Load vector
c_i	Unknown coefficients
f	Body force
h	Height of the beam
h_1	Left end thickness of tapered beam
h_2	Right end thickness of tapered beam
$h(x)$	Thickness of tapered beam as a function of the length axis
k	Volume fraction index
n	Taperness parameter
nu	Number of the functions for approximating u
nw	Number of the functions for approximating w
t	Surface traction
u_0	Solution obtained by minimizing the quadratic functional
$u(x)$	Displacement field along the length-axis of the beam
$w(x)$	Displacement field along the thickness-axis of the beam
x	Axis along length of the beam
y	Axis along width of the beam
z	Axis along thickness of the beam
$[A]$	Stiffness matrix
A_1, A_2, A_3	Stiffness coefficients
E	Elastic modulus
E_c	Elastic modulus of the ceramic constituent
E_f	Effective elastic modulus

E_m	Elastic modulus of the metal constituent
F	Applied load
F_{cr}	Critical buckling load
G	Shear modulus
I_1	Area moment of inertia at the left end of the tapered beam
$I(u)$	Quadratic functional
K	Thermal conductivity coefficient
K_c	Thermal conductivity coefficient of the ceramic constituent
K_{cm}	Difference between the thermal conductivity coefficients of the ceramic and the metal rich layer
K_f	Effective thermal conductivity coefficient
K_m	Thermal conductivity coefficient of the metal constituent
$\left[K_{ij}\right]$	Conventional stiffness matrix
$\left[K_{ij}^{\sigma}\right]$	Stress stiffness matrix
L	Length of the beam
N_{th}	Pre-stress coefficient
$P_{-1}, P_0, P_1, P_2, P_3$	Coefficients of temperature which are specific to any material constituent
P_c	Material property of the ceramic constituent
P_f	Effective material property
P_m	Material property of the metal constituent
S	Total boundary
T	Temperature in Kelvin
T_0	Stress-free temperature in Kelvin
T_c	Ceramic-rich layer temperature in Kelvin
T_m	Metal-rich layer temperature in Kelvin
T_u	Uniform temperature in Kelvin of the beam for UTD
U	Total strain energy of the beam

U_0	Strain energy density function
U_N	Approximate solution in the Ritz method
V	Potential energy of the applied load
V_c	Volume fraction of the ceramic constituent
V_m	Volume fraction of the metal constituent
α	Thermal expansion coefficient
α_c	Thermal expansion coefficient of the ceramic constituent
α_f	Effective thermal expansion coefficient
α_m	Thermal expansion coefficient of the metal constituent
α_{m0}	Thermal expansion coefficient of the metal constituent at stress-free temperature
β_i	Set of orthogonal admissible functions for the displacement field w
υ	Poisson's ratio
υ_c	Poisson's ratio of the ceramic constituent
υ_f	Effective Poisson's ratio
υ_m	Poisson's ratio of the metal constituent
ΔT	Dimensional thermal load
δ	Variational operator
ε_x	Axial strain
σ_{th}	Compressive thermal stress
ε_{nl}	Non-linear part of the axial strain
ϕ_i	Set of orthogonal admissible functions for the displacement field u
η	Eigenvalue
λ	Non-dimensional thermal buckling load
δW	Total virtual work
Ω	Volume of the continuous material
σ_{ij}	Stress component

ε_{ij}	Strain component
δu	Virtual displacement
δW_{I}	Virtual work due to the internal forces
δW_{E}	Virtual work due to the external forces
Π	Total potential energy

List of Figures

Page No

Page No

Page No

List of Tables

Chapter 1

INTRODUCTION

1.1. Introduction

In material science, functionally graded material (FGM) may be characterized by the variation in composition and structure gradually over volume, resulting in corresponding changes in the properties of the material. Functionally graded materials can be designed for specific functions and applications by suitably varying the proportions of the constituent phases. The concept of FGM was first introduced in Japan in 1984 during a space plane project. In that project, a combination of materials served the purpose of a thermal barrier capable of withstanding a surface temperature of 2000 K and a temperature gradient of 1000 K across a 10 mm section. Presently, the major applications of FGM lie in the high-temperature environment.

A typical FGM is an inhomogeneous composite made from different phases of material constituents (usually ceramic and metal). By gradually varying the volume fraction of the constituent materials, the material properties exhibit a smooth and continuous change from one layer to another. It thus eliminates the interface problems and reduces the thermal stress concentrations which are commonly encountered in the conventional composites. This is due to the fact that the ceramic constituents of FGMs are able to withstand high-temperature environments due to their better thermal resistance characteristics, while the metal constituents exhibit excellent mechanical performance (Shen, 2009).

There are many areas of application of functionally graded materials. FGMs have found applications in high-temperature nuclear reactors and chemical plants, thermal-barrier coatings for turbine blades, armor protection for military applications, fusion energy

devices, biomedical materials, including bone and dental implants, high speed components in space/aerospace industries, automotive components etc. It has application in various branches of engineering like aerospace, mechanical, electrical, civil, bio-medical etc. The potential applications of FGM are diverse and numerous. It has enormous potential for technological and engineering applications, especially in the extreme thermal environment where stress concentration due to high temperature gradients can be either minimized or significantly reduced.

Various theoretical models are developed to evaluate the effective material properties of FGM components with material gradation along either length or thickness direction of the component. Micromechanics models based on Mori-Tanaka scheme (Mori and Tanaka, 1973), and self-consistent model (Hill, 1965) were used by some of the researchers to derive the effective material properties of FGM components for theoretical analysis. But the most popular theoretical model in this regard is the volume fraction approach. In this approach, the effective material property is evaluated by using the simple rule of mixture (Voigt rule) of the constituents (metal and ceramic for the present work) in accordance with its volume fraction.

The beam is one of the most important structural elements which are commonly found in various structures and machines. With the evolution of functionally graded materials over the past few years, beams made of FGM are being used in various applications. With prevailing and increasing application, various researchers are carrying out theoretical investigations on static, dynamic and stability behaviors of FGM beams. As the FGM components are known to be suitable for high temperature applications, modern day researchers are concentrating on the theoretical investigations of FGM components mostly in the thermal environment. With this background, the present work mainly deals with the thermal buckling analyses of FGM beams.

For an FGM beam, the material gradation may be either in the length direction or in the thickness direction. The first one, termed as the Axially Functionally Graded Material (AFGM or AFM), is considered by some of the researchers for investigating the theoretical behavior. On the other hand, the second one, in which the material properties vary along the thickness direction, is considered by many researchers as it has wider industrial applications.

The present work is based on the second model where the property gradation occurs across the thickness in accordance with the volume fraction of the constituents.

Of all of the modes of failure, buckling is probably the most common and most catastrophic. Leonhard Euler long ago showed that there was a critical load for buckling of a slender column. With any smaller load, the column would remain straight and support it. With any larger load, the least disturbance would cause the column to bend sideways with an indefinitely large displacement, i.e., it would buckle. The collapse of a slender element which is subjected to compression, leading to a sudden lateral deflection is called buckling. Mathematical analysis of buckling often makes use of an artificial axial load eccentricity, that introduces a secondary bending moment which is not a part of the primary applied load. As the applied load is increased on a member, such as a column, it will ultimately become large enough to cause the member to become unstable. Further load will cause significant and somewhat unpredictable deformations, possibly leading to complete loss of the member's load-carrying capacity. If the deformations that follow buckling are not catastrophic, the member will continue to carry the load that caused it to buckle.

The main subject of the present work is to investigate the thermal buckling load of FGM beams. Three different thermal loadings are considered in the present thesis work. The first one considers the uniform temperature rise of the member. The second one considers linear temperature gradient across the thickness. And the third one assumes thermal loading at steady-state condition. In the third case, heat flows through the thickness from one surface to the other when the extreme surfaces of the beam are kept at different temperatures. The temperature dependence of the material properties is appropriately considered in the present analysis.

Tapered beams are commonly found in various applications. The problem involving investigation of buckling load of the tapered FGM beam is also taken up in this thesis work. For this problem, uniformly tapered beam is considered under the application of mechanical load. This part of the thesis mainly focuses on determining the critical buckling load under different classical boundary conditions.

1.2. Literature Review

An analytical investigation predicting snap-through path of a compressed bi-stable buckled beam was performed by Vangbo (1998) using a classical theory. It was also shown that the model can be used for a class of non-homogeneous sandwich beams. A one-dimensional mathematical model was developed by Parlapalli and Shu (2004) to analyze the buckling behavior of a two-layer beam with single delamination under clamped and simply supported boundary conditions. Non-dimensionalized axial and bending stiffnesses are used to investigate the buckling behavior of tri-layer beams having different delaminations by MSRao et al. (2004), and by MSRao and Shu (2004). Bochicchio and Vuk (2010) investigated the buckling and longtime dynamic behavior of an extensible elastic homogeneous beam resting on a visco-elastic foundation with positive stiffness and damping constant. Kozic et al. (2014) presented an analytical theory to define the dynamic characteristics of elastically connected parallel-beams under compressive axial loading. Grognec and Saoud (2015) carried out a theoretical study of the local/global buckling and post-buckling behavior of sandwich columns under axial compression. Li and Qiao (2015) presented buckling and post-buckling behavior of shear deformable anisotropic laminated composite beams with initial imperfection subjected to axial compression. The next three sub-sections are devoted for discussing literatures for three different categories.

1.2.1. Literature survey on FGM beams in general

High-order flexural theories for short functionally graded (FG) symmetric beams under three-point bending was presented by Benatta et al. (2008). Ke et al. (2009) study post-buckling response of FGM beams containing an open edge crack based on Timoshenko beam theory and von Kármán type nonlinear kinematics. In that work, exponential through thickness distributions of material properties are assumed, and Ritz method is employed to derive the nonlinear governing equations. Various higher-order shear deformation beam theories for bending and free vibration of FG beams were developed by Thai and Vo (2012).

Wattanasakulpong et al. (2012) employed an improved third order shear deformation theory to formulate a governing equation for predicting free vibration of layered FG beams. The Ritz method is adopted to solve the governing equation for various types of boundary conditions, and the frequency results are validated by some available and experimental

results. Analytical relations between the critical buckling load of an FGM Timoshenko beam and that of the corresponding homogeneous Euler-Bernoulli beam subjected to axial compressive load had been derived by Li and Batra (2013) for clamped-clamped (CC), simply supported-simply supported (SS) and clamped-free (CF) edges. Şimşek and Yurtcu (2013) examined bending and buckling of a FG nano-beam based on the nonlocal Timoshenko and Euler-Bernoulli beam theory. The material properties of the FG nano-beam are assumed to vary in the thickness direction. Şimşek et al. (2013) developed a micro-scale FG Timoshenko beam model for the static bending analysis based on the modified couple stress theory.

Nie et al. (2013) studied the plane stress problem of an orthotropic FG beam with arbitrary graded material properties along the thickness direction by the displacement function approach for the first time. A differential equation of the homogenized FGM beam deflection and its solution were presented by Murin et al. (2013a) to investigate the free vibration analysis of the beams with polynomial continuous longitudinal and transversal variation of material properties. Murin et al. (2013b) studied the shear correction function and evaluated it in the modal analysis of the FGM beams. Aydin (2013) studied free vibration of beams made of FGM containing any arbitrary number of open edge cracks. The study is based on Euler-Bernoulli beam and massless rotational springs connecting two intact segments of the beam. Li et al. (2014a) studied the time-dependent behavior of a simply-supported laminated FG beam with visco-elastic interlayer. Sarkar and Ganguli (2014) studied the free vibration behavior of axially functionally graded (AFG) Timoshenko beams, with uniform cross-section and having fixed–fixed boundary.

The work of Sitar et al. (2014) discussed governing differential equation for determining large deflections of slender, non-homogeneous beam subjected to a combined loading and composed of a finite number of laminae, which are made of nonlinearly elastic, modified Ludwick's type of material with different stress-strain relations in tension and compression domain. A comprehensive dynamic model of a rotating hub FGM beam system was developed by Li et al. (2014b) based on a rigid-flexible coupled dynamics theory to study its free vibration characteristics. Zhang et al. (2014) developed size-dependent beam model made of FGM that contains both micro-scale and shear deformation effects. Liu and Shu (2014) developed an analytical solution to study the free vibration of exponential

functionally graded beams with a single delamination based on Euler-Bernoulli hypothesis. Xiao et al. (2014) developed an analytical solution to study the free vibration behavior of exponential functionally graded beams with a single delamination.

Nguyen et al. (2013) developed the first-order shear deformation beam theory for static and free vibration of axially loaded rectangular FG beams. The effects of the power-law index, material contrast and Poisson's ratio on the displacements, natural frequencies, buckling loads and load-frequency curves as well as the corresponding mode shapes are investigated. Vo et al. (2015) presented a finite element model for free vibration and buckling analyses of functionally graded (FG) sandwich beams by using a quasi-3D theory in which both shear deformation and thickness stretching effects are included.

1.2.2. Literature survey on FGM beams under thermal loading

Three-dimensional thermal buckling analysis was performed by Na and Kim (2004) for functionally graded materials for which material properties are assumed to be temperature dependent, and varied continuously in the thickness direction according to a simple power law distribution in terms of the volume fraction of ceramic and metal. They analyzed thermal buckling behavior under uniform or non-uniform temperature rise across the thickness. The buckling and vibration behavior of FGM sandwich beam having constrained visco-elastic layer was studied by Bhangale and Ganesan (2006) in thermal environment by using finite element formulation. The FGM sandwich beam was assumed to be clamped on both edges. Li & Song (2006) carried out large post-buckling behavior of clamped-clamped and pinned-pinned Timoshenko beams under non-uniform temperature rise across the thickness. Zhao et al. (2007) studied the thermal post buckling behavior of simply-supported FGM beams with temperature-independent material properties under uniform and non-uniform temperature rise.

Anandrao et al. (2010) performed thermal post-buckling analysis of clamped and simply-supported FGM beams using Rayleigh-Ritz and finite element method. Using Euler-Bernoulli beam theory, Kiani and Eslami (2010) investigated the thermal buckling load of Aluminum/Alumina FGM beams under various thermal gradients using temperature-independent material properties. Vaz et al. (2010) investigated the elastic buckling and initial post-buckling behavior of aluminum alloy beams with double hinged fixed ends and

subjected to uniform heating. Kiani et al. (2011a, 2011b) performed thermo-electrical and thermal stability analysis of piezoelectric FGM beams. Wattanasakulpong et al. (2011) investigated the thermal buckling load of FGM beams under uniform temperature rise using an improved third order shear deformation theory. Pi et al. (2011) carried out thermal buckling analysis of clamped slender beams considering the effects of the uncertainties of the material and geometric parameters.

Based on first-order shear deformation theory, Ma and Lee (2011) carried out thermal post-buckling analysis of FGM beams under uniform temperature rise using both temperature dependent material properties. Using Euler-Bernoulli beam theory, Fallah and Aghdam (2012) determined the thermal buckling load of FG beams resting on a nonlinear elastic foundation for uniform temperature rise using temperature-independent material properties. Ma and Lee (2012) obtained an exact, closed-form solution for the nonlinear static responses of beams made of functionally graded materials (FGM) subjected to a uniform in-plane thermal loading. The equations governing the axial and transverse deformations of FGM beam are derived based on the nonlinear first-order shear deformation beam theory and the physical neutral surface concept. The buckling behavior of piezoelectric FGM beams was studied by Fu et al. (2012) employing Euler-Bernoulli beam theory.

Thermal effect on buckling and free vibration behavior of FG micro-beams based on modified couple stress theory was presented by Nateghi and Salamat-talab (2013) using classical and first order shear deformation beam theories. The work of Komijani et al. (2013) dealt with the small free vibration of functionally graded piezoelectric material (FGPM) beams with rectangular cross sections in pre/post-buckling regimes. The beam is assumed to be under in-plane thermal and electrical excitations. Shegokar and Lal (2013) studied the stochastic nonlinear bending response of FGM beams with surface bonded piezoelectric layers subjected to thermo-electromechanical loadings with uncertain material properties. Non-linear bending analysis of shear deformable FGM beams was carried out by Zhang (2013) under combined mechanical and thermal loading. The post-buckling behavior of the FGM Timoshenko beam was studied by Rahimi et al. (2013) using an energy approach.

Kiani and Eslami (2013) studied the thermal buckling behavior of FG beams for various thermal gradients using Timoshenko beam theory. Thermal buckling and post-buckling analyses of FG Timoshenko beams lying on a non-linear elastic foundation are carried out by Esfahani et al. (2013) for uniform temperature rise. Ghiasian et al. [2013, 2015] studied the dynamic buckling behavior of FGM beams resting on elastic foundation and subjected to uniform temperature rise loading. The free vibration behavior of thermally pre/post buckled FGM beams supported on a nonlinear hardening elastic foundation was investigated by Esfahani et al. (2014). Thermal post-buckling and large amplitude free vibration (including the effect of rotary inertia) behavior of prismatic and shear flexible Timoshenko beams were investigated by Gunda (2014) in the form of simple closed-form solutions by making use of the Rayleigh-Ritz method. The research work of Shen and Wang (2014) dealt with the large amplitude vibration, nonlinear bending and thermal post-buckling of functionally graded material (FGM) beams resting on an elastic foundation in thermal environments. Li (2014) carried out thermal post buckling analysis of three-dimensional braided shear deformable beams subjected to various temperature distributions through the thickness.

Komijani et al. (2014) investigated the buckling and post-buckling analysis and small amplitude vibrations in the pre/post-buckling regimes of functionally graded beams resting on a nonlinear elastic foundation and subjected to in-plane thermal loads. The thermal effect on buckling and free vibration characteristics of FG size-dependent Timoshenko nano-beams subjected to an in-plane thermal loading were investigated by Ebrahimi and Salari (2015). Shen (2015a, 2015b) investigated the nonlinear vibration, nonlinear bending and thermal post-buckling behavior of uniformly distributed and functionally graded fiber reinforced cross-ply and angle-ply laminated beams resting on Pasternak elastic foundations under different sets of hygro-thermal environmental conditions.

1.2.3. Literature survey on tapered FGM beams

The free vibration behavior of axially functionally graded beam with a non-uniform cross-section was investigated by Huang and Li (2010) using Euler-Bernoulli beam theory and by Huang et al. (2013) using Timoshenko beam theory. Shahba et al. (2011) studied free

vibration and stability analysis of axially functionally graded tapered Timoshenko beams through a finite element approach. The free vibration and stability of axially functionally graded tapered Euler-Bernoulli beams were studied by Shahba and Rajasekaran (2011) using a new approach called differential transform element method (DTEM). Rajasekaran (2013a, 2013b) studied bending vibration behavior of centrifugally stiffened axially functionally graded Euler-Bernoulli and Timoshenko tapered beams. The large displacement response of tapered cantilever beams made of axially functionally graded material was investigated by Kien (2013) using the finite element method.

The large deflections of tapered functionally graded beams subjected to end forces were studied by Kien and Gan (2014) using the finite element method and employing a first order shear deformable beam element. The large displacement behavior of tapered cantilever FG beams subjected to end forces was performed by Kien (2014) using Euler-Bernoulli beam theory. Niknam et al. (2014) investigated non-linear bending behavior of tapered FGM beam subjected to thermal and mechanical loading employing Euler-Bernoulli beam theory. Free vibration dynamic analysis of axially functionally graded tapered beam was carried out by Rajasekaran and Tochaei (2014) using the various differential element method. Maganti and Nalluri (2015) investigated bending vibration behavior of rotating functionally graded double-tapered beam.

1.3. Mathematical Background

The present work is based on the energy principle of structural mechanics. The governing equation is derived using the principle of minimum total potential energy. The solution of the governing equation is obtained by approximating the displacement fields following Ritz method. A brief discussion of the principles and methodologies followed in the present thesis work is given in the present section.

1.3.1. Energy principles in structural mechanics

The energy principles of structural mechanics include the principles of virtual displacements and forces, the principle of minimum total potential energy and the principle of maximum total complementary energy (Shames and Dym, 2009; Reddy, 2002; Cook et

al. 2002). These principles in variational form are used to derive the equations of equilibrium or motion of deformable solids.

The virtual work is the work done on a particle or a deformable body by actual forces in moving through a hypothetical or virtual displacement that is consistent with the geometric constraints. The applied forces are considered to be constant during the imposed virtual displacement. The principle of virtual displacements states that the virtual work done by actual forces is zero, if and only if the body is in equilibrium.

If a particle is in equilibrium under the action of n concurrent forces $F_1, F_2, F_3....F_n$, and if the particle is given an arbitrary virtual displacement δu during which all forces along with their directions are fixed, then the total virtual work done by all forces is given by,

$$\delta W = F_1\delta u + F_2\delta u + F_3\delta u + ... + F_n\delta u = \left(\sum_{i=1}^{n} F_i\right)\delta u \qquad (1.1)$$

The expression $\left(\sum_{i=1}^{n} F_i\right)$ is the vector sum of all forces acting on the particle. From vector mechanics, it is known that the sum is zero if the particle is in equilibrium and thus giving $\delta W = 0$. Conversely, if $\delta W = 0$ and δu is arbitrary, it follows that $\sum_{i=1}^{n} F_i = 0$, i.e., the particle is in equilibrium. In other words, the particle is in equilibrium if and only if $\delta W = 0$ for any choice of δu.The statement $\delta W = 0$ is the mathematical statement of the principle of virtual displacements for a particle. Here, δ is the variational operator.

A generalization of the principle of virtual displacements for deformable bodies can now be considered. In deformable bodies, material points can move relative to one another and do internal work in addition to the work done by the external forces. Thus, it should consider the virtual work done by internal forces (i.e., stresses) as well as that done by external forces. Consider a continuous material occupying the volume Ω and in equilibrium under the action of body forces f and surface tractions t. Suppose that over portion S_1 of the boundary, displacements arc specified to be $\hat{u}$ and on portion S_2, tractions are specified to be $\hat{t}$. The boundary portions S_1 and S_2 are disjoint (i.e., do not overlap) and their sum is the total boundary S. Let $u = (u_1, u_2, u_3)$ be the displacement vector corresponding to the equilibrium configuration of the body, and let σ_{ij} and ε_{ij} be the associated stress and strain

components, respectively. No assumption is made in concerning the constitutive behavior of the material body.

The set of admissible configurations is defined by sufficiently differentiable displacement fields that satisfy the geometric boundary conditions: $u = \hat{u}$ on S_1. Of all such admissible configurations, the actual one corresponds to the equilibrium configuration with the prescribed loads. In order to determine the displacement field u corresponding to the equilibrium configuration, let the body experience a virtual displacement δu from the equilibrium configuration. The virtual displacements are arbitrary continuous functions except that they satisfy the homogeneous form of the specified geometric boundary conditions, i.e., $\delta u = 0$ on S_1. The principle of virtual work states that a continuous body is in equilibrium if and only if the virtual work of all forces (internal and external), acting on the body, is zero through a virtual displacement, i.e.,

$$\delta W = \delta W_{\mathrm{I}} + \delta W_{\mathrm{E}} = 0 \tag{1.2}$$

Here, δW_{I} is the virtual work due to the internal forces and δW_{E} is the virtual work done due to the external forces. The principle of virtual work is independent of any constitutive law. The principle may be used to derive the equilibrium equations of deformable solids.

The principle of virtual work discussed is applicable to any continuous body with arbitrary constitutive behavior (i.e., elastic or inelastic). A special case of the principle of virtual work that deals with elastic (linear as well as nonlinear) bodies is known as the principle of minimum total potential energy. For elastic bodies, there exists a strain energy density function U_0 such that,

$$\sigma_{ij} = \frac{\partial U_0}{\partial \varepsilon_{ij}} \tag{1.3}$$

The strain energy density U_0 is a function of strains at a point and is assumed to be positive definite. Let, $d\Omega$ is the elemental volume over the volume Ω. The principle of virtual displacements, i.e., $\delta W = 0$, can be expressed in terms of the strain energy density U_0 as follows:

$$\delta W = 0$$
$$\Rightarrow \delta W_{\mathrm{I}} + \delta W_{\mathrm{E}} = 0$$

$$\Rightarrow \int_{\Omega} \sigma_{ij} \delta\varepsilon_{ij} d\Omega - \left[\int_{\Omega} f \delta u d\Omega + \int_{S_2} \hat{t} \delta u dS \right] = 0$$

$$\Rightarrow \int_{\Omega} \frac{\partial U_0}{\partial \varepsilon_{ij}} \delta\varepsilon_{ij} d\Omega + \delta V = 0$$

$$\Rightarrow \int_{\Omega} \delta U_0 d\Omega + \delta V = 0$$

$$\Rightarrow \delta\left(U + V\right) = 0$$

$$\Rightarrow \delta(\Pi) = 0$$

where, $\delta V = -\left[\int_{\Omega} f \delta u d\Omega + \int_{S_2} \hat{t} \delta u dS \right]$, $V = -\left[\int_{\Omega} f u d\Omega + \int_{S_2} \hat{t} u dS \right]$ and $U = \int_{\Omega} U_0 d\Omega$.

Here, U is the strain energy and V is the work potential. The sum $\Pi = V + U$ is called the total potential energy of the elastic body. Hence the principle of minimum total potential energy is mathematically given by,

$$\delta(\Pi) = \delta(U + V) = 0 . \tag{1.4}$$

The principle of virtual displacements as well as the principle of minimum total potential energy provide, when applied to an elastic body, the equilibrium equations. The main difference between them is that principle of virtual displacements gives the equilibrium equations in terms of stresses (or stress resultants), whereas the principle of minimum total potential energy gives them in terms of the displacements, because a constitutive relation is assumed to replace the stresses in terms of the displacements.

1.3.2. Ritz method

The energy methods derived from the principles of virtual displacements and forces as applied to continuous systems are used to determine the governing equations and natural boundary conditions of the problem. By directly using the variational statements (i.e., virtual work principles, the principle of minimum total potential energy, or the principle of complementary energy), a powerful method is often used in structural mechanics for determining the approximate solutions to the governing equations of a problem. The method bypasses the derivation of the governing differential equations (Euler equations) and goes directly from a variational statement of the problem to the solution of the Euler equations.

One such direct method was proposed by German engineer W. Ritz (Shames and Dym, 2009; Reddy, 2002).

For a quadratic functional $I(u)$, let the solution u_0 is obtained by minimizing it, i.e., making $\delta I(u)=0$. In structural mechanics problems, the functional $I(u)$ represents the total potential energy and $\delta I(u)=0$ (the principle of minimum total potential energy) yields the Euler equation. An approximation is taken for $U_N(x)$ of $u_0(x)$, for a fixed and preselected N, in the form given below:

$$u_0(x) \approx U_N(x) = \sum_{i=1}^{N} c_i \phi_i(x) + \phi_0(x), \tag{1.5}$$

where, $\phi_0(x)$ is the function that satisfies the specified essential boundary conditions of the problem, $\phi_i(x)$ are the set of coordinate functions that satisfy the homogeneous form of the specified essential boundary conditions and c_i are the set of unknown real constants (coordinates). These constants are determined by the condition that $I(U_N)$ is the minimum.

In the Ritz method, an approximate solution U_N (which may be exact if the right kind of approximate solution is chosen) is taken to the problem as a finite linear combination of the form of equation (1.5). If ϕ_0 and ϕ_i are taken such that U_N satisfies the specified essential boundary condition, $u(0)=0$ and if U_N is substituted into the total potential energy functional Π, then, Π is obtained as a function of the parameters $c_1, c_2, ..., c_N$ (after carrying out the indicated integration with respect to *x*) as given below:

$$\Pi = \Pi(c_1, c_2, ..., c_N). \tag{1.6}$$

Then c_i are determined (or adjusted) such that $\delta\Pi = 0$, in other words, Π is minimized with respect to c_i, where $i = 1, 2, 3....N$. The minimization of Π is given mathematically as follows:

$$\delta\Pi = 0$$

$$\Rightarrow \frac{\partial \Pi}{\partial c_1}\delta c_1 + \frac{\partial \Pi}{\partial c_2}\delta c_2 + ... + \frac{\partial \Pi}{\partial c_N}\delta c_N = 0$$

$$\Rightarrow \sum_{j=1}^{N} \frac{\partial \Pi}{\partial c_j}\delta c_j = 0 \tag{1.7}$$

Since the set $\{c_i\}$ is linearly independent, it follows that:

$$\frac{\partial \Pi}{\partial c_i} = 0 \qquad \text{for } i = 1,2,3...N \tag{1.8}$$

or $$[A]\{c\} = \{b\} \tag{1.9}$$

The equation (1.9) represents a set of N linear equations among $c_1, c_2, ..., c_N$ whose solution together with equation (1.5) yields the approximate solution $U_N(x)$. This completes the description of the Ritz method. In equation (1.9), $[A]$ is termed as the stiffness matrix and $\{b\}$ is termed as the load vector.

1.4. Overview of the Thesis Problems

Two broad categories of problems are solved in the present thesis work. The first one involves determination of thermal critical buckling load of FGM beams under in-plane thermal loading. The second kind of problem deals with the determination of critical buckling load of FGM tapered beams. It is to be mentioned that the thermal buckling problem constitutes the major portion of the present thesis work.

FGM beam made of ceramic and metal constituents is considered. For modeling FGM, material gradation along the thickness direction is considered. Employing the simple rule of mixture (Voigt model; Shen, 2009), effective material properties are evaluated in accordance with the power law variation of volume fraction of the constituents. In the FGM model considered, the top and the bottom layers are pure ceramic and pure metal respectively. For the thermal problem, temperature dependence of the material properties is considered using the well-known cubic polynomial relationship (Reddy and Chin, 1998).

Euler-Bernoulli beam theory is used to model the slender FGM beam. The governing equations are derived using the principle of minimum total potential energy. The formulation is based on unknown displacement fields. The governing equations, obtained as an eigenvalue problem, are solved by approximating the displacement fields following Ritz method. The descriptions of the specific problems are given in following sub-sections.

1.4.1. Thermal buckling of FGM beams

If the temperature of an axially constrained beam layer is increased above the stress-free value, a compressive thermal stress is induced. Hence, a compressive thermal force is induced in an axially restrained beam with temperature rise. For an FGM beam, the induced thermal force generally does not pass through the centroidal axis, making it eccentric. So an FGM beam under temperature rise is prone to instability due to the effect of the thermal compressive force. For such a beam, the temperature change leading to the critical buckling condition must be calculated as it is very important parameter for the design.

Three different thermal loadings are considered (Javaheri and Eslami, 2002): (a) Uniform temperature distribution or UTD, in which the temperature of the entire beam is increased uniformly; (b) Linear temperature distribution or LTD, in which the top (pure ceramic) layer is kept at a higher temperature than that of the bottom one (pure metal kept at stress-free temperature always), and a linear temperature gradient is assumed along the thickness direction; and, (c) Non-linear temperature distribution or NLTD, in which the extreme layers are kept at different temperatures as considered in LTD but a non-linear thermal gradient is induced at steady-state heat conduction condition.

Three different boundary conditions are considered for this category of the problems, namely, beam with both ends clamped (CC), beam with both ends simply supported (SS) and, beam with one end clamped and the other simply supported (CS). In all these cases, axial displacements at the ends are restricted. For this study, three different metal-ceramic functionally graded material compositions are used. These are Stainless Steel (SUS304)/Alumina (Al_2O_3), Stainless Steel/Silicon Nitride (Si_3N_4) and Stainless Steel/Zirconia (ZrO_2).

1.4.2. Buckling of tapered FGM beams

For this problem, critical buckling load of uniformly tapered FGM beams is determined. The beam with constant width is assumed to be tapered along the length direction where the thickness changes uniformly from one end to the other. Three different boundary conditions are considered, namely, beam with both ends clamped (CC), beam with both ends simply supported (SS) and, beam with one end clamped and the other simply supported (CS). It is to be mentioned that for CS beam, the clamped end is assumed to be of

higher thickness compared to that at the simply supported end. Two FGMs such as Stainless Steel (SUS304)/Zirconia (ZrO_2) and Titanium alloy (Ti-6Al-4V)/Zirconia are considered for this study.

1.5. Layout of the Thesis

The mathematical formulation of the thermal buckling problem is described in chapter 2. The description of FGM modeling and its temperature dependence are discussed in detail. The temperature coefficients for various material properties are given for different FGM constituents. Mathematical modeling of various thermal loadings is discussed. The governing equation is derived and the solution algorithm is described as the problem is physically non-linear. The assumed coordinate functions for the approximate displacement fields are listed.

In the present thesis work, the graphical variations of non-dimensional thermal buckling load with volume fraction index are presented. These variations are presented in two different forms; one for different length-thickness ratios for a fixed FGM and the other for different FGMs for a fixed length-thickness ratio. The results in these formats along with appropriate discussions are presented in chapter 3, chapter 4 and chapter 5 for UTD, LTD and NLTD respectively. Additional considerations for limit thermal loads are discussed in chapter 5. It is to be mentioned that the limit thermal load is defined as the load at which the material property responsible for thermal stress calculation becomes zero.

Chapter 6 discusses the entire problem of determination of critical buckling load of FGM beams starting from the mathematical formulation to the results obtained and its corresponding discussion. The variation of non-dimensional buckling load with taperness parameter is presented graphically for different volume fraction indices. Tapered beam up to ninety percent reductions in end thicknesses are considered. The buckling mode shape plots for different taperness parameters are also presented.

Chapter 2

MATHEMATICAL FORMULATION FOR THERMAL BUCKLING PROBLEM

2.1. Problem Description

The term beam has a very specific meaning in structural mechanics. It is a component that is designed to support transverse loads, that is, loads that act perpendicular to the longitudinal axis of the beam. Here, Euler-Bernoulli beam theory is followed and, thus the effect of shear deformation is neglected. Generally, for a beam with a length-thickness ratio 20 or more, Euler Bernoulli beam theory can be used. A beam with length L, width b and height h is considered as shown in Figure 1. As shown in Figure 1, *x*, *y* and *z* denote the coordinate axes along the length, width and thickness directions respectively. It is to be mentioned that the coordinate *z* originates from the mid-plane of the beam. In the present work, the graded material properties are assumed to be through the thickness direction.

The FGM beam considered consists of metal and ceramic constituents. The bottom layer ($z=-h/2$) consists of fully metal constituent, i.e., it is a metal rich layer. For any layer, moving from bottom to top, the metal constituent decreases and the ceramic constituent increases. Finally, the top layer ($z=+h/2$) consists of fully ceramic constituent, i.e., it is a ceramic rich layer. The bottom layer (metal rich) is considered to be at temperature T_m, the top layer (ceramic rich) is considered to be at temperature T_c and the stress free temperature is taken as T_0. It is to be noted that T_0=300 K is considered throughout this work. It is to be mentioned that $T_c > T_m$ for non-uniform temperature distribution across the beam thickness.

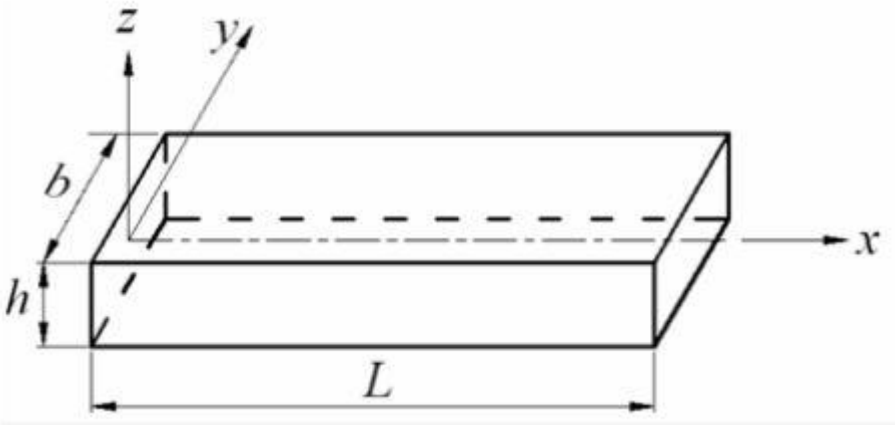

Figure 2.1: Beam with dimension and coordinate axes.

If the temperature of an axially constrained beam layer is increased above the stress-free value, a compressive thermal stress is induced. Hence, a compressive thermal force is induced in an axially restrained beam with temperature rise. For an FGM beam, the induced thermal force generally does not pass through the centroidal axis, making it eccentric. So an FGM beam under temperature rise is prone to instability due to the effect of the thermal compressive force. At critical condition, an FGM beam under in-plane thermal load attains a bent equilibrium configuration in the neighborhood of its straight configuration under external disturbance. The present work deals with the determination of temperature rise at critical condition where, the equilibrium conditions are applicable at the bent configuration.

Three different thermal loadings are considered: (a) Uniform temperature distribution (UTD), in which the entire beam temperature is raised to a temperature $T_u > T_0$, (b) Linear temperature distribution (LTD), in which the thermal gradient is linear across the beam thickness and, (c) Non-uniform temperature distribution (NLTD), where a non-linear thermal gradient is set up across the beam thickness due to steady-state heat conduction. The temperature dependence of the relevant material properties, namely elastic modulus E, shear modulus G, thermal expansion coefficient α and Poisson's ratio υ are considered. The thermal conductivity coefficient K is assumed to be independent of temperature for the present study. It is to be mentioned that the material property is assumed to be linear elastic obeying Hooke's law.

Three different boundary conditions are considered, namely, beam with both ends clamped (CC), beam with both ends simply supported (SS) and, beam with one end clamped and the other end simply supported (CS). For all these cases, axial displacements at the ends are fully constrained.

2.2. Modeling of FGM

The volume fraction V_c of the ceramic constita power lawssumed to follow power law given by, $V_c = \left(\frac{z}{h}+\frac{1}{2}\right)^k$. Accordingly, the volume fraction V_m of the other constituent (metal) is given by, $V_m = 1 - V_c = 1 - \left(\frac{z}{h}+\frac{1}{2}\right)^k$. Here k $(0 \le k \le \infty)$ is the volume fraction index.

The effective material property P_f of any layer *z* is determined using the simple rule of mixture (Voigt rule) of the metal and ceramic constituents as given below (Shen, 2009):

$$P_f = P_m V_m + P_c V_c = P_m + \left(P_c - P_m\right)\left(\frac{z}{h}+\frac{1}{2}\right)^k , \tag{2.1}$$

where, P_c and P_m are the material properties of the ceramic and metal constituents respectively, and, V_c and V_m are the volume fraction of the ceramic and metal constituents respectively. The value of k equal to zero represents a fully ceramic beam $(V_c = 1)$. Hence the various effective material properties are given as follows:

$$E_f = E_m + \left(\frac{z}{h}+\frac{1}{2}\right)^k \left(E_c - E_m\right), \tag{2.1a}$$

$$\alpha_f = \alpha_m + \left(\frac{z}{h}+\frac{1}{2}\right)^k \left(\alpha_c - \alpha_m\right), \tag{2.1b}$$

$$\nu_f = \nu_m + \left(\frac{z}{h}+\frac{1}{2}\right)^k \left(\nu_c - \nu_m\right), \tag{2.1c}$$

$$K_f = K_m + \left(\frac{z}{h}+\frac{1}{2}\right)^k \left(K_c - K_m\right). \tag{2.1d}$$

Table 2.1: Temperature coefficients for different material properties.

Material	Property	P_{-1}	P_0	P_1	P_2	P_3
Stainless Steel (SUS304)	α (K^{-1})	0	12.33e-6	8.086e-4	0	0
	E (Pa)	0	201.04e+9	3.079e-4	-6.534e-7	0
	K ($W\ m^{-1}\ K^{-1}$)	0	15.379	-1.264e-3	-2.092e-6	-7.223e-10
	υ	0	0.3262	-2.002e-4	3.797e-7	0
Alumina (Al_2O_3)	α (K^{-1})	0	6.8269e-6	1.838e-4	0	0
	E (Pa)	0	349.55e+9	-3.853e-4	4.027e-7	-1.673e-10
	K ($W\ m^{-1}\ K^{-1}$)	-1123.6	-14.087	-6.227e-3	0	0
	υ	0	0.2600	0	0	0
Silicon Nitride (Si_3N_4)	α (K^{-1})	0	5.8723e-6	9.095e-4	0	0
	E (Pa)	0	348.43e+9	-3.07e-4	2.16e-7	-8.946e-11
	K ($W\ m^{-1}\ K^{-1}$)	0	13.723	-1.032e-3	5.466e-7	-7.876e-11
	υ	0	0.2400	0	0	0
Zirconia (ZrO_2)	α (K^{-1})	0	12.766e-6	-1.491e-3	1.006e-5	-6.778e-11
	E (Pa)	0	244.27e+9	-1.371e-3	1.214e-6	-3.681e-10
	K ($W\ m^{-1}\ K^{-1}$)	0	1.7	1.276e-4	6.6485e-6	0
	υ	0	0.2882	1.133e-4	0	0

The effective shear modulus is determined using the relation, $G_f = \frac{E_f}{2(1+\upsilon_f)}$. It is to be mentioned that the subscripts c, m and f correspond to the ceramic, metal and effective material constituents respectively.

As the present problem involves increase of the temperature of the beam layers above the stress-free temperature, the material properties should be calculated in accordance with the temperature. The temperature-dependent material properties of the individual constituents (P_c or P_m) are calculated using a cubic polynomial relationship (Touloukian, 1967) given by,

$$P_c \text{ or } P_m = P_0(P_{-1}T^{-1} + 1 + P_1T + P_2T^2 + P_3T^3) \tag{2.2}$$

where, P_{-1}, P_0, P_1, P_2, P_3 are the coefficients of temperature, which are specific to the materials considered and T is the temperature in K. Except the thermal conductivity, all other material properties are now functions of both the thickness coordinate and the temperature. Various temperature coefficients for different material properties corresponding to different material constituents are listed in Table 2.1.

2.3. Temperature Distribution

As already mentioned that an increase in the beam temperature above the stress-free value gives rise to a thermal compressive force. In this thesis work, three different thermal loadings are considered with T_c and T_m being the temperatures of the top and bottom layers. These are as follows:

(i) Uniform Temperature Distribution (UTD)

(ii) Linear Temperature Distribution (LTD)

(iii) Non-Linear Temperature Distribution (NLTD) at steady-state heat conduction condition.

2.3.1. Uniform Temperature Distribution (UTD)

Under this category, the beam temperature is uniformly increased to a value of $T_u > T_0$. This leads to same temperature rise for all the beam layers above T_0. But as the

different FGM beam layers are having different thermo-mechanical properties, the thermal compressive stress are different for different layers. For any layer *z*, the temperature is given by,

$$T(z) = T_0 + \Delta T \quad , \tag{2.3}$$

where, ΔT is given by $\Delta T = T_u - T_0$. Here, ΔT is defined as the dimensional thermal load for UTD.

2.3.2. Linear Temperature Distribution (LTD)

Generally, the temperature distribution for any given surface temperatures (top & bottom surfaces) is obtained by solving the steady-state heat conduction equation along the beam thickness. But, if the beam is thin enough, the temperature distribution is approximated as linear through the thickness. Hence, the temperature as a function of thickness coordinate *z* can be written in the following equation form:

$$T(z) = T_m + \left(T_c - T_m\right)\left(\frac{z}{h} + \frac{1}{2}\right). \tag{2.4}$$

From equation (2.4), it is clear that the layer wise temperature $T(z)$ is a function of z which follows a linear relation between T_c and T_m. In this case, the temperature field is considered to be uniform over the beam length, but vary linearly along its thickness. Here, $\Delta T = \left(T_c - T_m\right)$ is defined as the dimensional thermal load for LTD.

2.3.3. Non-Linear Temperature Distribution (NLTD)

In this case, heat conduction across the thickness is assumed at steady-state condition. The temperature field is considered to be uniform over the beam length, but varies along its thickness. In this case, it is assumed that no source of heat generation exists within the beam system. Hence, the temperature distribution along the thickness direction can be obtained by solving the one-dimensional steady-state heat conduction equation through the thickness of the beam. The one-dimensional heat conduction equation is given by equation (2.5) below:

$$K(z)\frac{d^2T}{dz^2}+\frac{dK(z)}{dz}\frac{dT}{dZ}=0$$

$$\Rightarrow \frac{d}{dz}\left(K(z)\frac{dT}{dz}\right)=0. \tag{2.5}$$

Here, $K(z)$ is the thermal conductivity, which is also varying along the thickness of the FGM beam. The above equation is solved with the given temperature boundary conditions at the bottom and the top surfaces of the beam. The boundary conditions are:

$$T\big|_{z=+\frac{h}{2}}=T_c \tag{2.6a}$$

and $$T\big|_{z=-\frac{h}{2}}=T_m \tag{2.6b}$$

The solution of equation (2.5) results in a non-linear temperature distribution across the beam thickness. The approximate solution of equation (2.5) is obtained by Javaheri and Eslami (2002) in the form of a polynomial series. The layer-wise temperature distribution across the thickness (z) is given by the polynomial series (containing six terms) below:

$$T(z)=T_m+\frac{\Delta T}{D}\left[\left(\frac{z}{h}+\frac{1}{2}\right)-\frac{K_{cm}}{(k+1)K_m}\left(\frac{z}{h}+\frac{1}{2}\right)^{k+1}+\frac{K_{cm}^2}{(2k+1)K_m^2}\left(\frac{z}{h}+\frac{1}{2}\right)^{2k+1}\right.$$
$$\left.-\frac{K_{cm}^3}{(3k+1)K_m^3}\left(\frac{z}{h}+\frac{1}{2}\right)^{3k+1}+\frac{K_{cm}^4}{(4k+1)K_m^4}\left(\frac{z}{h}+\frac{1}{2}\right)^{4k+1}-\frac{K_{cm}^5}{(5k+1)K_m^5}\left(\frac{z}{h}+\frac{1}{2}\right)^{5k+1}\right] \tag{2.7}$$

where, $D=1-\frac{K_{cm}}{(k+1)K_m}+\frac{K_{cm}^2}{(2k+1)K_m^2}-\frac{K_{cm}^3}{(3k+1)K_m^3}+\frac{K_{cm}^4}{(4k+1)K_m^4}-\frac{K_{cm}^5}{(5k+1)K_m^5}$,

$\Delta T=T_c-T_m$ and $K_{cm}=K_c-K_m$.

From the above equation of temperature distribution, it is clear that the layer wise temperature $T(z)$ is a function of z, where in the equation, z is in the increasing power from beginning to the end of the equation. So the layer wise temperature varies non-linearly from layer to layer. Here, K_{cm} is the difference between the thermal conductivities of the ceramic rich layer and metal rich layer, and ΔT is defined as the temperature difference between the ceramic-rich and the metal-rich surfaces of the beam. Here, $\Delta T=(T_c-T_m)$ is defined as the dimensional thermal load for NLTD.

2.4. Governing Equation

The governing equation of the beam at critical condition is derived using the principle of minimum total potential energy, shown in equation (1.4) in the previous chapter. It is again given below:

$$\delta(U+V)=0 \tag{1.4}$$

where, U is the total strain energy of the beam, V is the potential energy of the applied load and δ is the variational operator.

The present formulation is displacement based, where the displacement fields along the *x* and *z* directions are taken as $u(x)$ and $w(x)$ respectively. The displacement fields are defined at the mid-plane of the beam. The strain along the axial direction is contributed by the bending deformation and the stretching deformation of the mid-plane. The expression of axial strain is given by,

$$\varepsilon_x = \frac{d}{dx}\left(u - z\frac{dw}{dx}\right)$$

$$= \frac{du}{dx} - z\frac{d^2w}{dx^2}. \tag{2.8}$$

In equation (2.8), the first term is due to stretching effect and the second term is due to bending action.

The strain energy U is derived as follows:

$$U = \frac{1}{2}\int \sigma\varepsilon_x dv$$

$$= \frac{1}{2}\int E_f \varepsilon_x^2 dv \qquad \text{(assuming linear elastic stress-strain material behavior)}$$

$$= \frac{1}{2}\int_{-\frac{h}{2}}^{+\frac{h}{2}}\int_0^L E_f\left(\frac{du}{dx} - z\frac{d^2w}{dx^2}\right)^2 b\,dz\,dx$$

$$= \frac{b}{2}\int_{-\frac{h}{2}}^{+\frac{h}{2}}\int_0^L E_f\left\{\left(\frac{du}{dx}\right)^2 - 2z\left(\frac{du}{dx}\right)\left(\frac{d^2w}{dx^2}\right) + z^2\left(\frac{d^2w}{dx^2}\right)^2\right\}dz\,dx$$

$$= \frac{A_1}{2}\int_0^L\left(\frac{du}{dx}\right)^2 dx - A_2\int_0^L\left(\frac{d^2w}{dx^2}\right)\left(\frac{du}{dx}\right)dx + \frac{A_3}{2}\int_0^L\left(\frac{d^2w}{dx^2}\right)^2 dx \tag{2.9}$$

where, the stiffness coefficients A_1, A_2 and A_3 are defined as below:

$$A_1 = b\int_{-\frac{h}{2}}^{+\frac{h}{2}} E_f\, dz\,,\ A_2 = b\int_{-\frac{h}{2}}^{+\frac{h}{2}} E_f z\, dz \text{ and } A_3 = b\int_{-\frac{h}{2}}^{+\frac{h}{2}} E_f z^2 dz\,. \tag{2.10}$$

For any layer, the temperature rise above the stress-free temperature T_0 induces compressive thermal stress σ_{th} which is given by,

$$\sigma_{th}(z) = E_f(z)\alpha_f(z)\left[T(z) - T_0\right]. \tag{2.11}$$

The potential energy V due to applied compressive thermal stress is derived as follows:

$$\begin{aligned} V &= -\int \sigma_{th}\varepsilon_{nl}\, dv \\ &= -\frac{b}{2}\int_{-\frac{h}{2}}^{+\frac{h}{2}}\int_{0}^{L} \sigma_{th}\left\{\left(\frac{dw}{dx}\right)^2 + \left(\frac{du}{dx}\right)^2\right\} dx dz \\ &= -\frac{N_{th}}{2}\int_0^L \left(\frac{du}{dx}\right)^2 dx - \frac{N_{th}}{2}\int_0^L \left(\frac{dw}{dx}\right)^2 dx \end{aligned} \tag{2.12}$$

where, the pre-stress coefficient N_{th} is given by,

$$N_{th} = b\int_{-\frac{h}{2}}^{+\frac{h}{2}} \sigma_{th}\, dz\,. \tag{2.13}$$

In deriving equation (2.12), the non-linear part of the axial strain ε_{nl} is used, which is given by, $\varepsilon_{nl} = \frac{1}{2}\left[\left(\frac{dw}{dx}\right)^2 + \left(\frac{du}{dx}\right)^2\right]$

Following Ritz method, the displacement fields are approximated as finite linear combinations of admissible functions and unknown coefficients c_i given by,

$$u = \sum_{i=1}^{nu} c_i \phi_i\,, \tag{2.14a}$$

$$w = \sum_{i=1}^{nw} c_{nu+i}\beta_i\ . \tag{2.14b}$$

Table 2.2: List of lowest order functions for different boundary conditions.

Type of Boundary	Boundary Conditions	Function
CC	$u\|_{x=0}=0, u\|_{x=L}=0$	$\phi_1(x)=\left(\frac{x}{L}\right)\left\{1-\left(\frac{x}{L}\right)\right\}$
	$w\|_{x=0}=0, w\|_{x=L}=0,$ $\left.\frac{dw}{dx}\right\|_{x=0}=0, \left.\frac{dw}{dx}\right\|_{x=L}=0$	$\beta_1=\left(\frac{x}{L}\right)^2\left\{1-2\left(\frac{x}{L}\right)+\left(\frac{x}{L}\right)^2\right\}$
SS	$u\|_{x=0}=0, u\|_{x=L}=0$	$\phi_1(x)=\left(\frac{x}{L}\right)\left\{1-\left(\frac{x}{L}\right)\right\}$
	$w\|_{x=0}=0, w\|_{x=L}=0,$ $\left.\frac{dw}{dx}\right\|_{x=0}\neq 0, \left.\frac{dw}{dx}\right\|_{x=L}\neq 0$	$\beta_1=\sin\left(\frac{\pi x}{L}\right)$
CS	$u\|_{x=0}=0, u\|_{x=L}=0$	$\phi_1(x)=\left(\frac{x}{L}\right)\left\{1-\left(\frac{x}{L}\right)\right\}$
	$w\|_{x=0}=0, w\|_{x=L}=0,$ $\left.\frac{dw}{dx}\right\|_{x=0}=0, \left.\frac{dw}{dx}\right\|_{x=L}\neq 0$	$\beta_1=\left(\frac{x}{L}\right)^2\left\{3-5\left(\frac{x}{L}\right)+2\left(\frac{x}{L}\right)^2\right\}$

Here, ϕ_i and β_i are the sets of orthogonal admissible functions for the field variables u and w; and nu and nw are the number of the functions for approximating u and w respectively. The set of orthogonal functions ϕ_i and β_i are generated numerically from the lowest order admissible functions by Gram-Schmidt orthogonalization scheme. The lowest order functions for each of these displacement fields along with the boundary conditions are given in Table 2.2. The orthogonal set of functions is selected in order to

ensure convergence of the solution. The lowest order functions for each displacement field are selected in order to satisfy the geometric boundary conditions of the beam.

Using the approximate displacement fields in the expressions of U and V given by equations (2.9) and (2.12), and applying the minimum potential energy principle given by equation (1.4), the governing equation is obtained in the following form:

$$\left[K_{ij}\right]\left\{c_j\right\}-\left[K_{ij}^{\sigma}\right]\left\{c_j\right\}=0 \tag{2.15}$$

where, $\left[K_{ij}\right]$ is the conventional stiffness matrix and $\left[K_{ij}^{\sigma}\right]$ is the stress stiffness matrix, each of dimension $nu+nw$. Equation (2.15) is transformed into an eigenvalue problem of the form given below:

$$\left[K_{ij}^{\sigma}\right]^{-1}\left[K_{ij}\right]\left\{c_j\right\}-\eta\left[I\right]\left\{c_j\right\}=0 \tag{2.16}$$

where, η represents the eigenvalue and $\left\{c_j\right\}$ represents the corresponding eigenvector. The elements of $\left[K_{ij}\right]$ and $\left[K_{ij}^{\sigma}\right]$ are given below:

Elements of the conventional stiffness matrix:

$$\left[K_{ji}\right]_{\substack{j=1,nu\\ i=1,nu}}=A_1\int_0^L\frac{d\phi_j}{dx}\frac{d\phi_i}{dx}dx,$$

$$\left[K_{ji}\right]_{\substack{j=1,nu\\ i=nu+1,nu+nw}}=-A_2\int_0^L\frac{d\phi_j}{dx}\frac{d^2\beta_{i-nu}}{dx^2}dx,$$

$$\left[K_{ji}\right]_{\substack{j=nu+1,nu+nw\\ i=1,nu}}=-A_2\int_0^L\frac{d^2\beta_{j-nu}}{dx^2}\frac{d\phi_i}{dx}dx,$$

$$\left[K_{ji}\right]_{\substack{j=nu+1,nu+nw\\ i=nu+1,nu+nw}}=A_3\int_0^L\frac{d^2\beta_{j-nu}}{dx^2}\frac{d^2\beta_{i-nu}}{dx^2}dx.$$

Elements of the stress stiffness matrix:

$$\left[K_{ji}^{\sigma}\right]_{\substack{j=1,nu\\ i=1,nu}}=N_{th}\int_0^L\frac{d\phi_j}{dx}\frac{d\phi_i}{dx}dx,$$

$$\left[K_{ji}^{\sigma}\right]_{\substack{j=1,nu\\ i=nu+1,nu+nw}}=0,$$

$$\left[K_{ji}^{\sigma}\right]_{\substack{j=nu+1,nu+nw \\ i=1,nu}} = 0,$$

$$\left[K_{ji}^{\sigma}\right]_{\substack{j=nu+1,nu+nw \\ i=nu+1,nu+nw}} = N_{th}\int_0^L \frac{d\beta_{j-nu}}{dx}\frac{d\beta_{i-nu}}{dx}dx.$$

The present work aims at finding the thermal buckling load for the first buckling mode. Hence, the purpose of solving equation (2.16) is to find the lowest eigenvalue as it corresponds to the fundamental buckling load. The eigenvector $\{c_j\}$ corresponding to the lowest eigenvalue is used to find the buckling mode shape of the fundamental mode. It is to be noted that η represents a value which is equivalent to the thermal buckling load.

2.5. Solution Methodology

The eigenvalue to be found out represents the fraction of the thermal load at critical condition. The elements of the conventional stiffness matrix depend on the stiffness coefficients A_1, A_2 and A_3. Also the elements of the stress stiffness matrix depend on the pre-stress coefficient N_{th}. These coefficients are dependent on the material properties as can be seen from equations (2.10) and (2.13). As temperature dependent material properties are considered in the present work, the elements of the matrix $\left[K_{ij}^{\sigma}\right]^{-1}\left[K_{ij}\right]$ in equation (2.16) are also dependent on the thermal load. Hence, to find out the thermal buckling load at critical condition, an iterative method is used to obtain the correct solution. In the present work, for the case of LTD and NLTD, the bottom layer (metal rich surface) is always considered to be at stress-free temperature T_0 , i.e., $T_m = T_0$ =300 K.

The step-wise algorithm of the iterative method used to solve equation (2.16) is briefly given below:

***Step 1*:**

For UTD: Increase T_u by a suitable amount to provide a new value of thermal load $(\Delta T)_{assumed} = T_u - T_0$.

For LTD and NLTD: Increase T_c by a suitable amount to provide a new value of thermal load $(\Delta T)_{assumed} = T_c - T_m$.

It is to be mentioned that before beginning the first iteration, it is considered that $T_u = T_0$ for UTD or, $T_c = T_m$ for LTD and NLTD.

***Step 2*:** Determine the through-thickness temperature distribution with the assumed value of the thermal load $(\Delta T)_{assumed}$ (as discussed in section 2.3).

***Step 3*:** Evaluate the stiffness coefficients and pre-stress coefficients using equations (2.10) and (2.13) respectively.

***Step 4*:** Determine the elements of the conventional stiffness matrix $\left[K_{ij}\right]$ and the stress stiffness matrix $\left[K_{ij}^{\sigma}\right]$.

***Step 5*:** Solve equation (2.16) to get the solution value $(\Delta T)_{solved}$ from the determined eigenvalue.

***Step 6*:** Calculate the percentage error as $\varepsilon = \left|\left\{(\Delta T)_{assumed} - (\Delta T)_{solved}\right\} / (\Delta T)_{assumed}\right| \times 100$.

***Step 7*:** Check if $\varepsilon \le \varepsilon_{max}$, where, ε_{max} is a predefined small number to check the convergence. If yes, consider $(\Delta T)_{solved}$ as the solution for the current load step. Otherwise, go to step 1 and repeat steps 1-7.

Chapter 3

RESULTS & DISCUSSION - UNIFORM TEMPERATURE DISTRIBUTION (UTD)

3.1. Introduction

A uniform temperature distribution corresponds to the case when the temperature of the entire beam is raised to a higher value T_u. The results are presented in graphical form in which the thermal buckling load in non-dimensional form is presented with the variation of volume fraction index k of the FGMs considered. The variation of k is considered to be from 0 to 50. Non-dimensional thermal buckling load λ is defined as $\lambda = 12\alpha_{m0}(L/h)^2(T_c - T_m)_{cr}$, where α_{m0} is the thermal expansion coefficient of the metal constituent at T_0. As mentioned in the previous chapter, the dimensional thermal load is given as $(T_u - T_0)$. The results are presented for three boundary conditions, namely, clamped-clamped (CC), simply supported-simply supported (SS) and, clamped-simply supported (CS). It is to be mentioned that the value of T_0 is taken as 300 K. The results are generated for *h*= 0.01 m and *b*= 0.02 m.

Three different metal-ceramic functionally graded material compositions are considered. These are Stainless Steel (SUS304)/Alumina (Al_2O_3), Stainless Steel/Silicon Nitride (Si_3N_4) and Stainless Steel/Zirconia (ZrO_2). Two different categories of λ vs. k plots are shown. The first one is the variation of λ with k for different length-thickness (L/h) ratios, and these are presented for different combinations of boundary conditions and materials. The second category represents the variation of λ with k for different FGM compositions, and these are presented for different combinations of boundary conditions and length-thickness ratios.

3.2. Validation Study

The validation plot showing the variation of non-dimensional thermal buckling load λ with volume fraction index k is shown in Figure 3.1 for L/h=25. The validation is carried out with the results of Kiani and Eslami (2013) for Stainless Steel/Silicon Nitride beam with clamped-clamped boundary condition. The comparison shows good agreement and thus validates the present mathematical model. The comparison does not show an exact matching as the present work is based on Euler-Bernoulli beam theory, whereas, the work of Kiani and Eslami (2013) is based on Timoshenko beam theory.

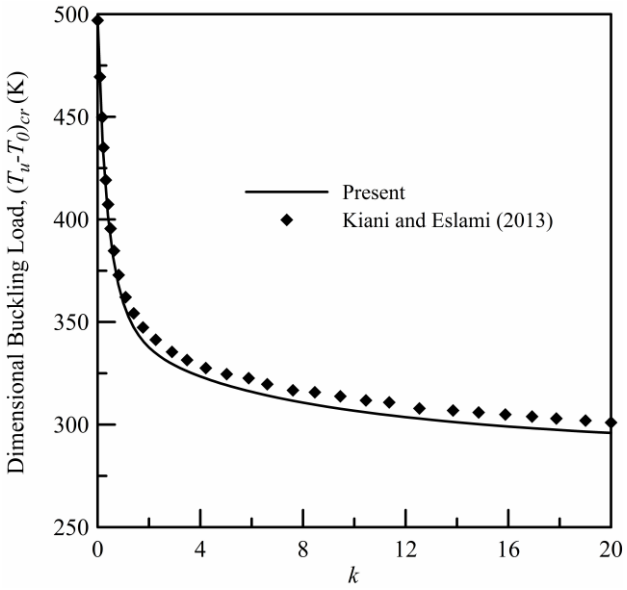

Figure 3.1: Validation plot showing variation of dimensional thermal buckling load $\left((T_u - T_0)_{cr}\right)$ with volume fraction index (k) for CC Stainless Steel/Silicon Nitride beam for L/h=25 with UTD.

3.3. Comparative Plots For Different Length-Thickness Ratios

The variation of non-dimensional thermal buckling load λ with volume fraction index k for Stainless Steel/Alumina (SUS304-Al_2O_3) beam is shown in Figure 3.2a-c for CC, SS and CS boundary conditions respectively. Similar plots are shown in Figure 3.3a-c for Stainless Steel/Silicon Nitride (SUS304-Si_3N_4) beam and in Figure 3.4a-c for Stainless

Steel/Zirconia (SUS304-ZrO_2) beam. In each of the figures, plots are presented for L/h=25, 40, 50, 75, 100, 150.

It is seen from Figure 3.2 that the non-dimensional thermal buckling load decreases with an increase in the volume fraction index. The decrease is sharp for low values of the volume fraction index (0 to 2). But then it becomes gradual up to k=50. It is also seen that, with increase in length-thickness ratio, the non-dimensional thermal buckling load increases for any particular value of the volume fraction index. The natures of the plots are quite similar irrespective of the boundary conditions and length-thickness ratios. It is also seen that for the same volume fraction index, the non-dimensional thermal buckling load is maximum for CC beam and minimum for SS beam, with the CS beam coming in between the other two.

The plots shown in Figure 3.3 for SUS304-Si_3N_4 beam are found to be similar in nature with the plots of Figure 3.2. This is true irrespective of the boundary conditions and length-thickness ratios. The thermal loads for the SUS304-Si_3N_4 beam are observed to be slightly lesser than that of the SUS304-Al_2O_3 beam.

The k vs. λ plots for SUS304-ZrO_2 beam, as shown in Figure 3.4, are found to be of different nature compared to the plots of SUS304-Al_2O_3 and SUS304-Si_3N_4 beams. Here, for SUS304-ZrO_2 beam, the non-dimensional thermal buckling load increases with increase in volume fraction index. The increase is observed to be sharp for k=0 to 5, and becomes gradual beyond k=5 up to k=50. Similar to the other two FGM beams, it is seen that the non-dimensional thermal buckling load increases with increase in length-thickness ratios for any particular value of the volume fraction index.

3.4. Comparative Plots For Different Materials

The variation of non-dimensional thermal buckling load λ with volume fraction index k for three different FGMs are presented in Figure 3.5a-c for CC, SS and CS beam respectively having L/h=25. Similar plots are presented in Figures 3.6-3.9 for L/h=50, 75, 100, 150 respectively. It is clear from Figures 3.5-3.9 that the natures of the λ vs. k plots are almost identical for Stainless Steel/Alumina and Stainless Steel/Silicon Nitride beams. The plots for these two FGMs are found to coincide with each other. Comparisons among

three FGMs reveal that the thermal buckling load for Stainless Steel/Zirconia beam is lower than that of the other two FGM beams. The relative differences in the thermal buckling loads are found to be decreasing with increases in the values of the volume fraction index. The observations made are true for all the L/h ratios and boundary conditions considered.

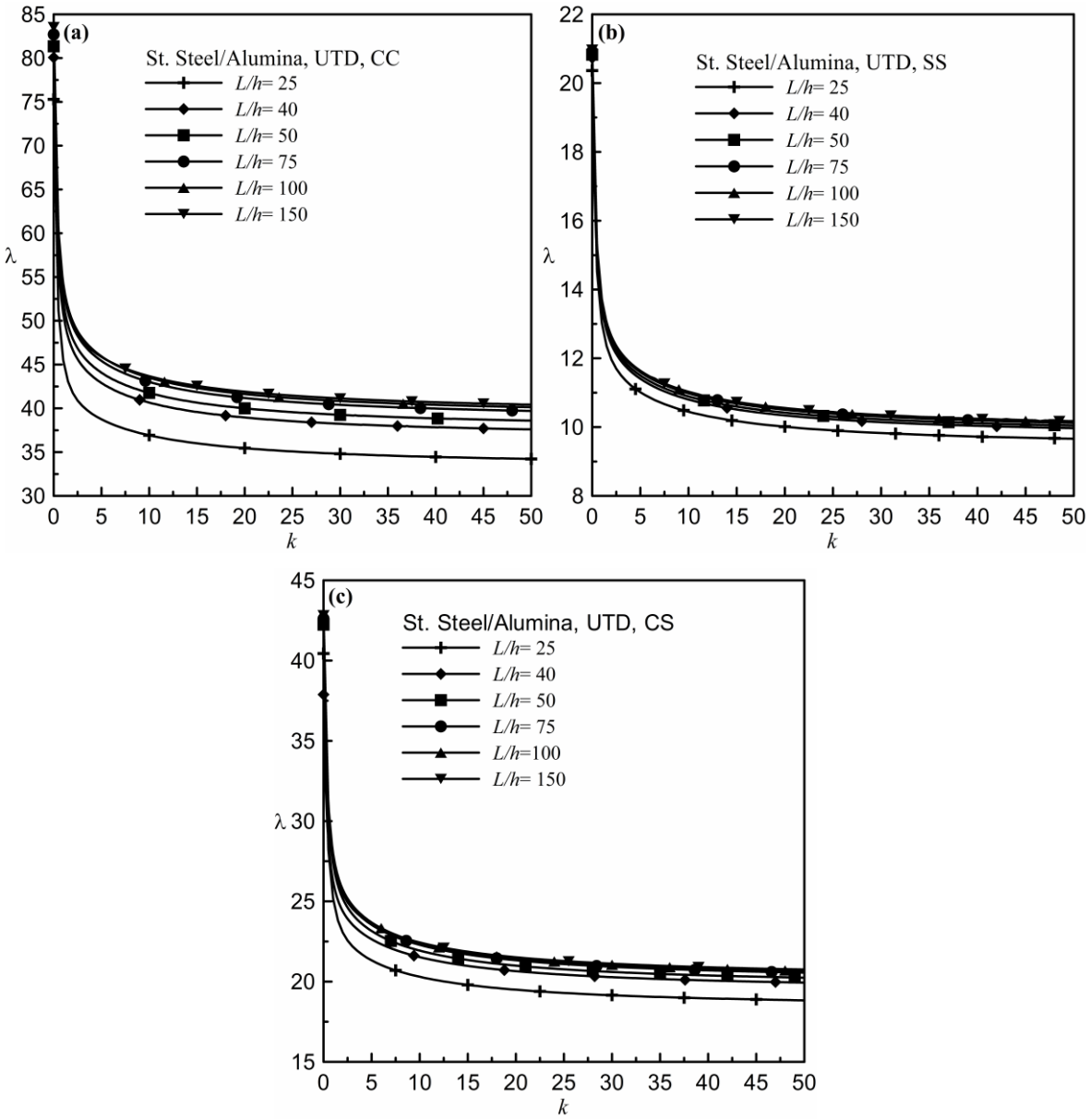

Figure 3.2: Variation of non-dimensional thermal buckling load (λ) with volume fraction index (k) for different length-thickness ratios of Stainless Steel/Alumina beams for UTD: (a) CC, (b) SS and (c) CS.

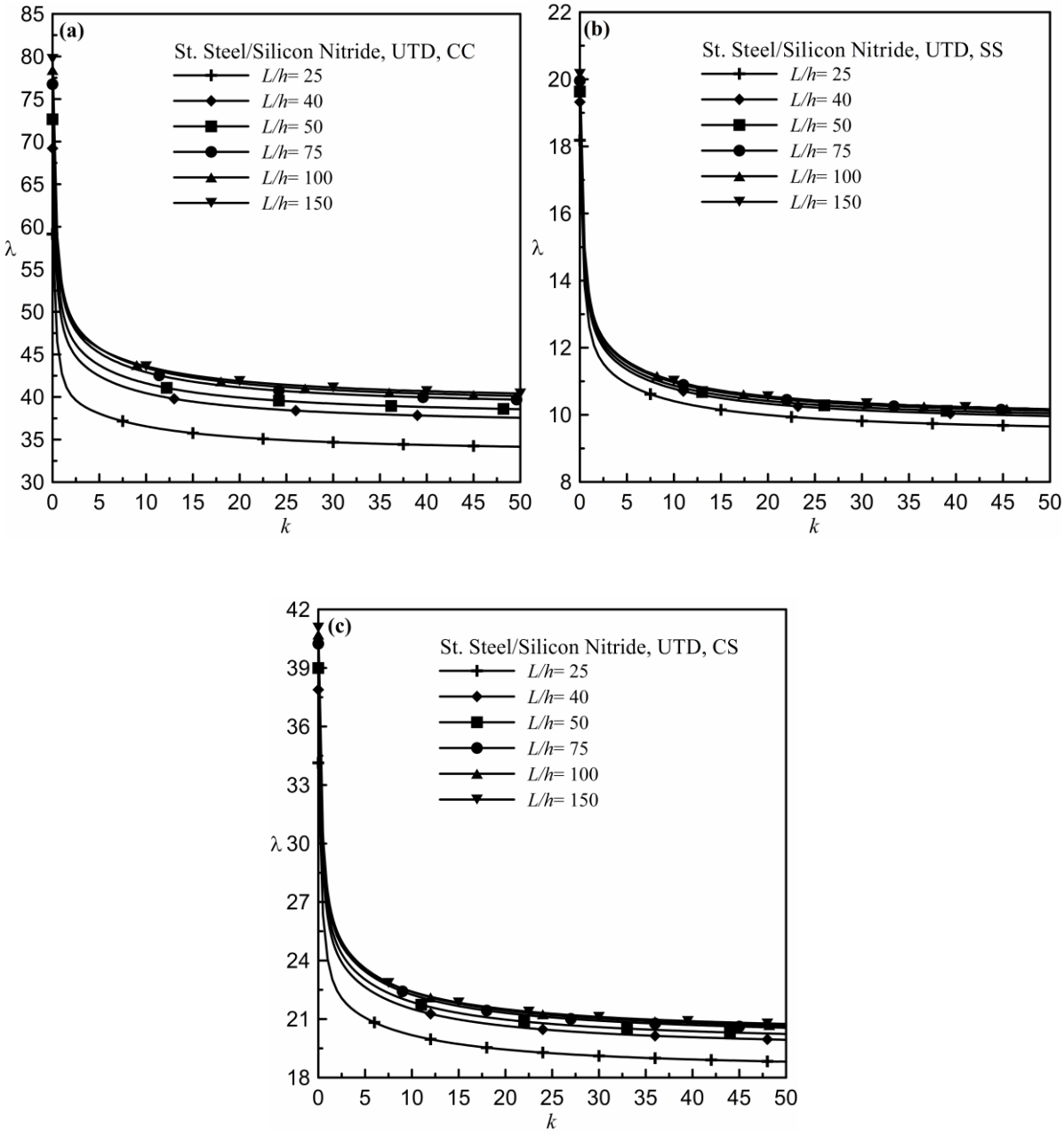

Figure 3.3: Variation of non-dimensional thermal buckling load (λ) with volume fraction index (k) for different length-thickness ratios of Stainless Steel/Silicon Nitride beams for UTD: (a) CC, (b) SS and (c) CS.

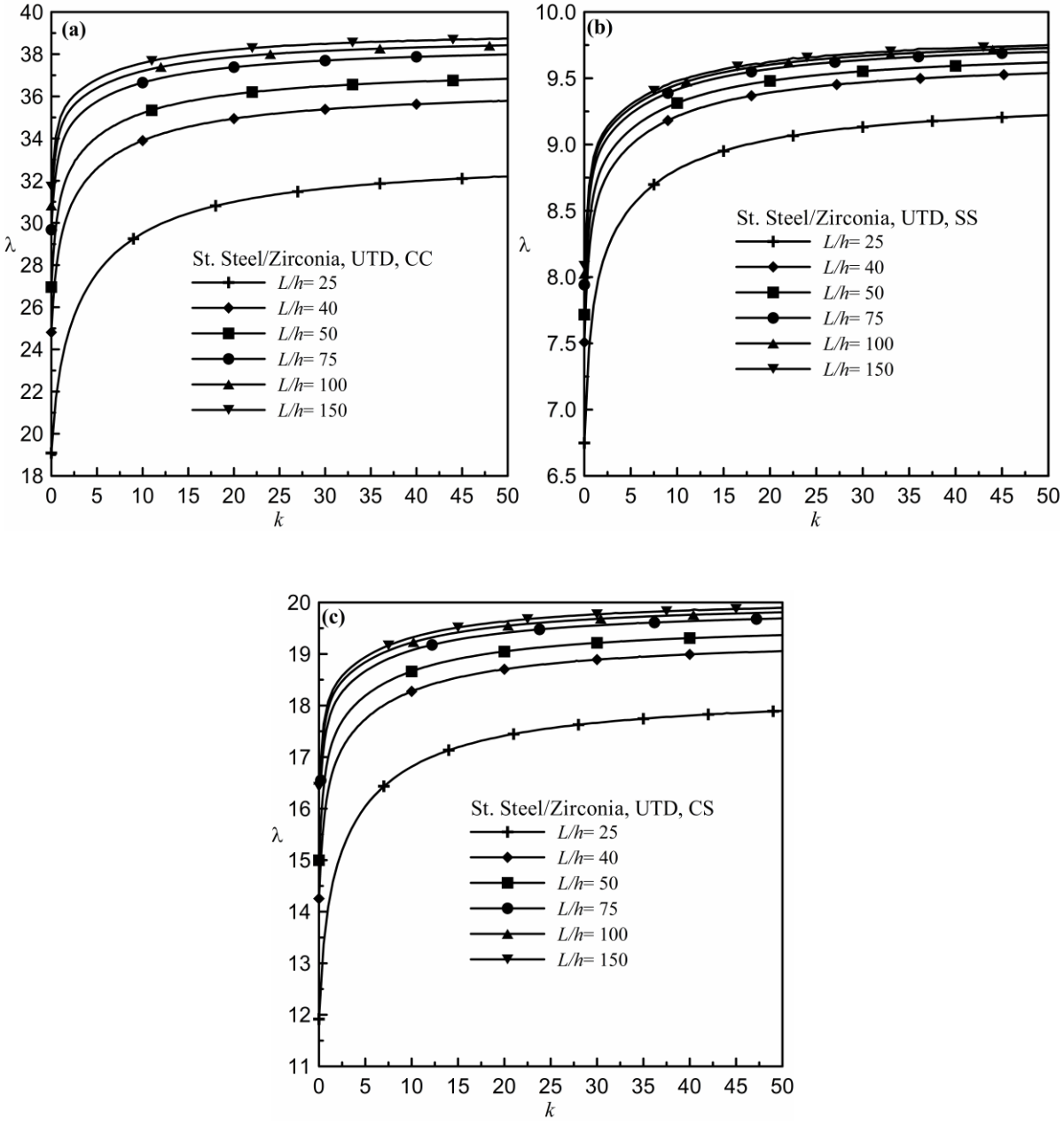

Figure 3.4: Variation of non-dimensional thermal buckling load (λ) with volume fraction index (k) for different length-thickness ratios of Stainless Steel/Zirconia beams for UTD: (a) CC, (b) SS and (c) CS.

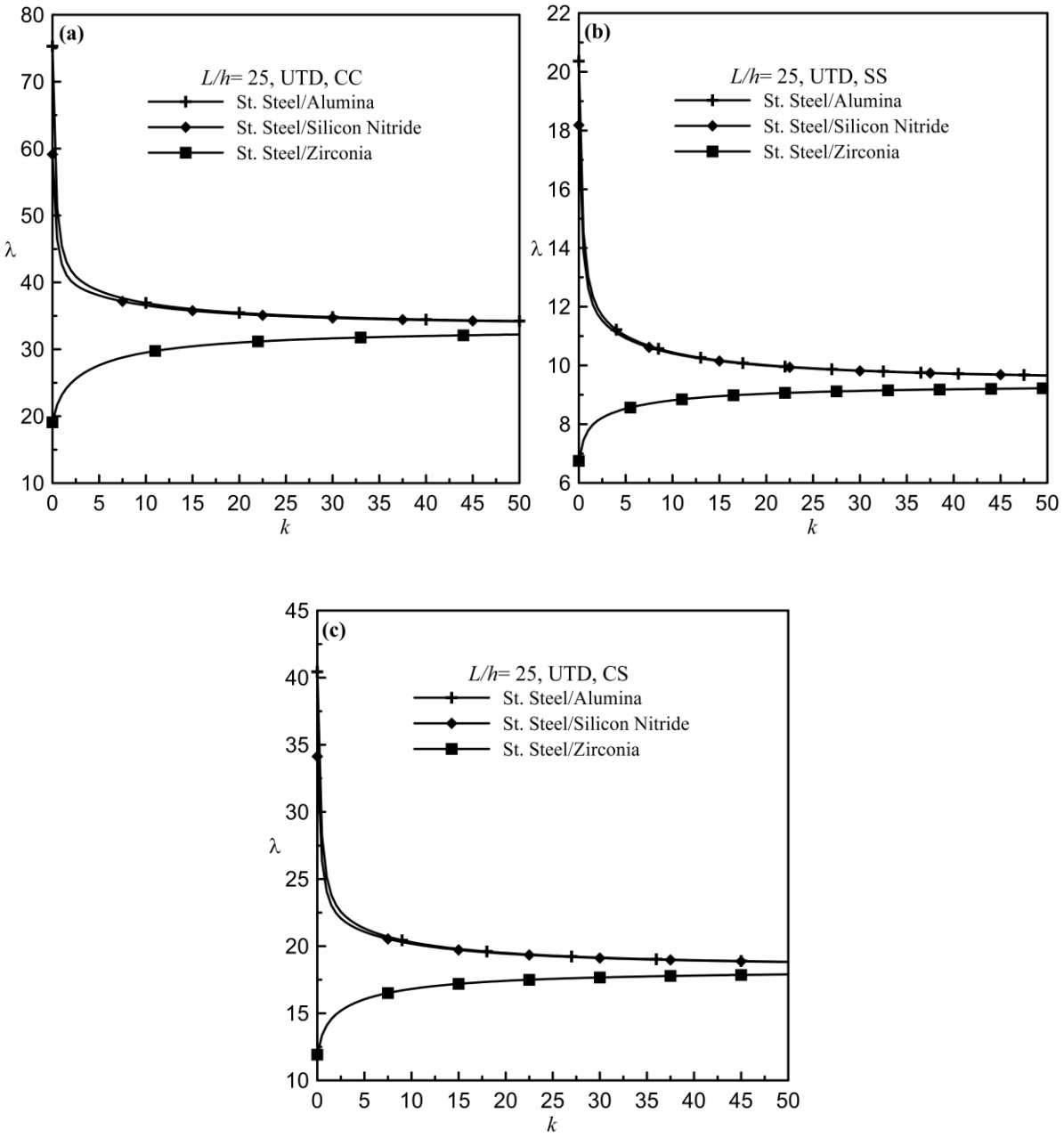

Figure 3.5: Variation of non-dimensional thermal buckling load (λ) with volume fraction index (k) for different FGM compositions having L/h =25 for UTD: (a) CC, (b) SS and (c) CS.

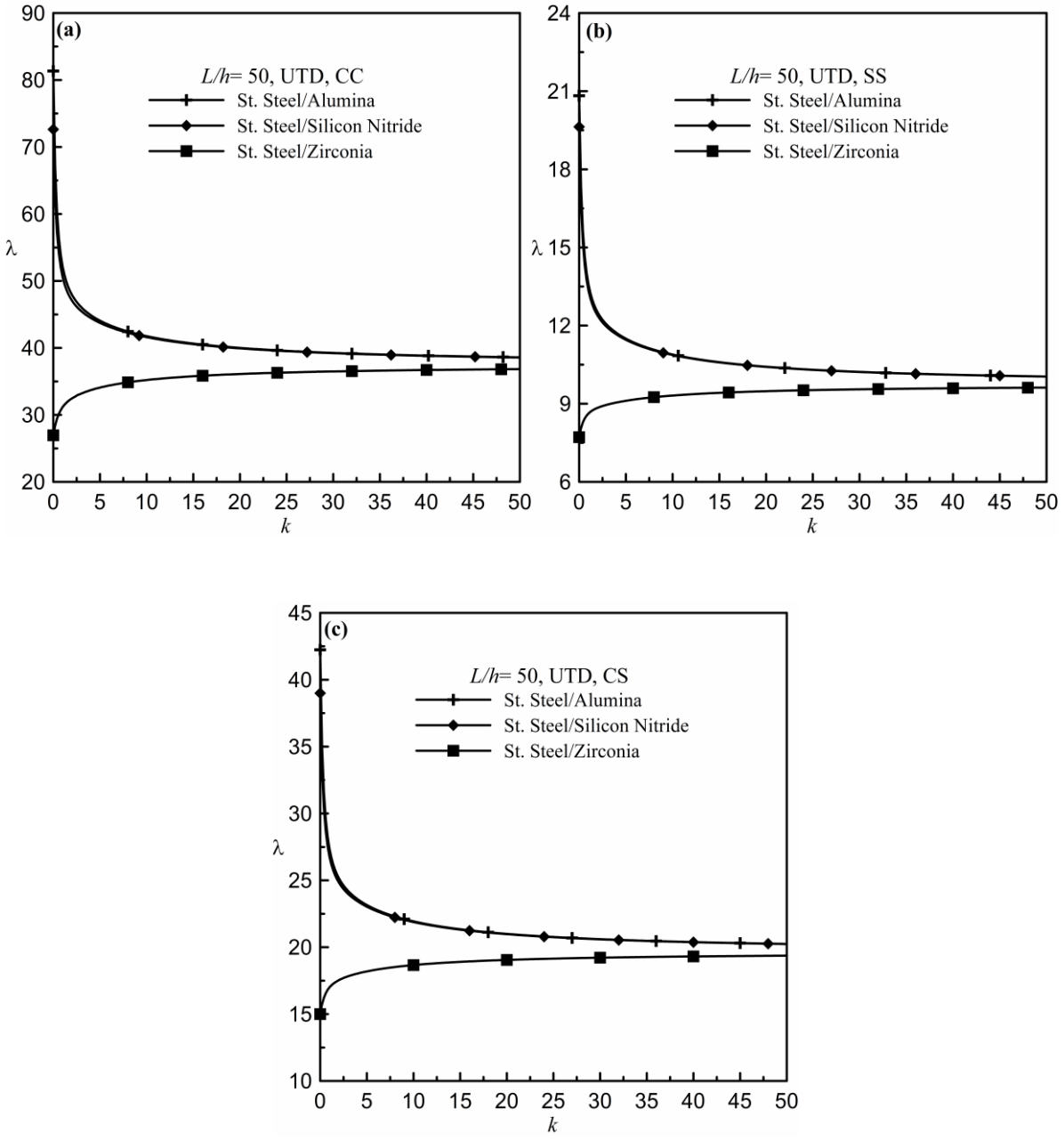

Figure 3.6: Variation of non-dimensional thermal buckling load (λ) with volume fraction index (k) for different FGM compositions having L/h =50 for UTD: (a) CC, (b) SS and (c) CS.

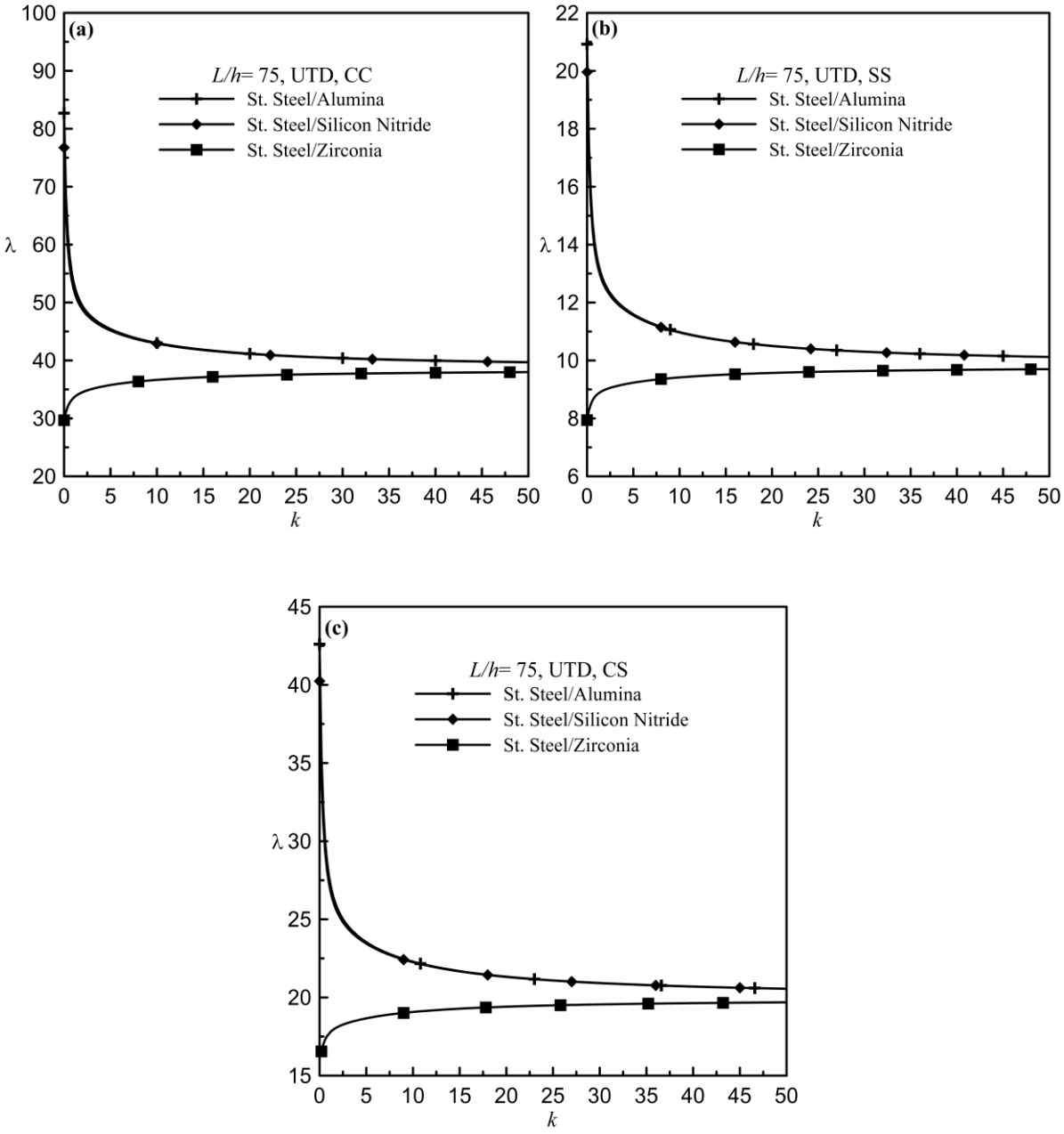

Figure 3.7: Variation of non-dimensional thermal buckling load (λ) with volume fraction index (k) for different FGM compositions having L/h =75 for UTD: (a) CC, (b) SS and (c) CS.

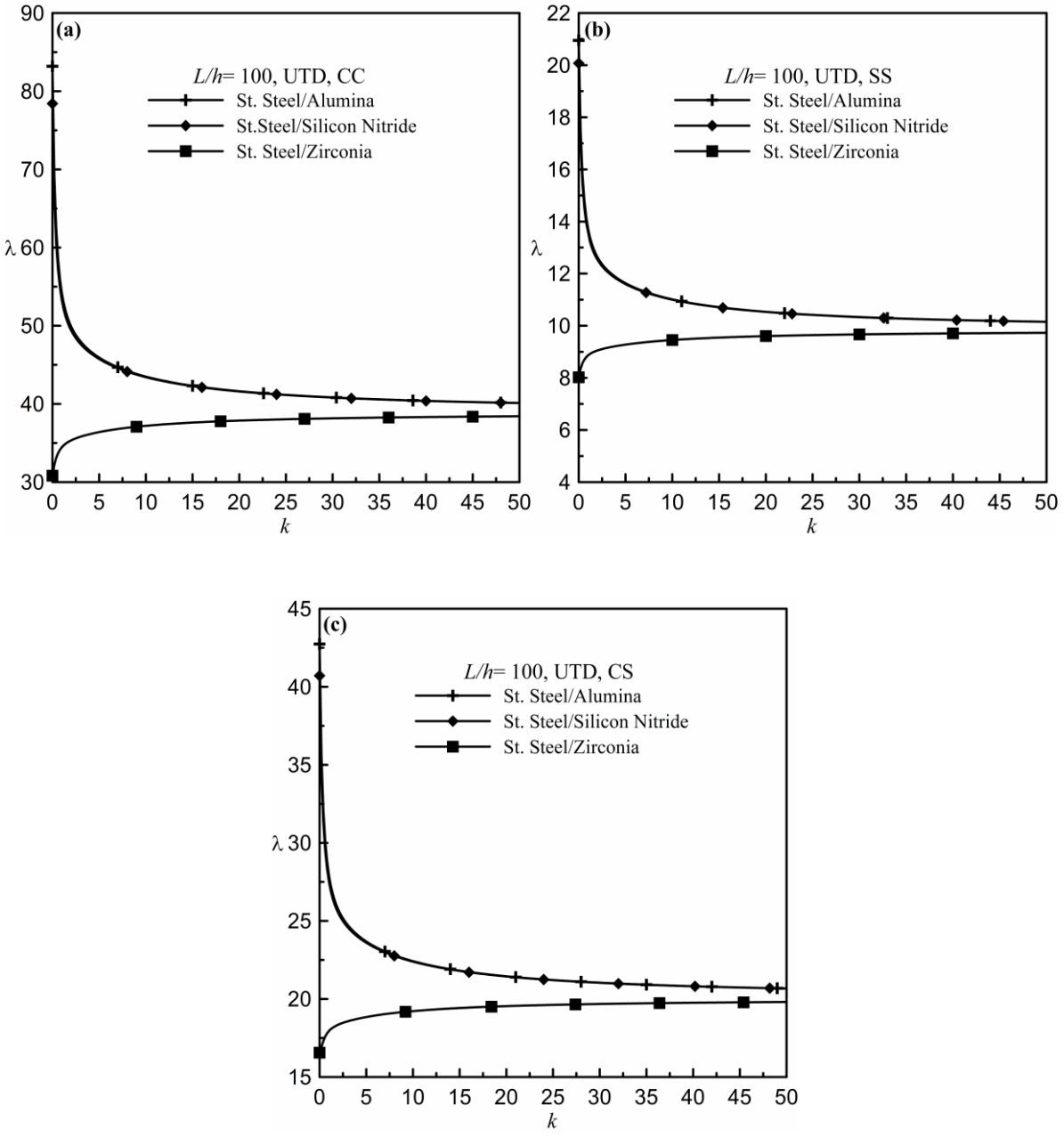

Figure 3.8: Variation of non-dimensional thermal buckling load (λ) with volume fraction index (k) for different FGM compositions having L/h=100 for UTD: (a) CC, (b) SS and (c) CS.

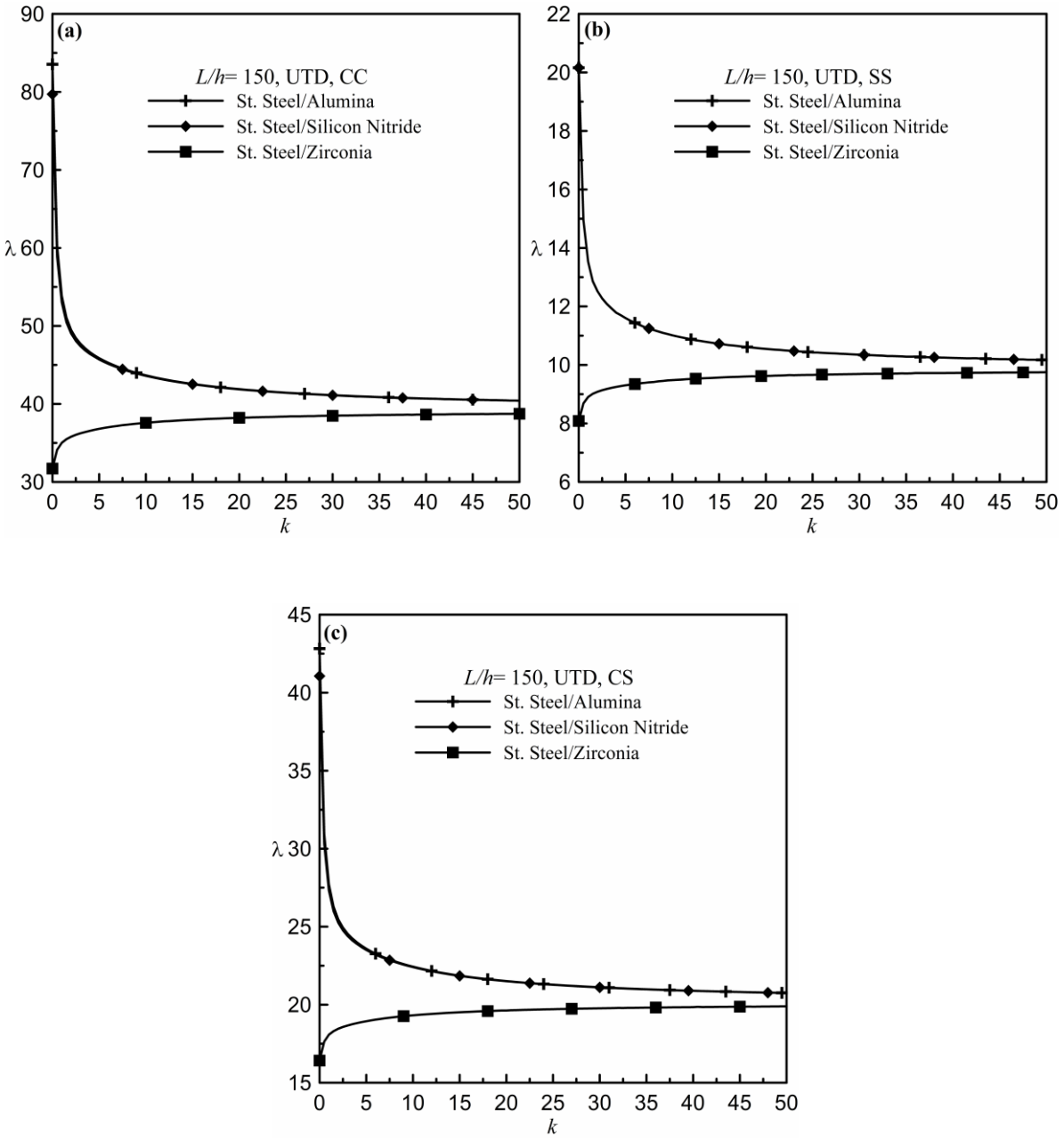

Figure 3.9: Variation of non-dimensional thermal buckling load (λ) with volume fraction index (k) for different FGM compositions having L/h=150 for UTD: (a) CC, (b) SS and (c) CS.

Chapter 4

RESULTS & DISCUSSION - LINEAR TEMPERATURE DISTRIBUTION (LTD)

4.1. Introduction

In the case of linear temperature distribution (LTD), a linear temperature gradient is assumed through the thickness of the beam. The top (ceramic-rich) and the bottom (metal-rich) layers of the beam are considered to be at temperatures T_c and T_m respectively, where, $T_c > T_m$ and T_m is assumed to be equal to the stress-free temperature T_0 (300 K). In this case, the equation governing the through-thickness temperature distribution is given by equation (2.4), which is given by, $T(z) = T_m + (T_c - T_m)\left(\frac{z}{h} + \frac{1}{2}\right)$. It is to be mentioned that a temperature distribution at steady-state condition can be approximated to be linear for a thin beam.

The results are shown in graphical form in which the non-dimensional thermal buckling loads are presented for different values of the volume fraction index k of the FGMs considered. It is considered that k ranges from 0 to 50. Non-dimensional thermal buckling load λ is defined as $\lambda = 12\alpha_{m0}(L/h)^2(T_c - T_m)_{cr}$, where α_{m0} is the thermal expansion coefficient of the metal constituent at T_0. As previously mentioned, the dimensional thermal load is given as $(T_c - T_m)$. Three boundary conditions are considered, namely, clamped-clamped (CC), simply supported-simply supported (SS) and, clamped-simply supported (CS). The results are generated for h= 0.01 m and b= 0.02 m.

Three different metal-ceramic functionally graded materials are considered. These are Stainless Steel/Alumina (Al_2O_3), Stainless Steel (SUS304)/Silicon Nitride (Si_3N_4) and

Stainless Steel/Zirconia (ZrO_2). Two different categories of k vs. λ plots are shown. The first one corresponds to the variation of λ with k for different length-thickness (L/h)

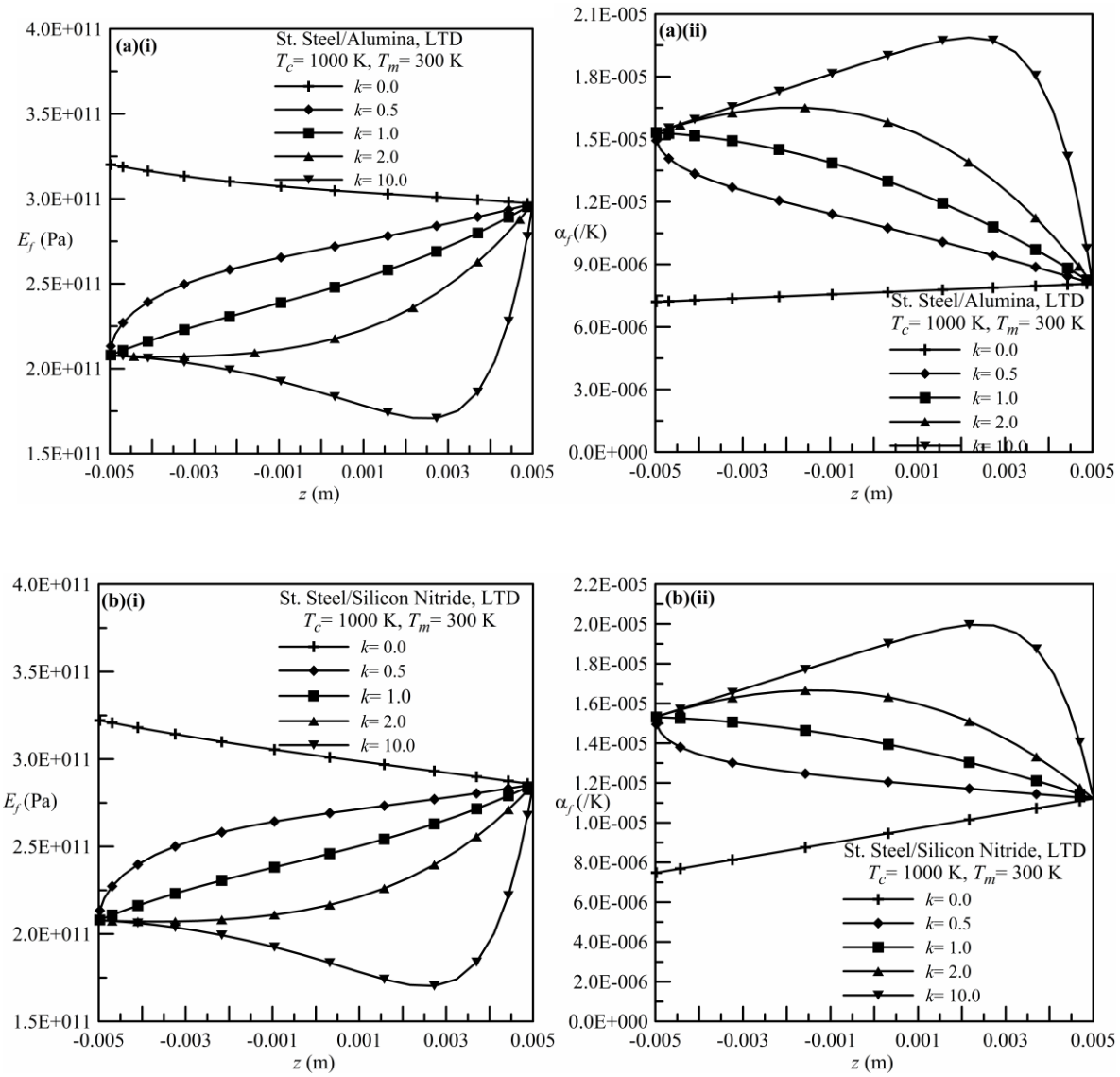

Figure 4.1: Variation of (i) effective elastic modulus and (ii) effective thermal expansion coefficient along the thickness direction for T_c =1000K for LTD: (a) Stainless Steel/Alumina, (b) Stainless Steel/Silicon Nitride and (c) Stainless Steel/Zirconia.

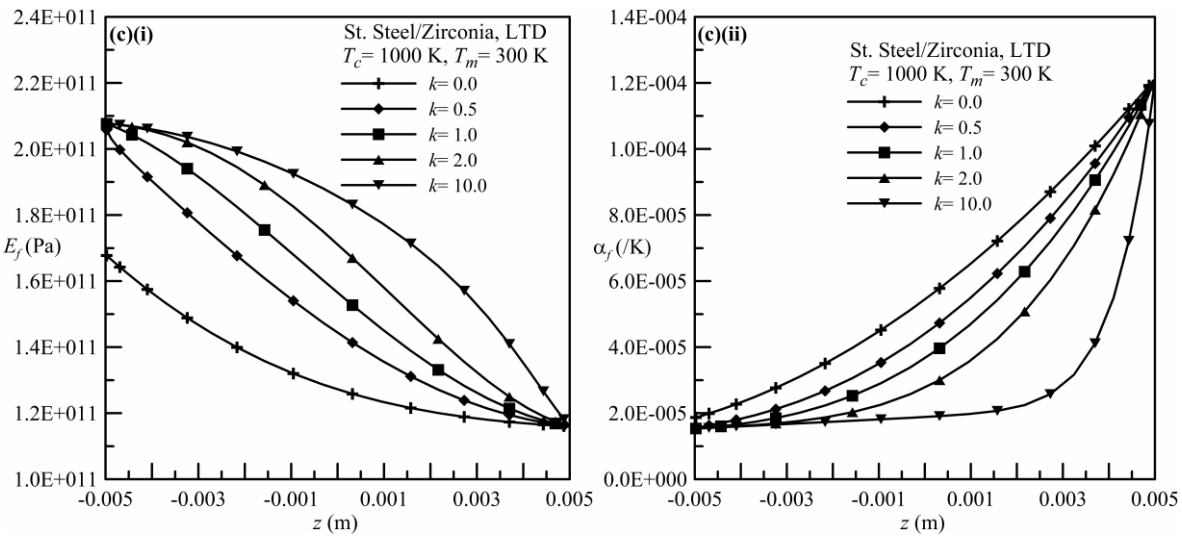

Figure 4.1: Continued.

ratios, and these are presented for different combinations of boundary conditions and materials. The second one considers the variation of λ with k for different FGM compositions, and these are shown for different combinations of boundary conditions and length-thickness ratios.

The present problem involving thermal buckling of FGM beam for LTD is strongly dependent on the how the effective thermal expansion coefficient and effective elastic modulus vary with temperature. In this case, the temperature profile is essentially considered to be linear through the thickness. Hence the variation of through-thickness material properties for any given thermal load $(T_c - T_m)$ strongly governs the present problem. For illustration purpose, Figure 4.1 is presented which shows the variation of through-thickness material properties for $(T_c - T_m)$=700 K for the three FGMs considered. In each of the figures, the through- thickness variation of the material properties are shown for different values of *k*.

4.2. Validation Study

The variation of non-dimensional thermal buckling load λ with volume fraction index k is compared with the results of Kiani and Eslami (2013) for Stainless Steel/Silicon Nitride beam with clamped-clamped boundary condition. The same is also compared with

the results generated by ANSYS (version 10.0). The comparison plots are shown in Figure 4.2 for L/h=40. Figure 4.2 shows very good agreement of the present plot with ANSYS. It also shows that the trend of the present plot matches with that of Kiani and Eslami (2013). The reason for deviation of the present result from that of Kiani and Eslami (2013) can be attributed to the fact that the present work is based on Euler-Bernoulli beam theory, whereas, the work of Kiani and Eslami (2013) is based on Timoshenko beam theory. The finite element model in ANSYS is created using SHELL91 elements with layered variation of material properties across the thickness. Thus, Figure 4.2 validates the present model for LTD.

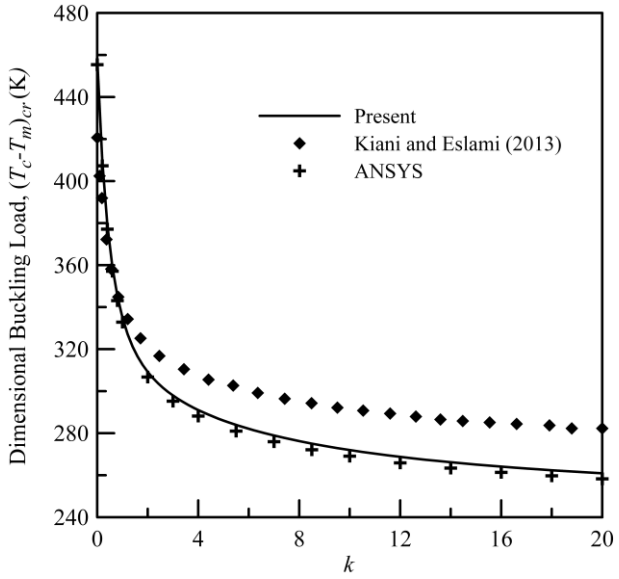

Figure 4.2: Validation plot showing variation of dimensional thermal buckling load with volume fraction index for CC Stainless Steel/Silicon Nitride beam for L/h=40 with LTD.

4.3. Comparative Plots For Different Length-Thickness Ratios

The variation of non-dimensional thermal buckling load λ with volume fraction index k for Stainless Steel/Alumina beam is presented in Figure 4.3a-c for CC, SS and CS boundary conditions respectively. Similar kinds of plots are presented in Figure 4.4a-c for Stainless Steel/Silicon Nitride beam and in Figure 4.5a-c for Stainless Steel/Zirconia beam. In each case, plots are presented for L/h=25, 40, 50, 75, 100, 150.

It is observed from Figure 4.3 that the non-dimensional thermal buckling load decreases with an increase in the volume fraction index. The decrease is sharp for low values of the volume fraction index. Beyond that, the decreasing nature is quite gradual up to k=50. Moreover, with an increase in the length-thickness ratio, the non-dimensional thermal buckling load is found to be increasing for any value of the volume fraction index. The natures of the plots are quite similar irrespective of the boundary conditions and length-thickness ratios. It is also seen that for the same volume fraction index, the non-dimensional thermal buckling load is maximum for clamped-clamped beam, followed by clamped-simply supported beam and minimum for simply supported-simply supported beam.

The k vs. λ plots for SUS304-Si_3N_4 beam, shown in Figure 4.4, are found to be of similar nature with that for Stainless Steel/Alumina beam. This is true irrespective of the boundary conditions and length-thickness ratios considered. Apparently, the thermal loads for the SUS304-Si_3N_4 beam are observed to be slightly lesser than that of the SUS304-Al_2O_3 beam.

The k vs. λ plots for SUS304-ZrO_2 beam, shown in Figure 4.5, are seen to be of completely different nature compared to the plots of SUS304-Al_2O_3 and SUS304-Si_3N_4 beams. In this case, the non-dimensional thermal buckling load is seen to be increasing with increase in volume fraction index values. The increase is observed to be sharp for lower value of k and it becomes gradual for moderate to high values of k. Similar to the other two FGM beams, it is seen that the non-dimensional thermal buckling load increases with increase in length-thickness ratios for any particular value of the volume fraction index. Unlike the other FGMs, the effects of length-thickness ratio are seen to be more prominent for the SUS304-ZrO_2 beam.

4.4. Comparative Plots For Different Materials

The variation of non-dimensional thermal buckling load λ with volume fraction index k for three different FGMs are presented in Figure 4.6a-c for CC, SS and CS beam respectively having L/h=25. Similar plots for L/h=50, 75, 100, 150 are presented in Figures 4.7-4.10 respectively. It is seen that the natures of the λ vs. k plots are almost identical for Stainless Steel/Alumina and Stainless Steel/Silicon Nitride beams. The plots for

these two FGMs are seen to coincide with each other. This is more prominent for higher length-thickness ratios. Comparisons among three FGMs reveal that the thermal buckling load for Stainless Steel/Zirconia beam is lower than that of the other two FGM beams. The relative differences in the thermal buckling loads are found to be decreasing with increases in the values of the volume fraction index. The observations made are true for all the L/h ratios and boundary conditions considered.

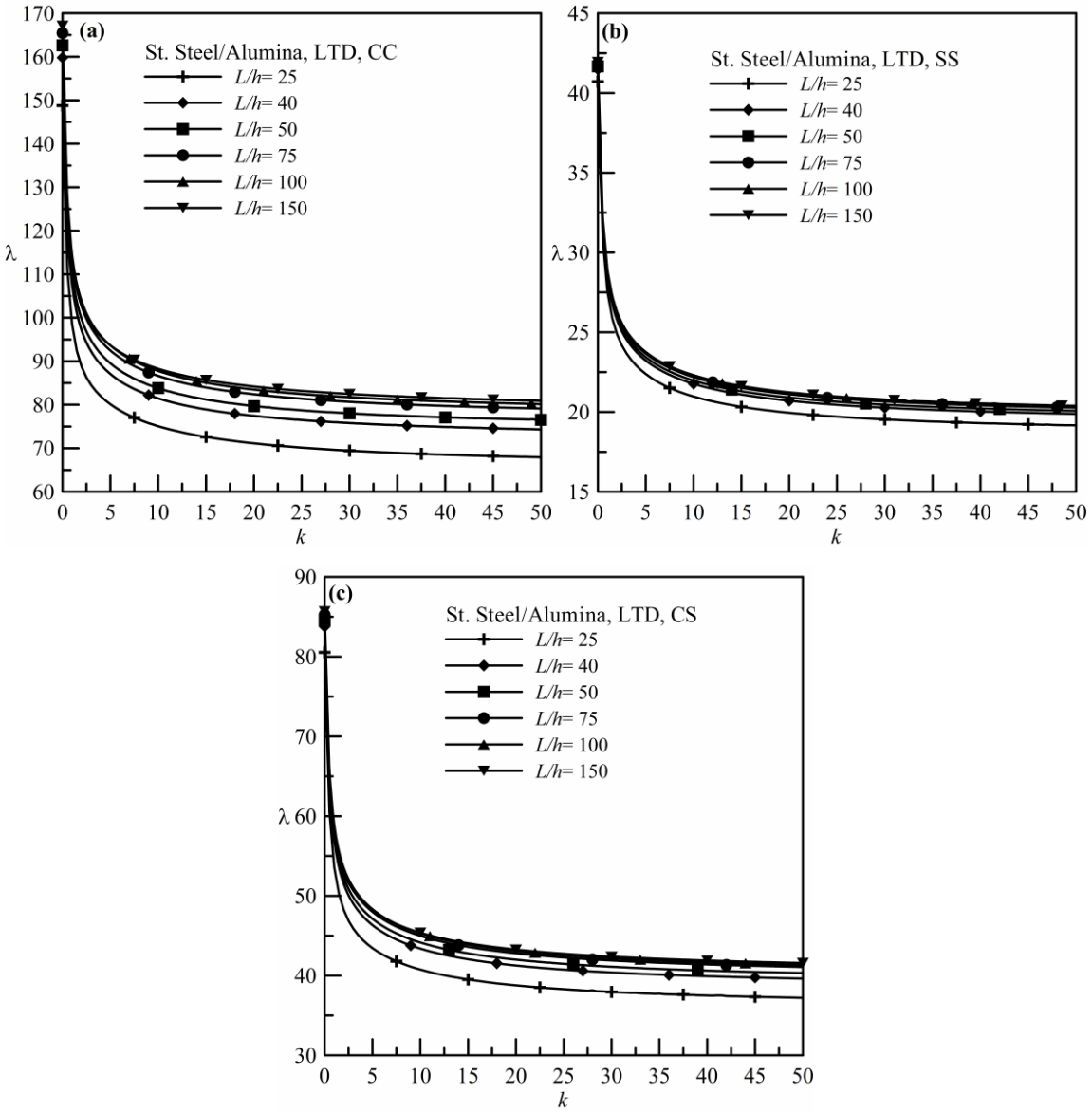

Figure 4.3: Variation of non-dimensional thermal buckling load (λ) with volume fraction index (k) for different length-thickness ratios of Stainless Steel/Alumina beams for LTD: (a) CC, (b) SS and (c) CS.

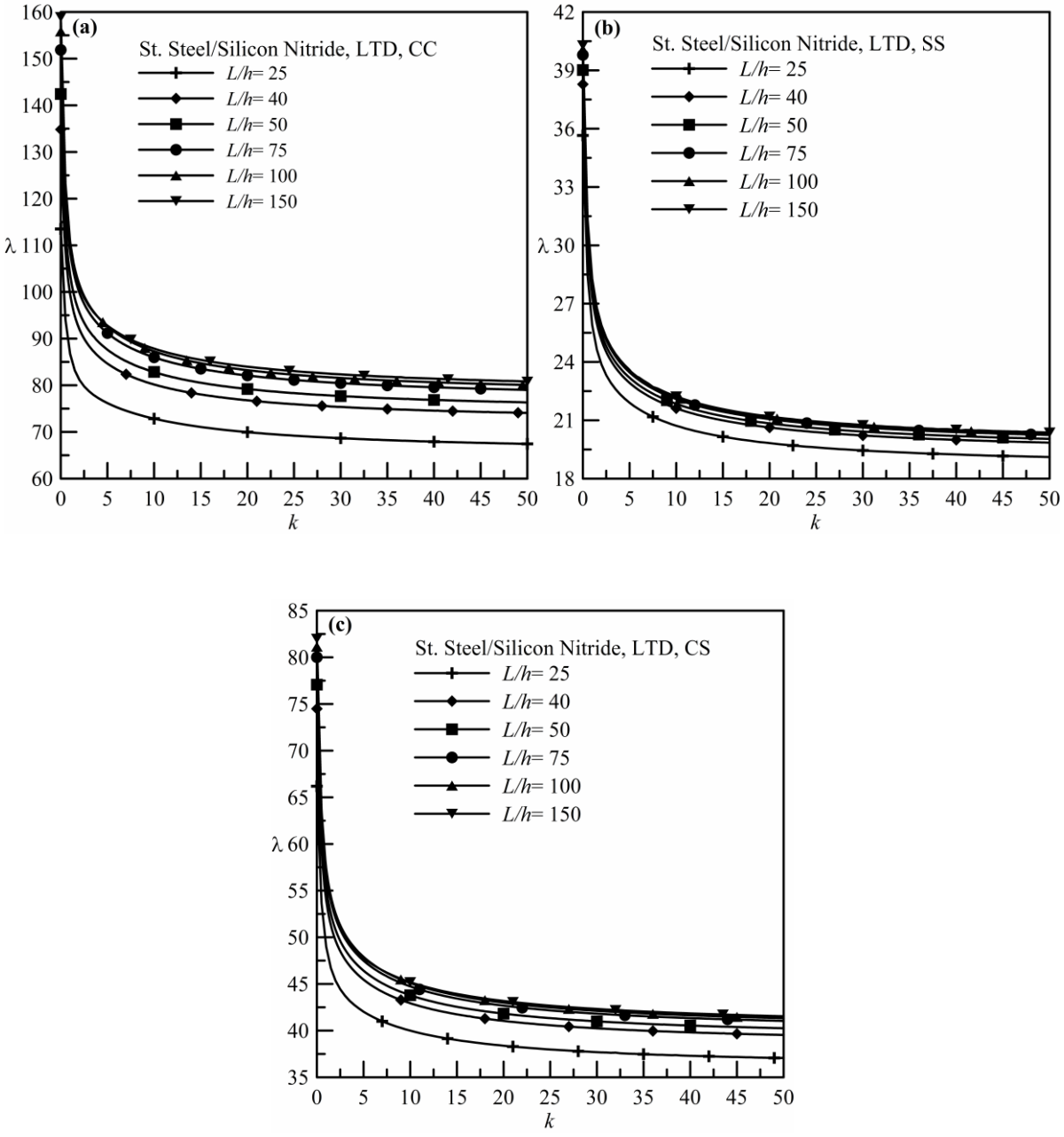

Figure 4.4: Variation of non-dimensional thermal buckling load (λ) with volume fraction index (k) for different length-thickness ratios of Stainless Steel/Silicon Nitride beams for LTD: (a) CC, (b) SS and (c) CS.

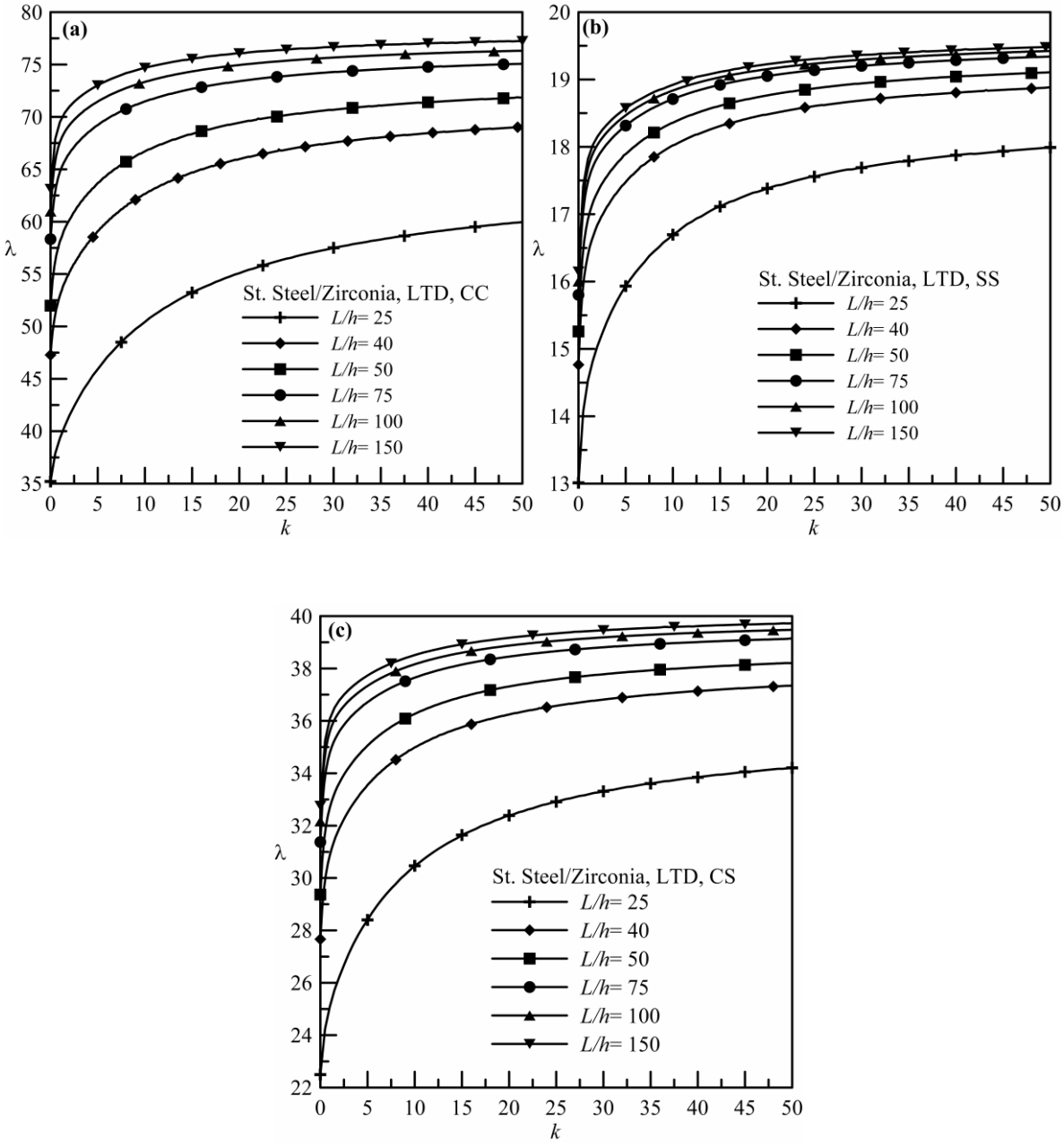

Figure 4.5: Variation of non-dimensional thermal buckling load (λ) with volume fraction index (k) for different length-thickness ratios of Stainless Steel/Zirconia beams for LTD: (a) CC, (b) SS and (c) CS.

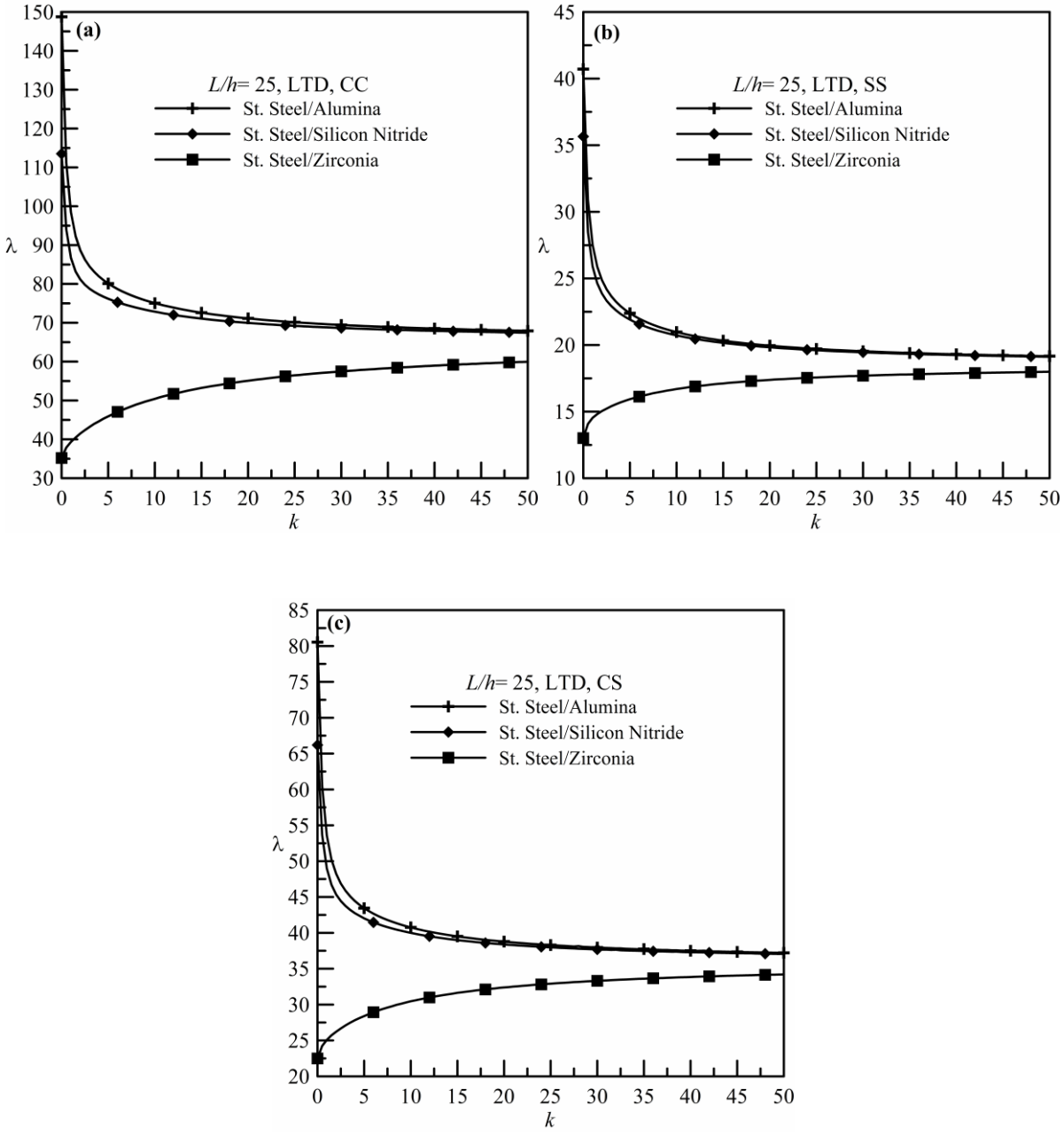

Figure 4.6: Variation of non-dimensional thermal buckling load (λ) with volume fraction index (k) for different FGM compositions having L/h=25 for LTD: (a) CC, (b) SS and (c) CS.

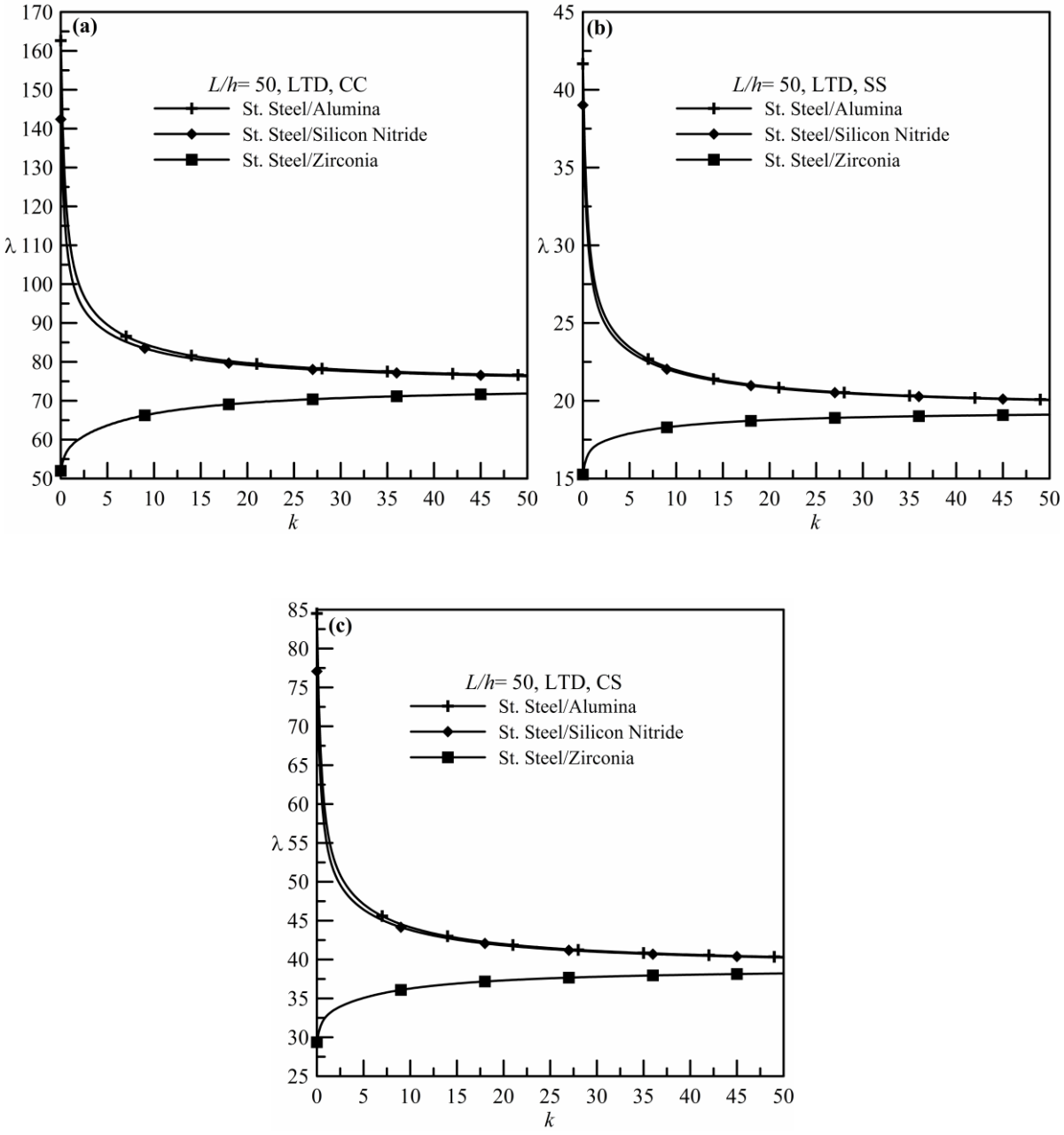

Figure 4.7: Variation of non-dimensional thermal buckling load (λ) with volume fraction index (k) for different FGM compositions having L/h=50 for LTD: (a) CC, (b) SS and (c) CS.

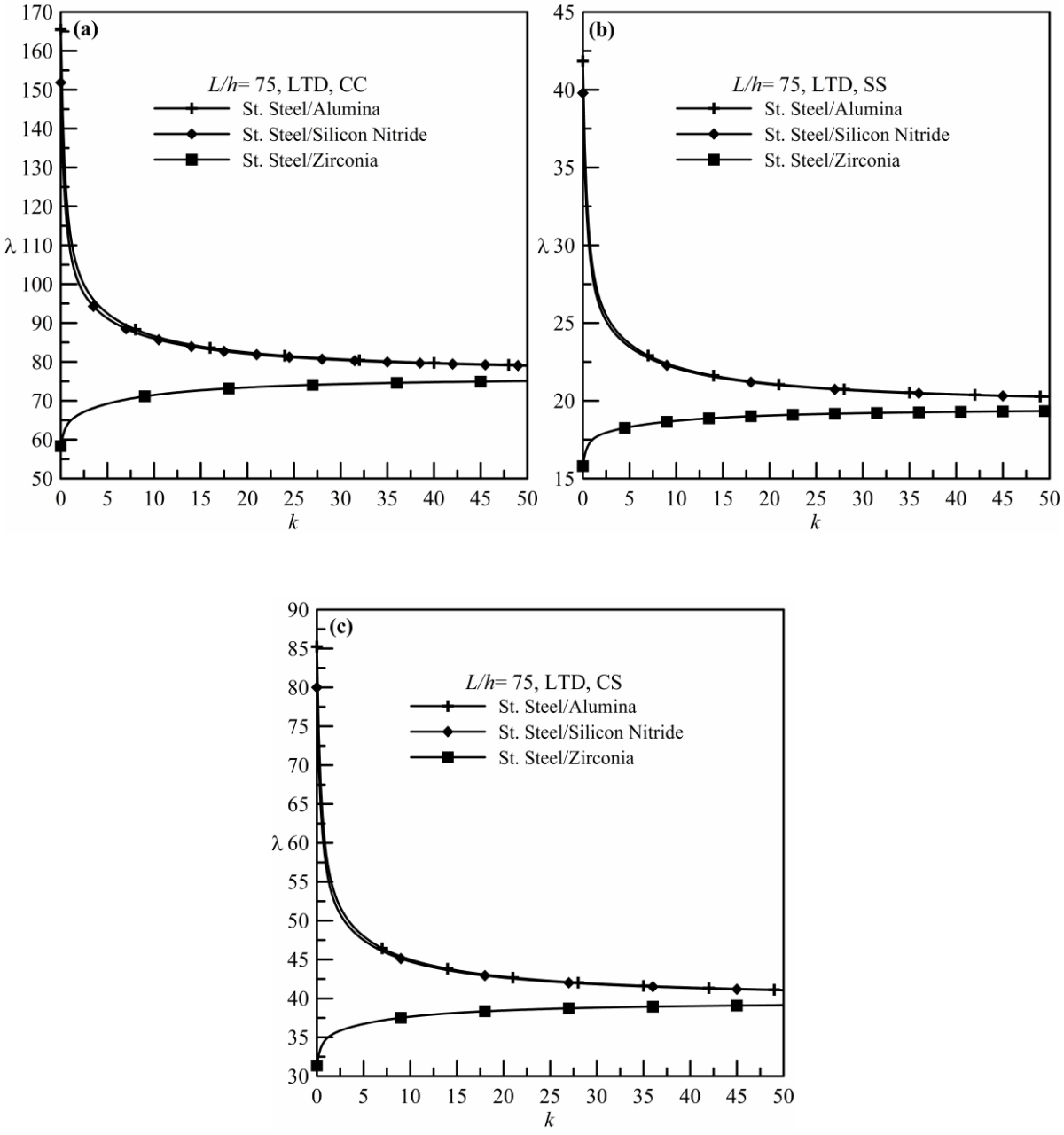

Figure 4.8: Variation of non-dimensional thermal buckling load (λ) with volume fraction index (k) for different FGM compositions having L/h=75 for LTD: (a) CC, (b) SS and (c) CS.

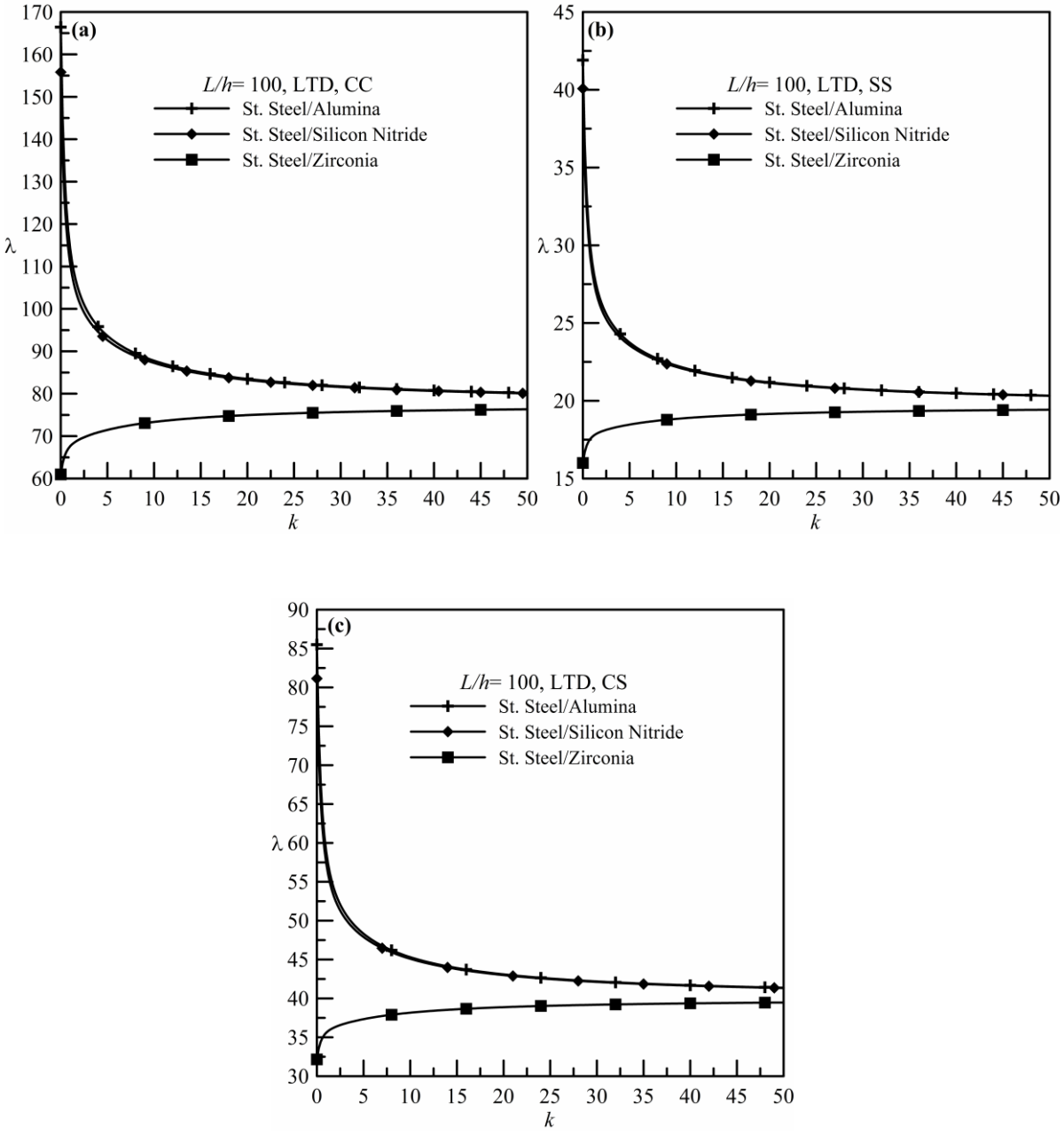

Figure 4.9: Variation of non-dimensional thermal buckling load (λ) with volume fraction index (k) for different FGM compositions having L/h=100 for LTD: (a) CC, (b) SS and (c) CS.

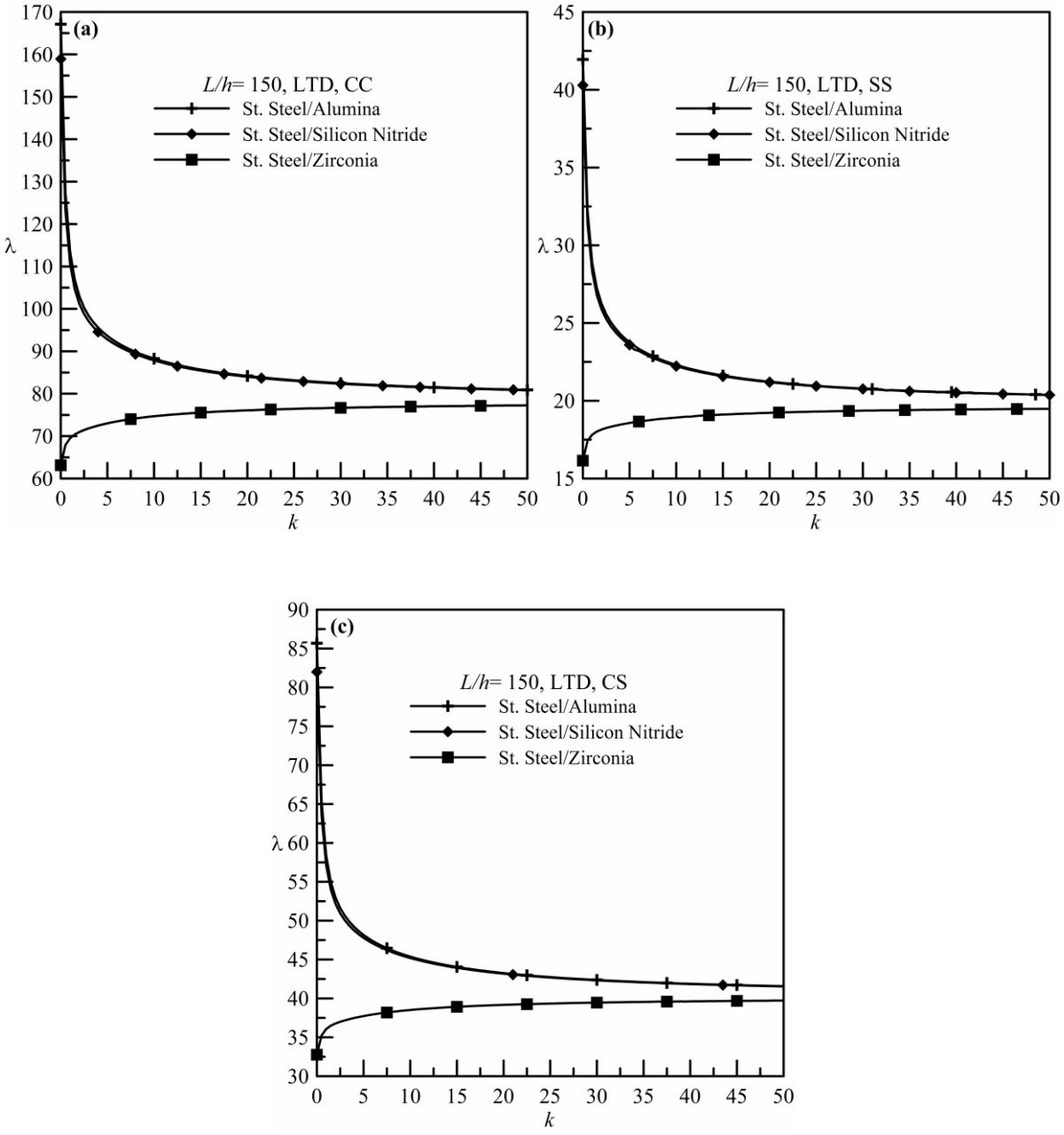

Figure 4.10: Variation of non-dimensional thermal buckling load (λ) with volume fraction index (k) for different FGM compositions having L/h=150 for LTD: (a) CC, (b) SS and (c) CS.

Chapter 5

RESULTS & DISCUSSION – NON-LINEAR TEMPERATURE DISTRIBUTION (NLTD)

5.1. Introduction

In this case, steady-state heat conduction is considered where heat flows between the bottom surface (metal-rich having temperature T_m) and the top surface (ceramic-rich having temperature $T_c > T_m$). Here, T_m is assumed to be equal to the stress-free temperature T_0 (300 K) and the temperature field is considered to be uniform over the beam length. The temperature distribution is obtained by solving the one-dimensional heat conduction equation, given in equation (2.5). It is seen that the through-thickness temperature gradient in this case is non-linear in nature and this is given by equation (2.7).

The results are shown in graphical form in which the non-dimensional thermal buckling loads are presented for different values of the volume fraction index k. It is considered that k ranges from 0 to 50. Non-dimensional thermal buckling load λ is defined as $\lambda = 12\alpha_{m0}(L/h)^2(T_c - T_m)_{cr}$, where α_{m0} is the thermal expansion coefficient of the metal constituent at T_0. The dimensional thermal load is given as $(T_c - T_m)$. Three boundary conditions are considered, namely, clamped-clamped (CC), simply supported-simply supported (SS) and, clamped-simply supported (CS). The results are generated for h= 0.01 m and b= 0.02 m.

Three different metal-ceramic FGMs are considered. These are Stainless Steel/Alumina (Al_2O_3), Stainless Steel (SUS304)/Silicon Nitride (Si_3N_4) and Stainless Steel/Zirconia (ZrO_2). Two different categories of k vs. λ plots are shown. The first one considers the variation of λ with k for different length-thickness (L/h) ratios, and these are presented for different combinations of boundary conditions and materials. The second

case considers the variation of λ with k for different FGM compositions, and these are shown for different combinations of boundary conditions and length-thickness ratios.

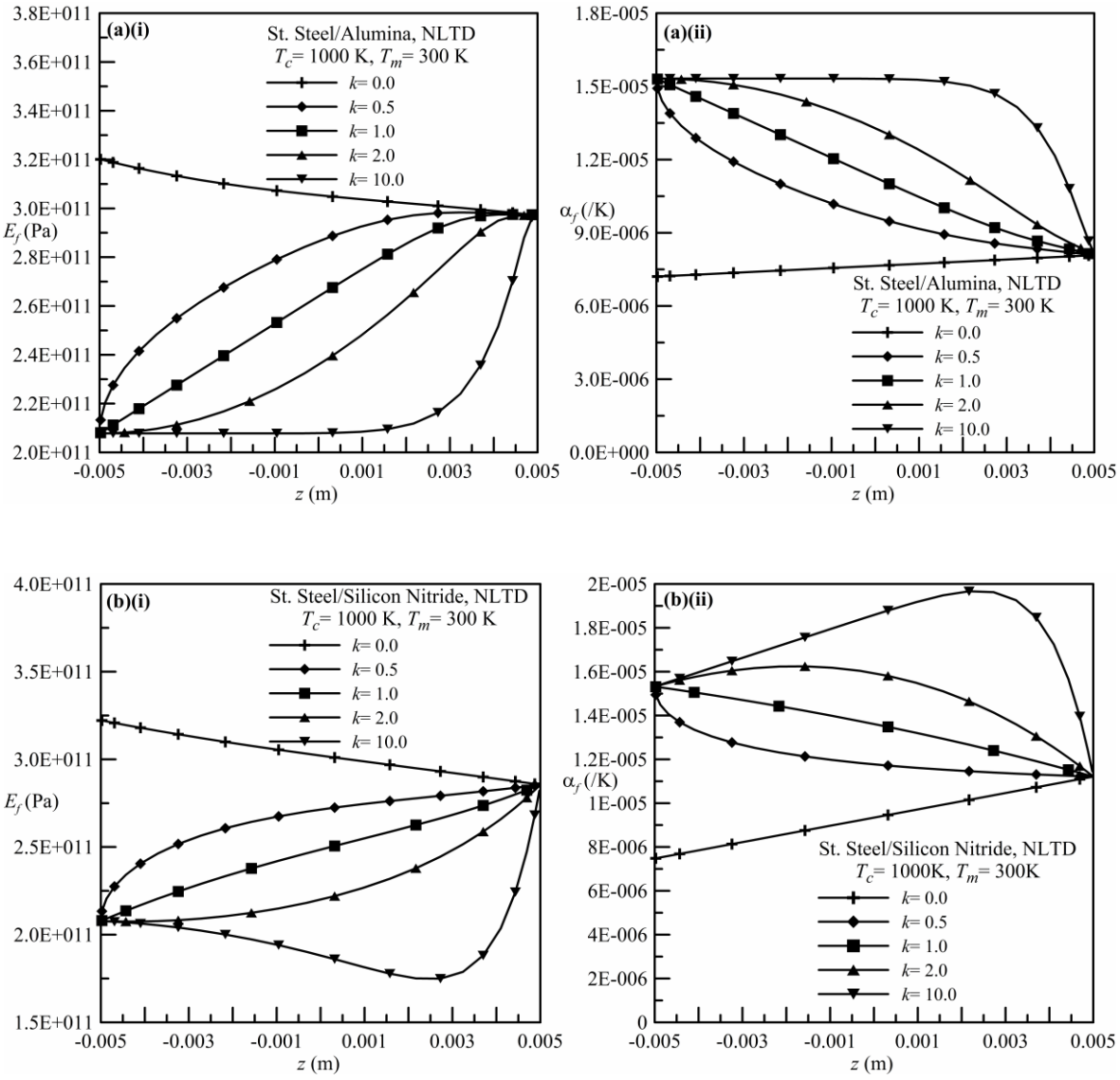

Figure 5.1: Variation of (i) effective elastic modulus and (ii) effective thermal expansion coefficient along the thickness direction for T_c =1000K for NLTD: (a) Stainless Steel/Alumina, (b) Stainless Steel/Silicon Nitride and (c) Stainless Steel/Zirconia.

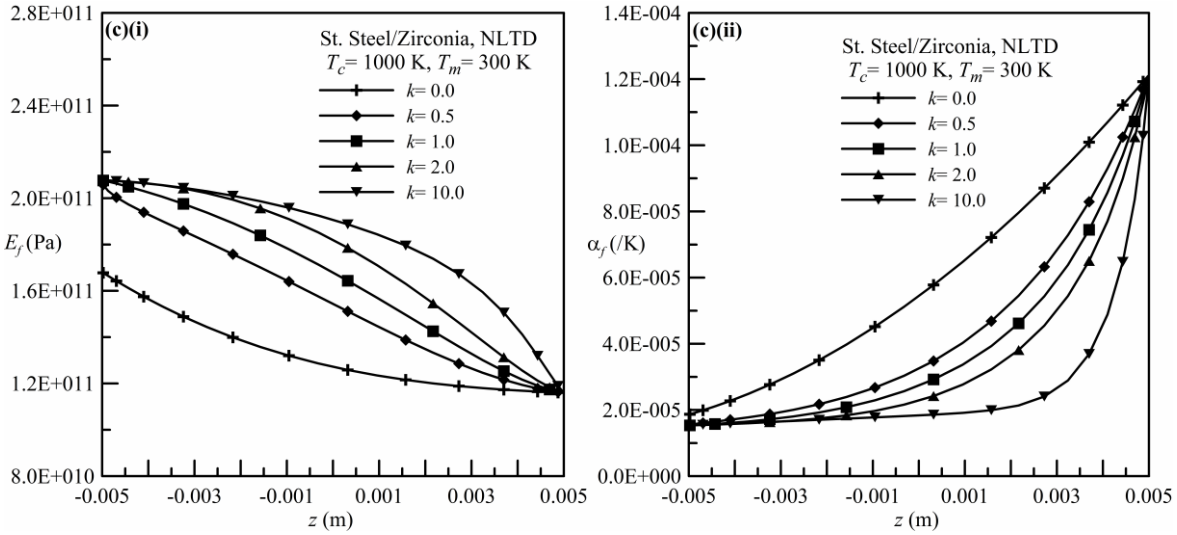

Figure 5.1: Continued.

The present problem is strongly dependent on the variation of effective elastic modulus and effective thermal expansion coefficient with temperature as these are considered to be dependent on temperature. For NLTD, the temperature profile is governed by the steady-state heat conduction equation, leading to a non-linear temperature distribution through the beam thickness. Hence the variation of through-thickness material properties for any specific thermal load $\left(T_c - T_m\right)$ strongly governs the present problem. For illustration purpose, Figure 5.1, showing the variation of through-thickness material properties, is presented for $\left(T_c - T_m\right)$=700K for the three FGMs considered.

5.2. Limit Thermal Load

The aim of this work is to determine the thermal buckling load for different combinations of L/h and k values for different FGMs. But it could not be obtained for certain parameters as the effective elastic modulus (E_f) becomes very low at high values of thermal load $\left(T_c - T_m\right)$. For the range of L/h and k values considered, this is encountered for Stainless Steel/Alumina beams. The thermal load for which E_f theoretically becomes zero is defined as limit thermal load $\left(T_c - T_m\right)_{limit}$ in dimensional form. Figure 5.2 shows the variations of limit thermal loads with volume fraction index for different FGMs. It is seen

that $(T_c - T_m)_{limit}$, while remaining constant initially, decreases with k for Stainless Steel/Silicon Nitride and Stainless Steel/Zirconia beams. On the other hand, it increases with k for Stainless Steel/Alumina beams. The limit thermal loads are found to be almost same for Stainless Steel/Silicon Nitride and Stainless Steel/Zirconia beams for moderate to high values of k. Although the dimensional value of limit thermal load is independent of the L/h ratio, its non-dimensional form varies with L/h.

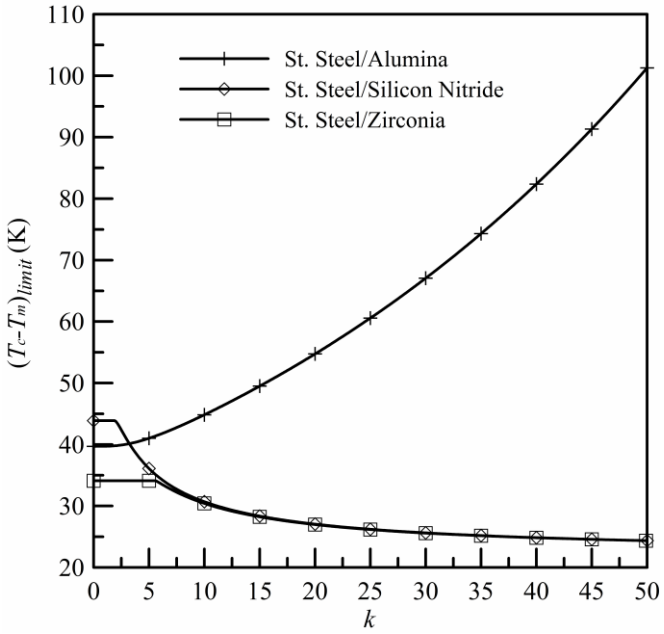

Figure 5.2: Limit thermal load vs. volume fraction index plots.

5.3. Validation Study

The validation of the present problem is carried out with ANSYS (version 10.0) and the validation plot is shown in Figure 5.3. It represents the comparison in the form of k vs. λ plots. The validation is obtained for Stainless Steel-Zirconia FGM beam for length-thickness ratio of 100. The finite element model in ANSYS is created using SHELL91 elements with layered variation of material properties across the thickness. The plots presented in Figure 5.3 match very well with each other and hence validates the present model.

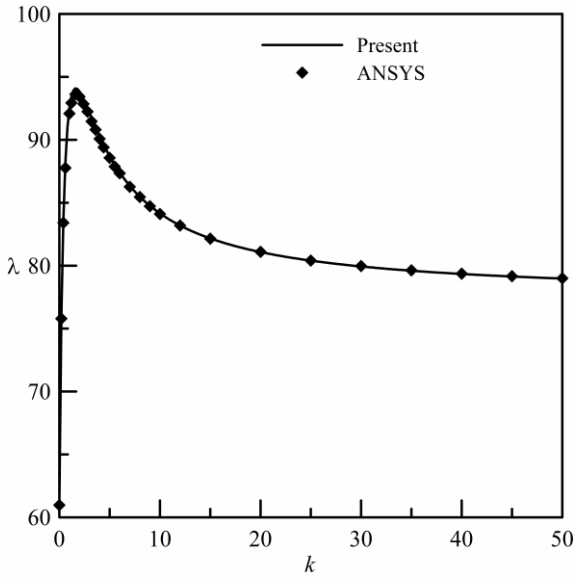

Figure 5.3: Validation plot showing variation of non-dimensional thermal buckling load (λ) with volume fraction index (k) for CC Stainless Steel/Zirconia beam for L/h=100 with NLTD.

5.4. Comparative Plots For Different Length-Thickness Ratios

The variation of non-dimensional thermal buckling load λ with volume fraction index k is presented in Figure 5.4a-c for CC, SS and CS boundary conditions respectively for Stainless Steel/Alumina beam. Similar plots are presented in Figure 5.5a-c for Stainless Steel/Silicon Nitride beam and in Figure 5.6a-c for Stainless Steel/Zirconia beam. In each of the figures, plots are presented for L/h=25, 40, 50, 75, 100, 150.

It is seen from Figure 5.4 that the non-dimensional thermal buckling load increases with an increase in the volume fraction index. The thermal buckling load is obtained up to certain values of k and this true for all the boundary conditions considered. This is due to the fact that, the limit thermal load is reached beyond a certain value of k before the beam buckling occurs. The value of k beyond which the thermal buckling load is not available is highest for SS beam and least for CC beam. Again the value of k beyond which the thermal buckling load is not available due to limit thermal load increases with increasing values of L/h. For any boundary condition and a specific value of k, the non-dimensional thermal buckling load is almost independent of the L/h ratio.

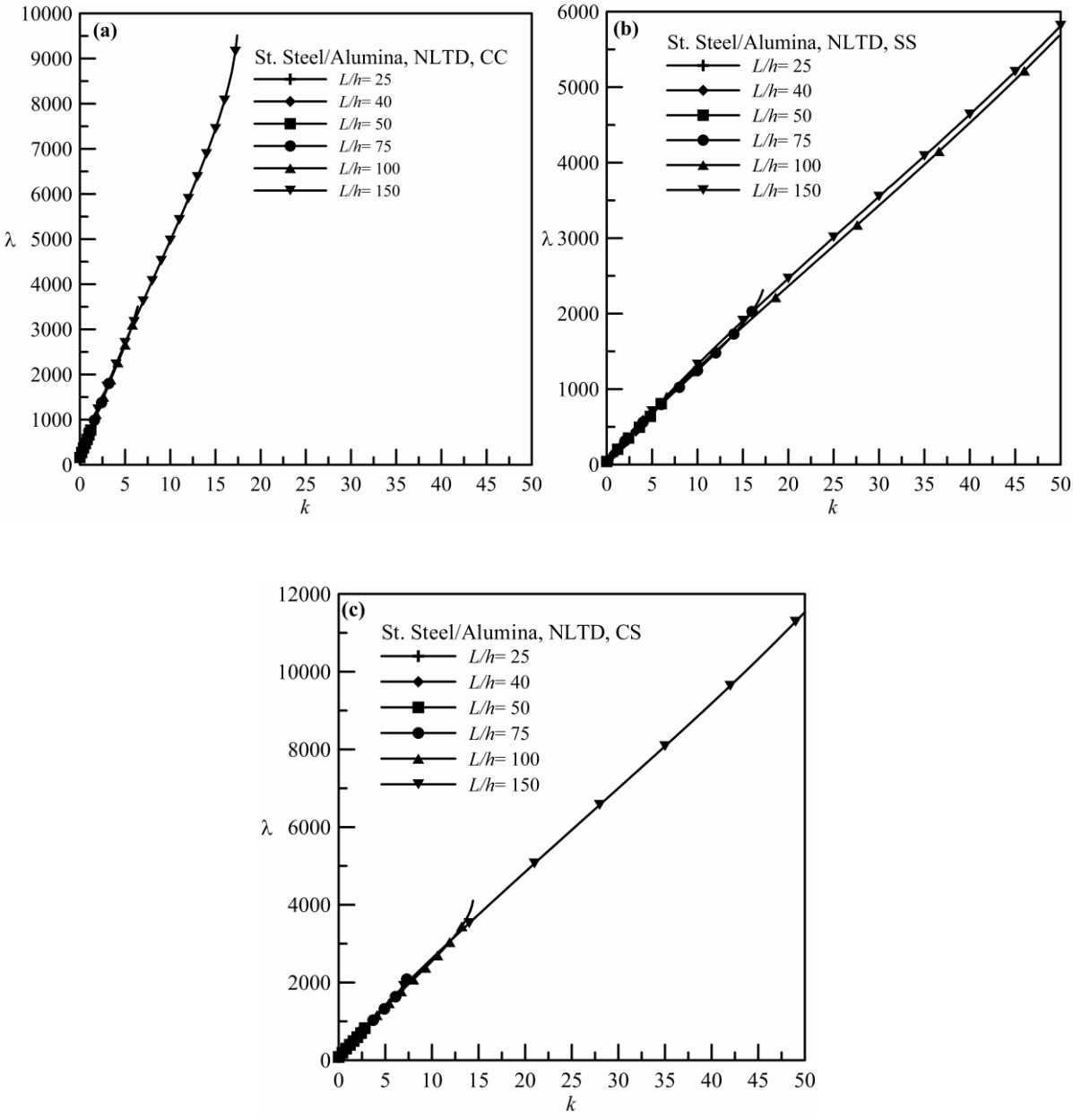

Figure 5.4: Variation of non-dimensional thermal buckling load (λ) with volume fraction index (k) for different length-thickness ratios of Stainless Steel/Alumina beams for NLTD: (a) CC, (b) SS and (c) CS.

It is observed from Figure 5.5 that the non-dimensional thermal buckling load decreases with an increase in the volume fraction index. The decrease is sharp for low values of the volume fraction index. Beyond that, the decreasing nature is gradual up to k=50. Moreover, with an increase in the length-thickness ratio, the non-dimensional thermal buckling load is found to be increasing for any value of the volume fraction index. The natures of the plots are quite similar irrespective of the boundary conditions and length-thickness ratios. It is also seen that for the same volume fraction index, the non-dimensional thermal buckling load is maximum for clamped-clamped beam, followed by clamped-simply supported beam and minimum for simply supported-simply supported beam.

It is seen from Figure 5.6 that the nature of the plots are entirely different from the other FGMs considered. Here, for Stainless Steel/Zirconia beam, it is found that the non-dimensional thermal buckling load increases initially sharply for low values of k. Then it decreases with k initially sharply and then gradually becomes independent of k. This trend is true for all the L/h values considered except for L/h=25 of CC and CS beams. For these cases, λ increases with k and, this increase in initially sharp and then gradual till k reaches the value of 50. It is also observed that the non-dimensional thermal buckling load increases with increase in the L/h value for any specific value of k.

5.5. Comparative Plots For Different Materials

The variation of non-dimensional thermal buckling load λ with volume fraction index k for three different FGMs are presented in Figure 5.7a-c for CC, SS and CS beam respectively having L/h=25. Similar plots for L/h=50, 75, 100, 150 are presented in Figures 5.8-5.11 respectively. The relative difference in non-dimensional thermal buckling load values between Stainless Steel/Alumina and the other two FGMs is significant. This effect becomes more pronounced for higher L/h ratios. Due to this, it becomes difficult to accommodate the λ vs. k plots in a single figure for all the three FGMs. So Figures 5.8-5.11 are presented with two different scales for the vertical axis representing thermal buckling load. The variation λ with k has been discussed in the previous section for different FGMs. The non-dimensional thermal buckling loads are not available beyond certain value of k due to limit thermal load for Stainless Steel/Alumina and this becomes more pronounced with decreasing L/h. Hence the plots showing variation of λ with k is

not clearly visible for L/h=25, as shown in Figure 5.7a. Comparisons among three FGMs reveal that the non-dimensional thermal buckling load for Stainless Steel/Alumina beam is much higher compared to the other two FGM beams. This is true for all the L/h values and boundary conditions considered. It is also seen that Stainless Steel/Zirconia beam exhibits lowest buckling load.

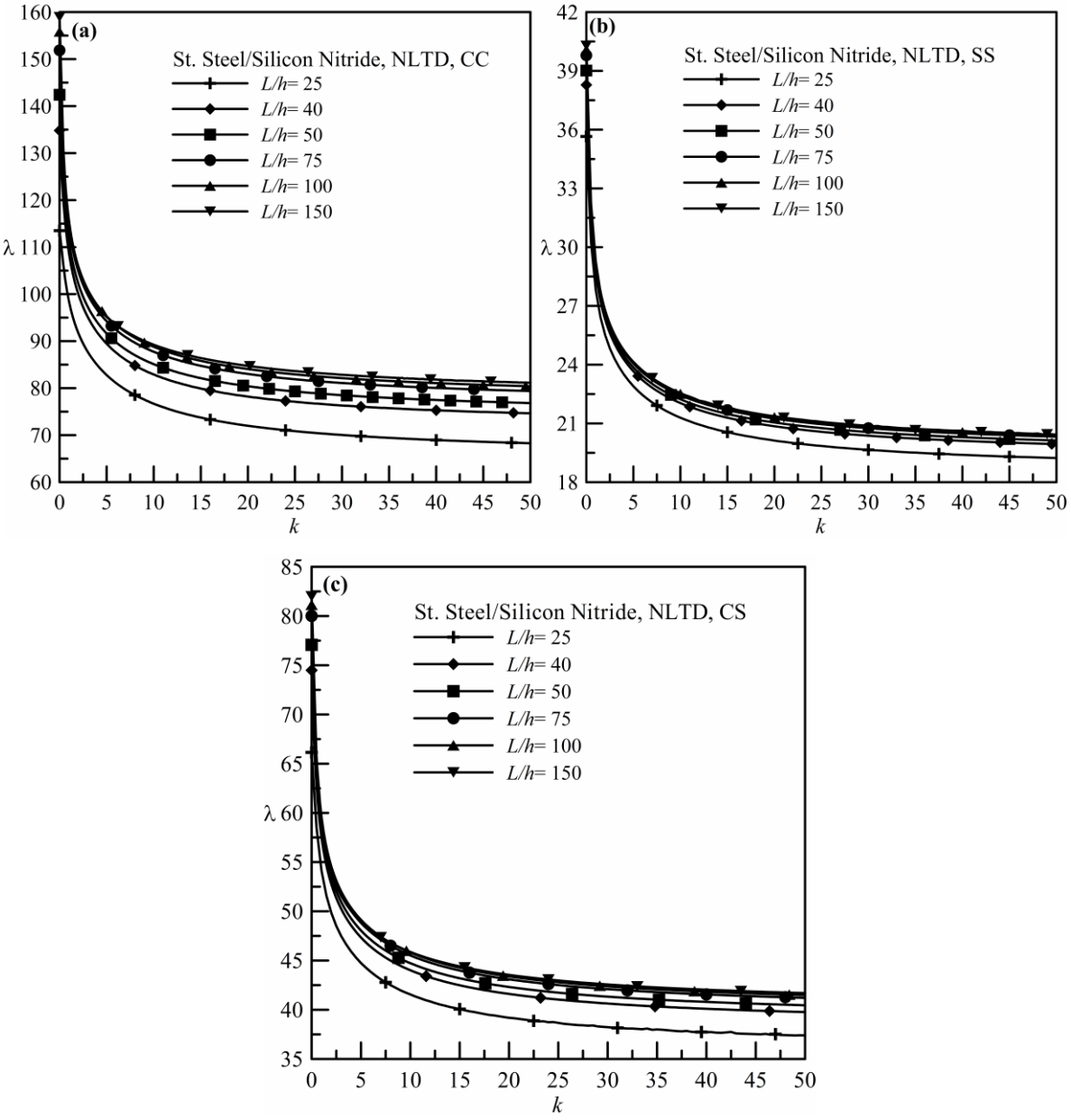

Figure 5.5: Variation of non-dimensional thermal buckling load (λ) with volume fraction index (k) for different length-thickness ratios of Stainless Steel/Silicon Nitride beams for NLTD: (a) CC, (b) SS and (c) CS.

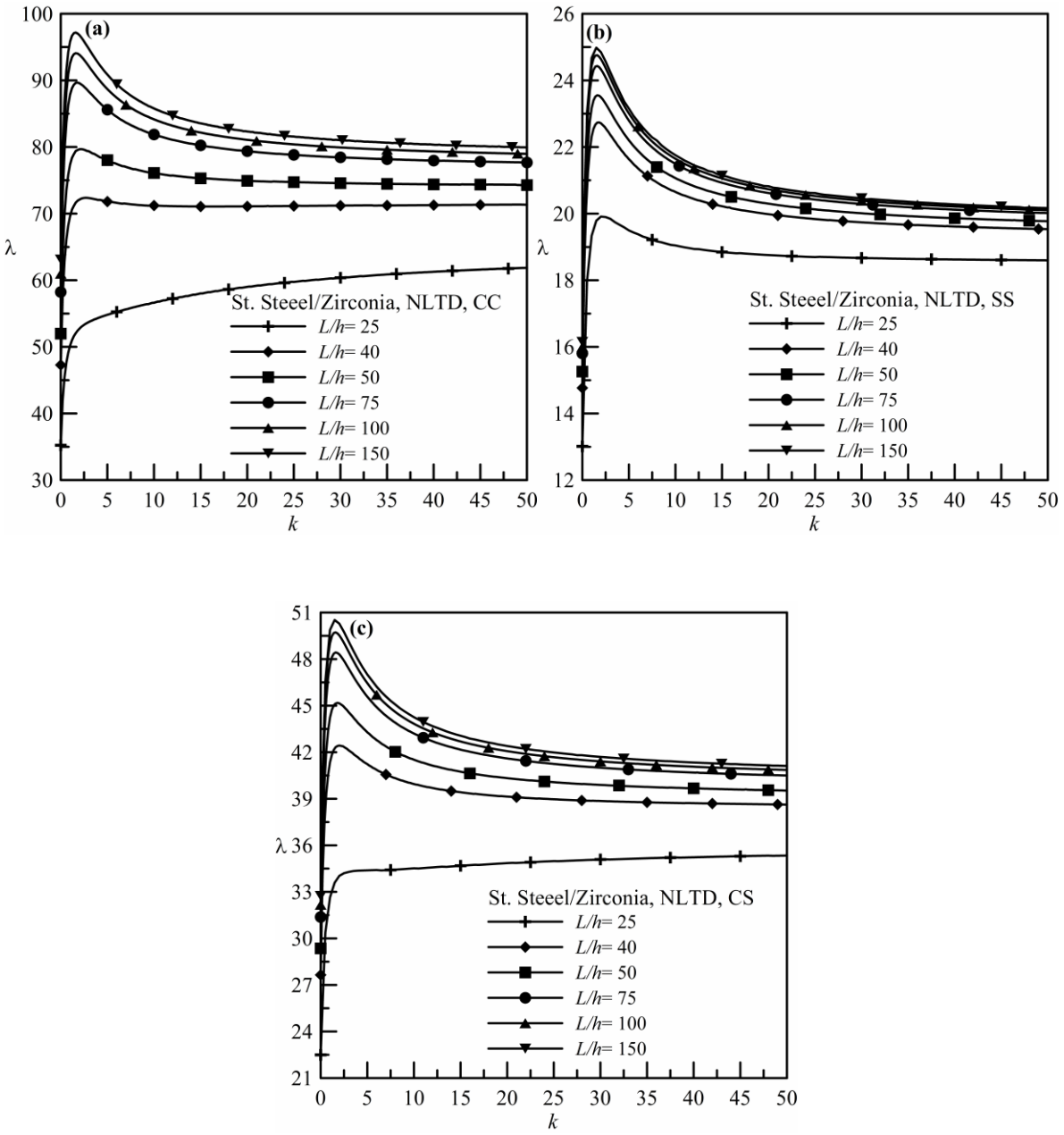

Figure 5.6: Variation of non-dimensional thermal buckling load (λ) with volume fraction index (k) for different length-thickness ratios of Stainless Steel/Zirconia beams for NLTD: (a) CC, (b) SS and (c) CS.

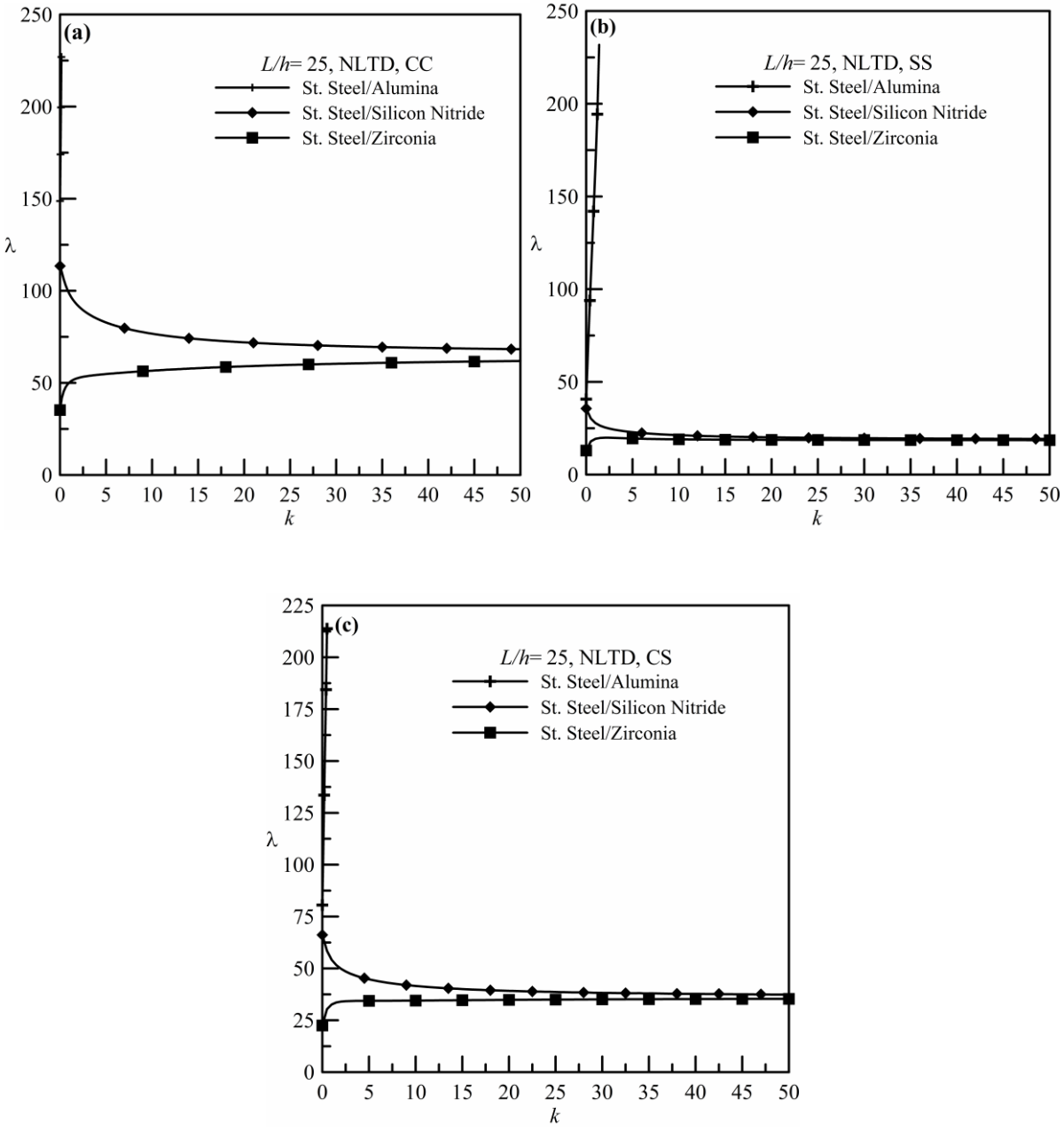

Figure 5.7: Variation of non-dimensional thermal buckling load (λ) with volume fraction index (k) for different FGM compositions having L/h=25 for NLTD: (a) CC, (b) SS and (c) CS.

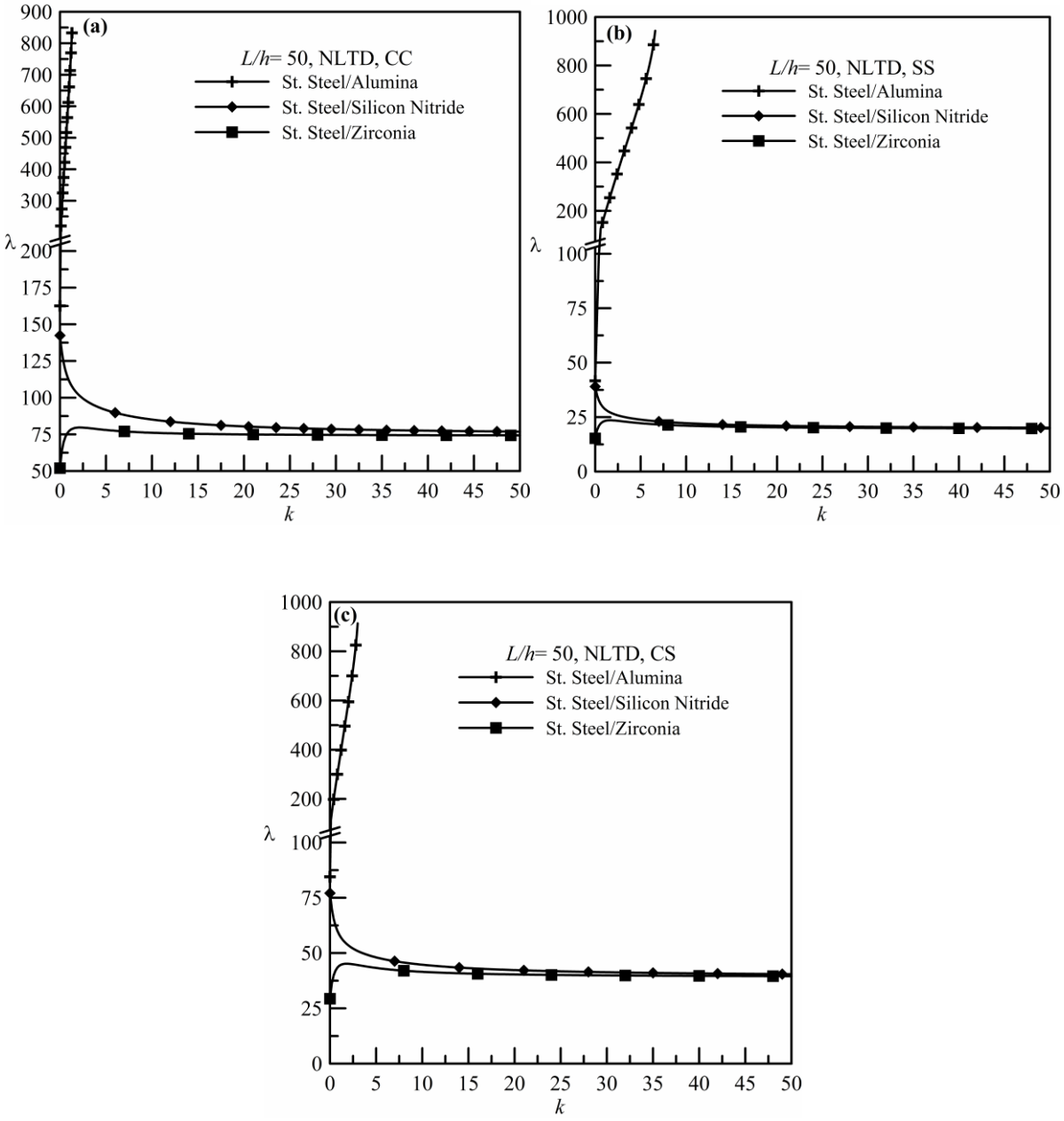

Figure 5.8: Variation of non-dimensional thermal buckling load (λ) with volume fraction index (k) for different FGM compositions having L/h=50 for NLTD: (a) CC, (b) SS and (c) CS.

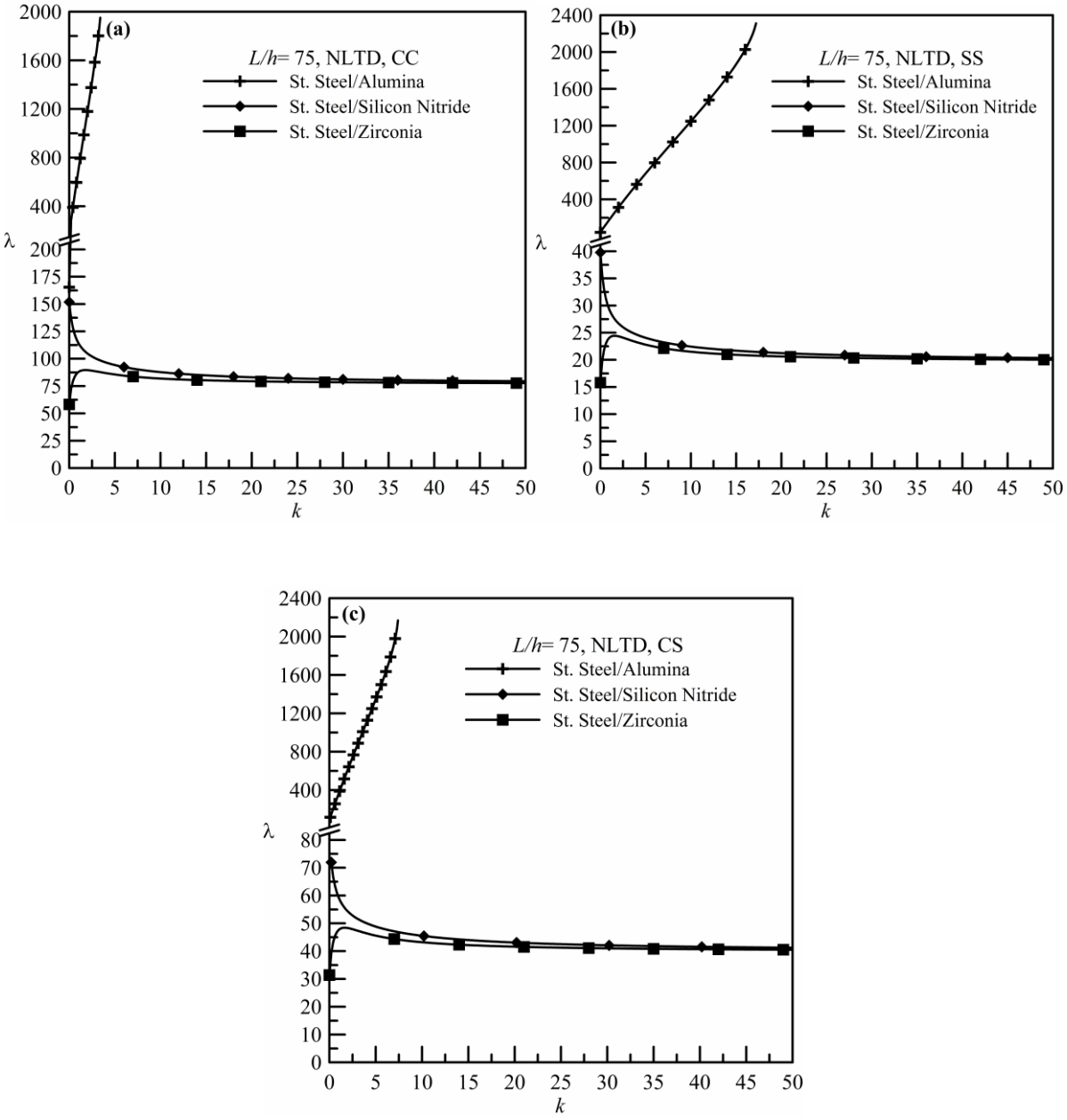

Figure 5.9: Variation of non-dimensional thermal buckling load (λ) with volume fraction index (k) for different FGM compositions having L/h=75 for NLTD: (a) CC, (b) SS and (c) CS.

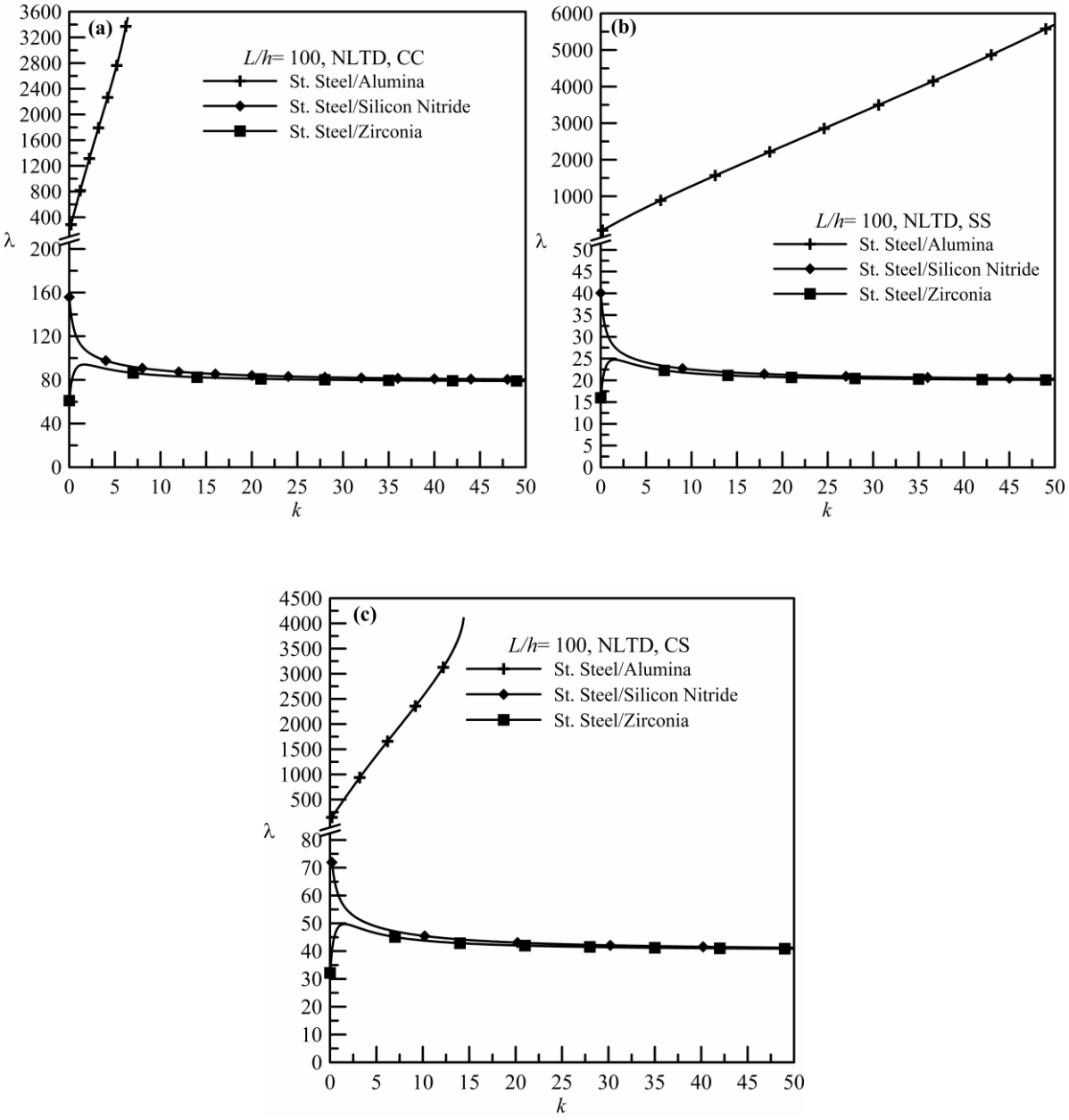

Figure 5.10: Variation of non-dimensional thermal buckling load (λ) with volume fraction index (k) for different FGM compositions having L/h=100 for NLTD: (a) CC, (b) SS and (c) CS.

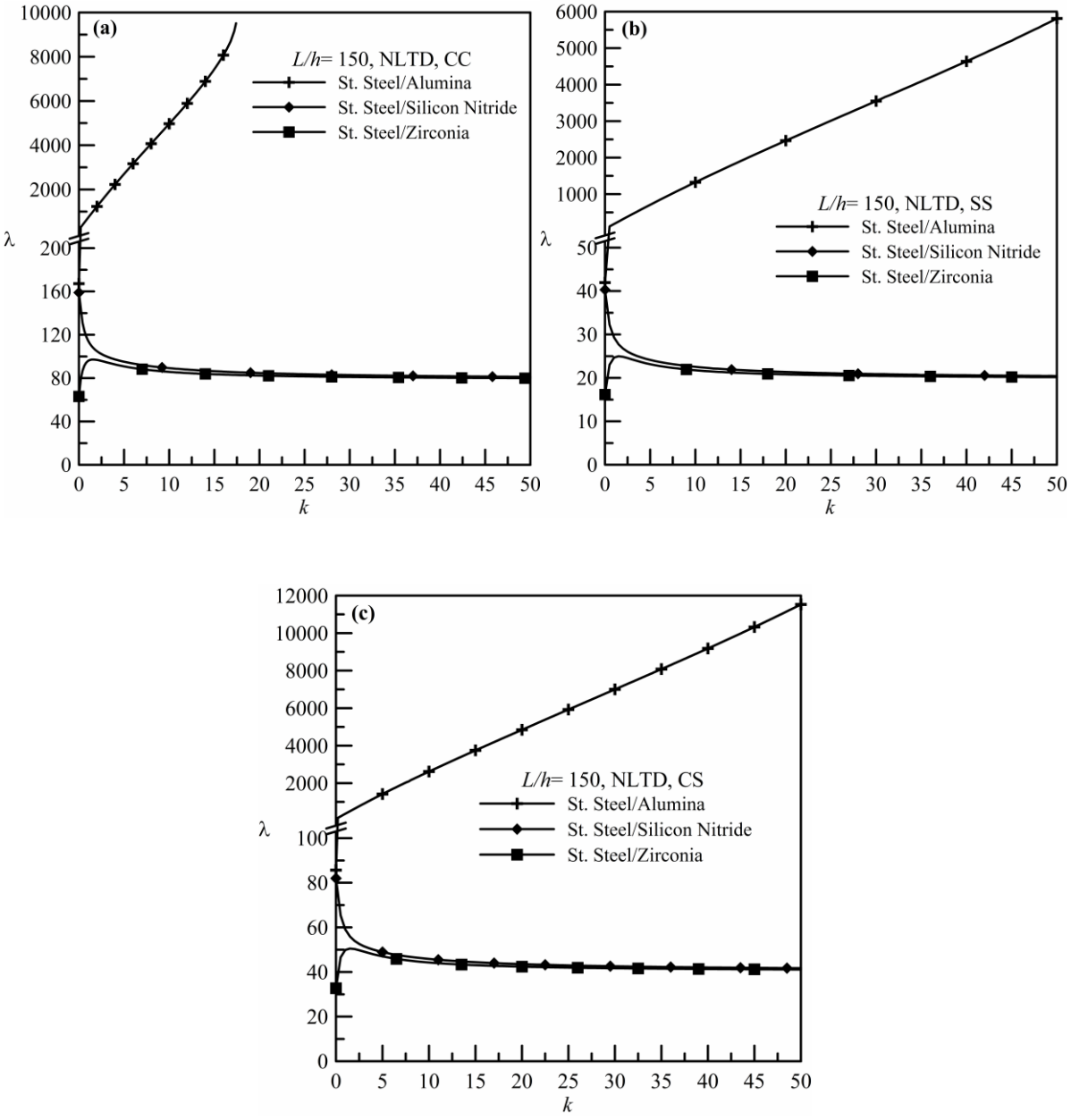

Figure 5.11: Variation of non-dimensional thermal buckling load (λ) with volume fraction index (k) for different FGM compositions having L/h=150 for NLTD: (a) CC, (b) SS and (c) CS.

Chapter 6

DETERMINATION OF CRITICAL BUCKLING LOAD OF UNIFORMLY TAPERED FGM BEAMS

6.1. Introduction

Tapered beams are often found in many industrial applications eg., aerospace structures, civil structures, mechanical structures etc. With the increasing application of functionally graded materials, tapered FGM beams are considered as useful structural components. Hence, the knowledge of critical buckling load of the tapered FGM beam is important for the engineering designers and analysts. Various researchers have started working on mechanical behavior of tapered FGM beams over the last few years. The literature survey on this has already been presented in section 1.2.3.

6.2. Problem Description

As shown in Figure 6.1, a beam with length L, width b, left end thickness h_1 and right end thickness h_2 is considered where $h_1 > h_2$. Here, a beam with uniformly varying thickness and constant width is considered. In the present problem, x and z are the coordinate axes along the length and thickness directions respectively, and u and w are the displacement fields along x and z directions respectively. The beam thickness at any axial location is given by, $h(x) = h_1\{1 - n(x/L)\}$, where $n = (1 - h_2/h_1)$ is defined as the taperness parameter. The taperness parameter n=0 corresponds to a uniform beam.

It is considered that the beam is axially restrained at the left end (x=0) and is free axially at the right end (x=L). When the beam is subjected to a load F at the right end, it is subjected to instability or buckling, when F reaches the critical value F_{cr}. In the present work, the critical buckling load is determined for different boundary conditions. At critical

condition, the beam attains equilibrium at a bent configuration when subjected to a small transverse disturbance. Hence the governing equations of equilibrium are formulated at the bent configuration.

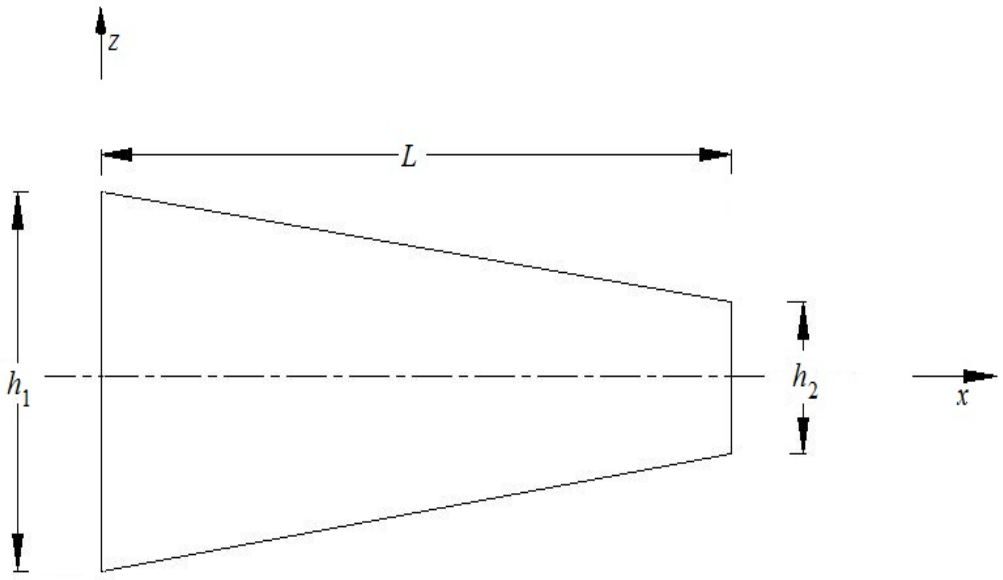

Figure 6.1: A tapered FGM Beam with dimensions and coordinate axes.

Three different classical boundary conditions are considered: (i) beam with both ends clamped (CC), (ii) beam with both ends simply supported (SS) and, (iii) beam with one end clamped and the other end simply supported (CS). Analysis of critical buckling load is carried out for two different FGMs namely, Stainless Steel (SUS304)/Zirconia (ZrO_2) and Titanium alloy (Ti-6Al-4V)/Zirconia.

The theoretical formulation is based on Euler-Bernoulli beam theory. Minimum potential energy principle in variational form is employed to deduce the governing equation in terms of the displacement fields. The governing equation is an eigenvalue problem for which the lowest eigenvalue gives the critical buckling load. The solution of the governing equation is obtained by approximating the displacement fields using the Ritz method.

6.3. Mathematical Formulation

The FGM beam is modeled using simple mixture of metal and ceramic constituents in accordance with power law variation of volume fraction, which for ceramic and metal constituents at any layer z is given by, $V_c = \left(\frac{z}{h(x)} + \frac{1}{2}\right)^k$ and. $V_m = 1 - V_c = 1 - \left(\frac{z}{h(x)} + \frac{1}{2}\right)^k$.

Here V_c and V_m are the volume fraction of ceramic and metal constituents respectively, and k $(0 \le k \le \infty)$ is the volume fraction index that controls the material gradation profile along the thickness direction. The effective elastic modulus E_f is calculated using the following relation: $E_f = E_m + \left(\frac{z}{h(x)} + \frac{1}{2}\right)^k (E_c - E_m)$ (6.1)

where, E_c and E_m are the elastic moduli for the ceramic and metal constituents respectively. Linear elastic stress-strain relation is used in the present formulation.

The governing equation is derived using the principle of minimum total potential energy given by equation (1.4). It is given by, $\delta(U+V) = 0$. The expression of axial strain is given by equation (2.8) and is as follows: $\varepsilon_x = \frac{du}{dx} - z\frac{d^2w}{dx^2}$. The strain energy of the tapered FGM beam is derived as follows:

$$U = \frac{1}{2}\int \sigma\varepsilon_x dv$$

$$= \frac{1}{2}\int E_f \varepsilon_x^2 dv \qquad \text{(assuming linear elastic stress-strain material behavior)}$$

$$= \frac{1}{2}\int_0^L \int_{-h(x)/2}^{h(x)/2} E_f \left(\frac{du}{dx} - z\frac{d^2w}{dx^2}\right)^2 b dz dx$$

$$= \frac{1}{2}\int_0^L \int_{-h(x)/2}^{h(x)/2} E_f \left\{\left(\frac{du}{dx}\right)^2 - 2z\left(\frac{d^2w}{dx^2}\right)\left(\frac{du}{dx}\right) + z^2\left(\frac{d^2w}{dx^2}\right)^2\right\} b dz dx$$

$$= \frac{1}{2}\int_0^L A_1\left(\frac{du}{dx}\right)^2 dx - \int_0^L A_2\left(\frac{d^2w}{dx^2}\right)\left(\frac{du}{dx}\right)dx + \frac{1}{2}\int_0^L A_3\left(\frac{d^2w}{dx^2}\right)^2 dx, \qquad (6.2)$$

Table 6.1: List of functions for different boundary conditions.

Type of Boundary	Boundary Conditions	Function
CC	$u\|_{x=0}=0, u\|_{x=L}\neq 0$	$\phi_1(x)=\left(\frac{x}{L}\right)$
	$w\|_{x=0}=0, w\|_{x=L}=0,$ $\left.\frac{dw}{dx}\right\|_{x=0}=0, \left.\frac{dw}{dx}\right\|_{x=L}=0$	$\beta_1=\left(\frac{x}{L}\right)^2\left\{1-2\left(\frac{x}{L}\right)+\left(\frac{x}{L}\right)^2\right\}$
SS	$u\|_{x=0}=0, u\|_{x=L}\neq 0$	$\phi_1(x)=\left(\frac{x}{L}\right)$
	$w\|_{x=0}=0, w\|_{x=L}=0,$ $\left.\frac{dw}{dx}\right\|_{x=0}\neq 0, \left.\frac{dw}{dx}\right\|_{x=L}\neq 0$	$\beta_1=\sin\left(\frac{\pi x}{L}\right)$
CS	$u\|_{x=0}=0, u\|_{x=L}\neq 0$	$\phi_1(x)=\left(\frac{x}{L}\right)$
	$w\|_{x=0}=0, w\|_{x=L}=0,$ $\left.\frac{dw}{dx}\right\|_{x=0}=0, \left.\frac{dw}{dx}\right\|_{x=L}\neq 0$	$\beta_1=\left(\frac{x}{L}\right)^2\left\{3-5\left(\frac{x}{L}\right)+2\left(\frac{x}{L}\right)^2\right\}$

where, the stiffness coefficients $A_1(x)$, $A_2(x)$ and $A_3(x)$ are defined below:

$$A_1(x)=b\int_{-\frac{h(x)}{2}}^{+\frac{h(x)}{2}} E_f\,dz,\ A_2(x)=b\int_{-\frac{h(x)}{2}}^{+\frac{h(x)}{2}} E_f z\,dz \text{ and } A_3(x)=b\int_{-\frac{h(x)}{2}}^{+\frac{h(x)}{2}} E_f z^2 dz. \tag{6.3}$$

The potential energy V due to applied load F is given as follows:

$$V = -\left[\frac{F}{2} \int_0^L \left(\frac{du}{dx} \right)^2 dx + \frac{F}{2} \int_0^L \left(\frac{dw}{dx} \right)^2 dx \right]. \tag{6.4}$$

The displacement fields are approximated as linear combinations of admissible functions and unknown coefficients. According to Ritz method, the displacement fields are assumed to be of the form of equation (2.13a) and (2.13b) i.e. $u = \sum_{i=1}^{nu} c_i \phi_i$ and $w = \sum_{i=1}^{nw} c_{nu+i} \beta_i$. Here, ϕ_i and β_i are the set of orthogonal admissible functions of the field variables u and w; nu and nw are the number of the functions for u and w respectively. The set of orthogonal functions ϕ_i and β_i are generated numerically from the lowest order admissible functions using Gram-Schmidt orthogonalization scheme. The list of lowest order orthogonal functions for u and w is given in Table 6.1.

Using the assumed displacement fields and applying the minimum potential energy principle, the governing equation for finding the critical buckling load F_{cr} is given by,

$$\left[K_{ji} \right] \{ c_i \} - \left[K_{ji}^s \right] \{ c_i \} = 0, \tag{6.5}$$

where, $\left[K_{ji} \right]$ and $\left[K_{ji}^s \right]$ are the structural stiffness matrix and stress stiffness matrix respectively. Equation (6.5) is an eigenvalue problem for which the lowest eigenvalue gives the critical buckling load F_{cr} . The non-zero elements of the stiffness matrices are given below:

$$\left[K_{ji} \right]_{\substack{j=1,nu \\ i=1,nu}} = \int_0^L A_1 \frac{d\phi_j}{dx} \frac{d\phi_i}{dx} dx,$$

$$\left[K_{ji} \right]_{\substack{j=1,nu \\ i=nu+1,nw+nu}} = -\int_0^L A_2 \frac{d\phi_j}{dx} \frac{d^2\beta_{i-nu}}{dx^2} dx,$$

$$\left[K_{ji} \right]_{\substack{j=nu+1,nw+nu \\ i=1,nw}} = -\int_0^L A_2 \frac{d\phi_{j-nu}}{dx} \frac{d^2\beta_i}{dx^2} dx,$$

$$\left[K_{ji} \right]_{\substack{j=nu+1,nu+nw \\ i=nu+1,nu+nw}} = \int_0^L A_3 \frac{d^2\beta_{j-nu}}{dx^2} \frac{d^2\beta_{i-nu}}{dx^2} dx,$$

$$\left[K_{ji}^{s}\right]_{\substack{j=1,nu \\ i=1,nu}} = F\int_{0}^{L}\frac{d\phi_j}{dx}\frac{d\phi_i}{dx}dx,$$

$$\left[K_{ji}^{s}\right]_{\substack{j=nw+1,nw+nu \\ i=nw+1,nw+nu}} = F\int_{0}^{L}\frac{d\beta_{j-nu}}{dx}\frac{d\beta_{i-nu}}{dx}dx.$$

6.4. Results and Discussion

The results are generated for h_1=0.01 m, b=0.02 m, $L/h_1 = 75$ and for the following values of elastic modulus of the FGM constituents: 208 GPa for Stainless Steel, 106 GPa for Titanium alloy and 168 GPa for Zirconia. The results are presented graphically in the form of non-dimensional buckling load vs. volume fraction index plots. The non-dimensional buckling load λ is defined as $\lambda = F_{cr}L^2/(E_m I_1)$, where, $I_1 = bh_1^3/12$, the moment of inertia at the left end and E_m is the effective elastic modulus of the corresponding metallic constituent.

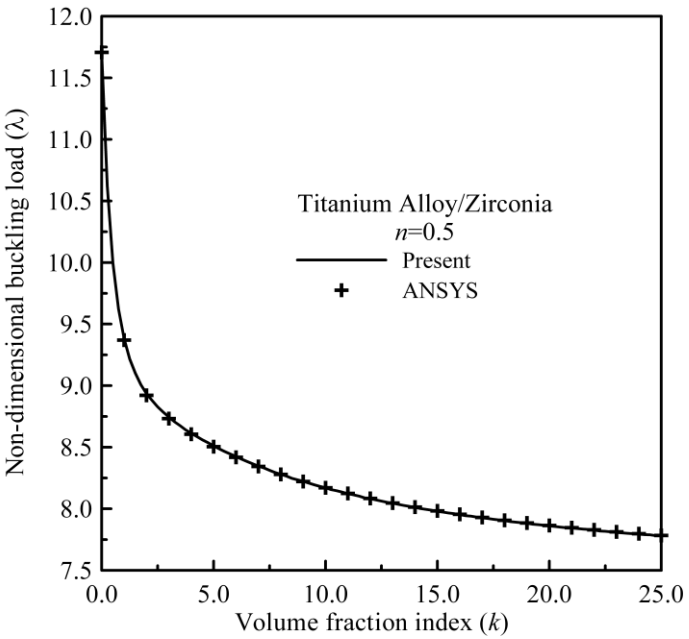

Figure 6.2: Validation plot with ANSYS.

6.4.1. Validation study

A comparative plot with finite element package ANSYS (version 10.0) showing variation of non-dimensional buckling load λ with volume fraction index n is presented in Figure 6.2 for n=0.5 for Titanium alloy/Zirconia beam. It shows very good agreement of the present result with ANSYS. The finite element model in ANSYS is built using SHELL91 elements with layered variation of material properties.

6.4.2. Comparative plots for different volume fraction indices

Figure 6.3a-c presents the non-dimensional buckling load(λ) vs. taperness parameter(n) plots for Stainless Steel/Zirconia beam under different boundary conditions. In each of the figures, the plots are shown for different volume fraction indices, including pure ceramic and pure metal beams. A wide range of taperness parameters including a uniform beam $(n=0)$ are considered. Similar plots for Titanium alloy/Zirconia beam are shown in Figure 6.4a-c. It is shown from the figures that the buckling load decreases with increase in taperness parameter. For Stainless Steel/Zirconia, it is found that for any fixed taperness ratio, the non-dimensional buckling load is lowest for the purely ceramic beam. Then increases gradually with a rise in volume fraction indices and becomes maximum for fully metallic beam. This is due to the fact that, for Stainless Steel/Zirconia beam, the elastic modulus value which is responsible for critical buckling is greater for metal than ceramic. The trend is completely reversing for Titanium alloy/Zirconia, i.e., for any fixed taperness ratio, the non-dimensional buckling load is lowest for purely metallic beam. Then it increases gradually with a rise in the volume fraction index and becomes maximum for fully ceramic beam. This is due to the fact that, for Titanium alloy/Zirconia beam, the elastic modulus value which contributes to the buckling load is greater for ceramic than metal.

Figures 6.3 and 6.4 also show that that the non-dimensional buckling load λ is almost invariant with the volume fraction index k for higher taperness parameters. It means the effect of material profile parameter k becomes insignificant with more thickness reductions between the beam ends. As expected, the CC beam corresponds to the highest critical buckling load and the SS beam exhibits the lowest buckling load.

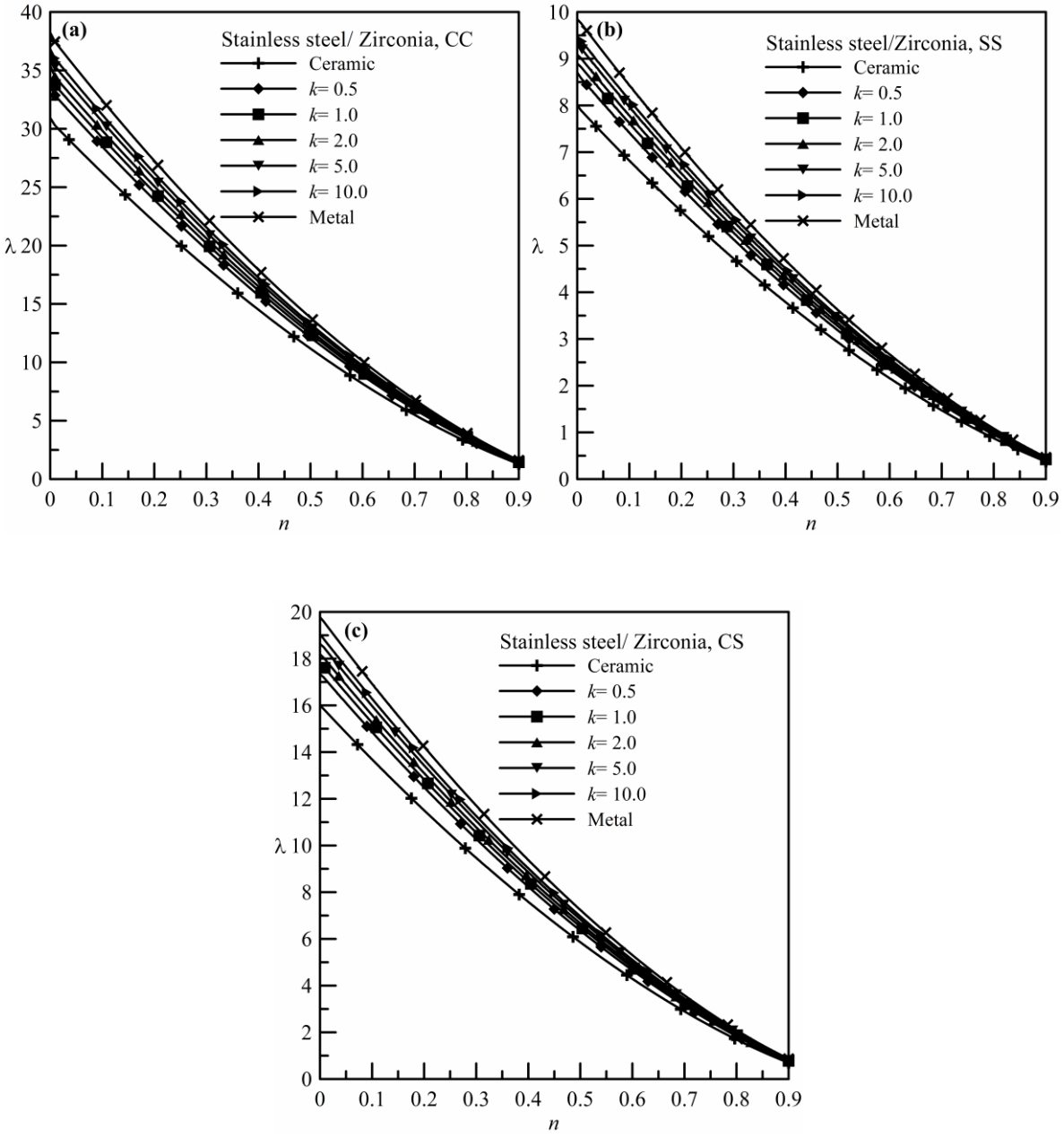

Figure 6.3: Non-dimensional buckling load vs. taperness parameter plots for different volume fraction indices of Stainless Steel/Zirconia beam: (a) CC, (b) SS and (c) CS.

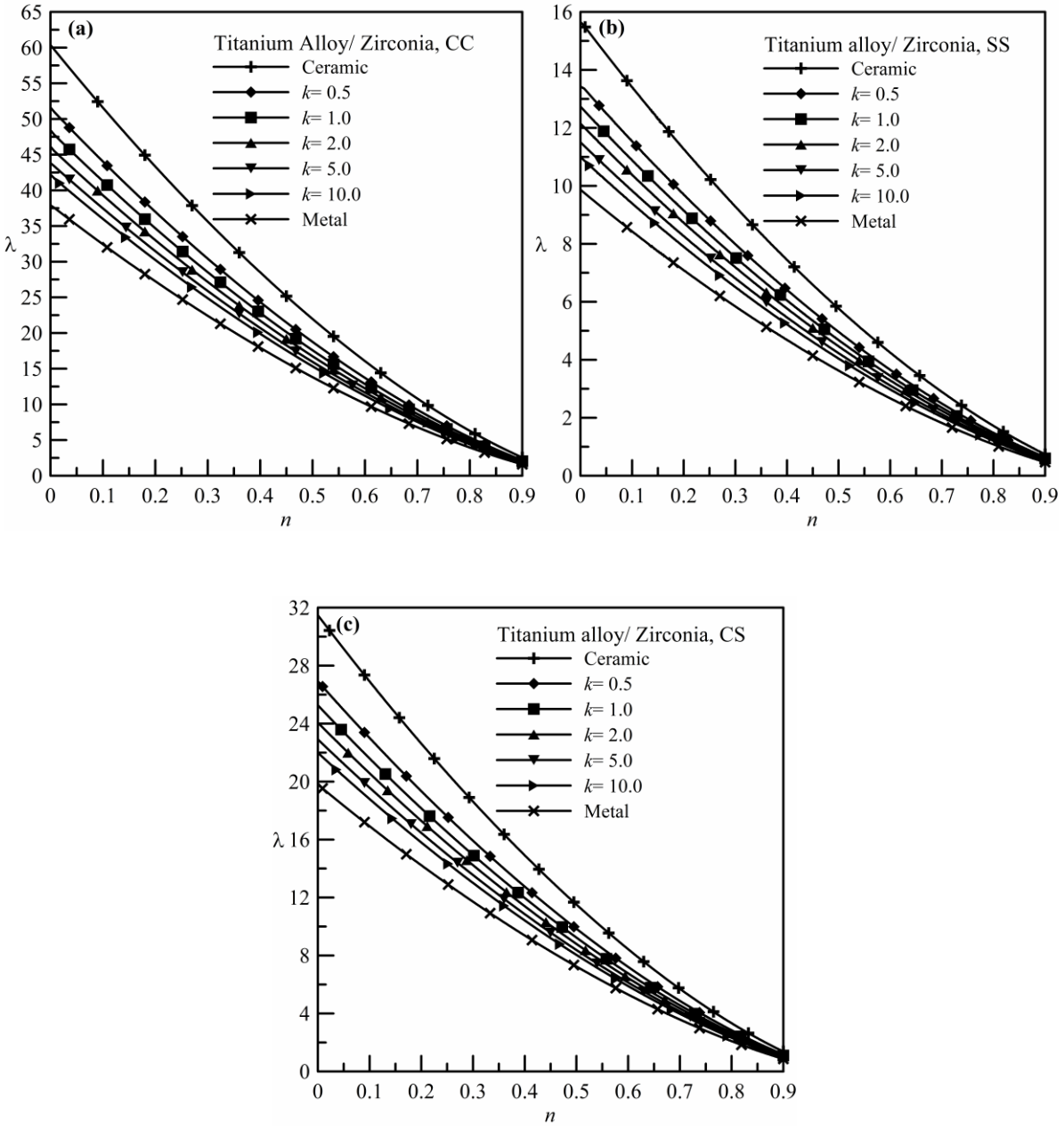

Figure 6.4: Non-dimensional buckling load vs. taperness parameter plots for different volume fraction indices of Titanium alloy/Zirconia beam: (a) CC, (b) SS and (c) CS.

.

Chapter 7

CONCLUSIONS

7.1. Conclusions

In the present work, the critical buckling load of FGM beam is analyzed. The critical buckling load is very much important for predicting the stability of any structures. It is an axial compressive load at which a beam is buckled or collapsed due to the loss of its configuration. So the study of critical buckling load is important for engineering design.

Two types of analyses are reported in the present thesis work: (i) Thermal buckling load of uniform FGM beams, and (ii) Critical buckling load of uniformly tapered FGM beams. The FGM is modeled using a simple rule of mixture of the metal and ceramic constituents using power-law variation of the volume fraction. The bottom layer is considered as fully metallic and the top layer is considered as fully ceramic. A mathematical formulation involving the principle of minimum total potential energy is reported. Ritz method is applied to solve the governing equations of the respective problems. The problem is formulated as an eigenvalue problem where the lowest eigenvalue gives the critical buckling load.

In the study of thermal buckling load of FGM beam, effective material properties are considered as a function of temperature. A thermal load is applied to the beam by making a temperature difference between the bottom and the top layer. Three different studies are considered: (a) A beam with uniform temperature distribution (UTD) in which the temperature of the beam is raised uniformly, (b) Linearly temperature distribution (LTD) in which the top (pure ceramic) layer is kept at a higher temperature than that of the bottom one (pure metal), and a linear temperature gradient is assumed along the thickness direction in the beam, and (c) Non-linear temperature distribution (NTD), in which the extreme layers are kept at different temperatures, and a non-linear thermal gradient is induced at steady-state heat conduction condition. The study is performed for three different FGM materials,

namely, Stainless Steel/Alumina, Stainless Steel/Silicon Nitride and Stainless Steel/Zirconia. Three different boundary conditions are considered, namely, beam with both ends clamped (CC), beam with both ends simply supported (SS), and beam with one end clamped and the other end simply supported (CS). For each of these cases, a study is carried out to predict the variation of non-dimensional thermal buckling load with the volume fraction index. The graphical results in comparative form are presented for (i) different materials and (ii) different length-thickness ratios.

In the other study, critical buckling load of a uniformly tapered FGM beam is determined, where, a load is applied at the right end of the beam. A beam with uniform width is assumed to be tapered along the length direction, in which the thickness reduces from the left to the right end. The study is carried out for two FGMs, namely, Stainless Steel/Zirconia and Titanium alloy/Zirconia, and for the above-mentioned boundary conditions such as CC, SS and CS. In this study, the variation of non-dimensional buckling load with taperness parameter is shown graphically for different volume fraction indices. Results are reported for tapered beams with up to ninety percent reductions in the end thicknesses.

7.2. Future Scope of Work

The present study can be extended to thermal buckling analysis of other materials such as conventional composites; FGMs involving other constituents etc. The methodologies adopted in the present work are robust and quite general in nature. Hence, it can be used for buckling analysis of any other structural elements, which are used in common engineering applications.

Bibliography

Anandrao KS, Gupta RK, Ramchandran P and Rao GV. 2010, Thermal post-buckling analysis of uniform slender functionally graded material beams, *Structural Engineering Mechanics*, **36**, 545-560.

Aydin K. 2013, Free vibration of functionally graded beams with arbitrary number of surface cracks, *European Journal of Mechanics A/Solids*, **42**, 112-124.

Benatta MA, Mechab I, Tounsi A and Bedia EAA. 2008, Static analysis of functionally graded short beams including warping and shear deformation effects, *Computational Materials Science*, **44**, 765-773.

Bhangale RK and Ganesan N. 2006, Thermo-elastic buckling and vibration behavior of a functionally graded sandwich beam with constrained viscoelastic core, *Journal of Sound and Vibration*, **295**, 294-316.

Bochicchio I and Vuk E. 2010, Buckling and longterm dynamics of a nonlinear model for the extensible beam, *Mathematical and Computer Modelling*, **51**, 833-846.

Cook RD, Malkus DS, Plesha ME and Witt RJ. 2002, *Concepts and Applications of Finite Element Analysis*, Fourth Ed., John Wiley & Sons Inc., USA.

Ebrahimi F and Salari E. 2015, Thermal buckling and free vibration analysis of size dependentTimoshenko FG nanobeams in thermal environments, *Composite Structures*, **128**, 363-380.

Esfahani SE, Kiani Y and Eslami MR. 2013, Non-linear thermal stability analysis of temperature dependent FGM beams supported on non-linear hardening elastic foundations, *International Journal of Mechanical Sciences*, **69**, 10-20.

Esfahani SE, Kiani Y, Komijani M and Eslami MR. 2014, Vibration of a temperature-dependent thermally pre/postbuckled FGM beam over a nonlinear hardening elastic foundation, *Journal of Applied Mechanics*, **81**, 011004-011004-13.

Fallah A and Aghdam MM. 2012, Thermo-mechanical buckling and nonlinear free vibration analysis of functionally graded beams on nonlinear elastic foundation, *Composites: Part B*, **43**, 1523-1530.

Fu Y,Wang J and Mao Y. 2012, Nonlinear analysis of buckling, free vibration and dynamic stability for the piezoelectric functionally graded beams in thermal environment, *Applied Mathematical Modelling*, **36**, 4324-4340.

Ghiasian SE, Kiani Y and Eslami MR. 2013, Dynamic buckling of suddenly heated or compressed FGM beams restingon nonlinear elastic foundation, *Composite Structures*, **106**, 225–234.

Ghiasian SE, Kiani Y, Eslami MR. 2015, Nonlinear Thermal Dynamic Buckling of FGM Beams, *European Journal of Mechanics - A/Solids*, **54**, 232-242.

Grognec PL and Saoud KS. 2015, Elastoplastic buckling and post-buckling analysis of sandwich columns, *International Journal of Non-Linear Mechanics*, **72**, 67-79.

Gunda JB. 2014, Thermal post-buckling & large amplitude free vibration analysis of Timoshenko beams: Simple closed-form solutions, *Applied Mathematical Modelling*, **38**, 4548-4558.

Hill R. 1965, A self-consistent mechanics of composite materials, *Journal of the Mechanics and Physics of Solids*, **13**, 213–222.

Huang Y and Li XF. 2010, A new approach for free vibration of axially functionally graded beams with non-uniform cross-section, *Journal of Sound and Vibration*, **329**, 2291-2303.

Huang Y, Yang LE and Luo QZ. 2013, Free vibration of axially functionally graded Timoshenko beams with non-uniform cross-section, *Composites: Part B*, **45**, 1493-1498.

Javaheri R and Eslami MR. 2002, Thermal Buckling of Functionally Graded Plates, *Journal of American Institute of Aeronautics and Astronautics*, **40**, 162-169.

Ke LL, Yang J. and Kitipornchai, S. 2009, Postbuckling analysis of edge cracked functionally graded Timoshenko beams under end shortening, *Composite Structures*, **90**, 152-160.

Kiani Y and Eslami MR. 2010, Thermal buckling analysis of functionally graded material beams, *International Journal of Mechanics and Materials in Design*, **6**, 229-238.

Kiani Y, Rezaei M, Taheri S and Eslami MR. 2011a, Thermo-electrical buckling of piezoelectric functionally graded material Timoshenko beams, *International Journal of Mechanics and Materials in Design*, **7**, 185-197.

Kiani Y, Rezaei M, Taheri S and Eslami MR. 2011b, Thermal buckling of piezoelectric functionally graded material beams, *Journal of Thermal Stresses*, **34**, 835-850.

Kiani Y and Eslami MR. 2013, Thermomechanical Buckling of Temperature-dependent FGM Beams, *Latin American Journal of Solids and Structures*, **10**, 223-246.

Kien ND and Gan BS. 2014 Large deflections of tapered functionally graded beams subjected to end forces, *Applied Mathematical Modelling*, **38**, 3054-3066.

Kien ND. 2013, Large displacement response of tapered cantilever beams made of axially functionally graded material, *Composites: Part B*, **55**, 298-305.

Kien ND. 2014, Large displacement behaviour of tapered cantilever Euler-Bernoulli beams made of functionally graded material, *Applied Mathematics and Computation*, **237**, 340-355.

Komijani M, Esfahani SE, Reddy JN, Liu YP and Eslami MR. 2014, Nonlinear thermal stability and vibration of pre/post-buckled temperature- and microstructure-dependent functionally graded beams resting on elastic foundation, *Composite Structures*, **112**, 292–307.

Komijani M, Kiani Y, Esfahani SE and Eslami MR. 2013, Vibration of thermo-electrically post-buckled rectangular functionally graded piezoelectric beams, *Composite Structures*, **98**, 143-152.

Kozic P, Pavlovic R and Karlicic D. 2014, The flexural vibration and buckling of the elastically connected parallel-beams with a Kerr-type layer in between, *Mechanics Research Communications*, **56**, 83–89.

Li J, Zhang B, Yang Q and Hu X. 2014a, Analysis on time-dependent behavior of laminated functionally graded beams with viscoelastic interlayer, *Composite Structures*, **107**, 30-35.

Li L, Zhang DG and Zhu WD. 2014b, Free vibration analysis of a rotating hub–functionally graded material beam system with the dynamic stiffening effect, *Journal of Sound and Vibration*, **333**, 1526-1541.

Li S and Song X. 2006, Large thermal deflections of Timoshenko beams under transversely non-uniform temperature rise, *Mechanical Research Communication*, **33**, 84-92.

Li Z. 2014, Thermal postbuckling behavior of 3D braided beams with initial geometric imperfection under different type temperature distributions, *Composite Structures*. **108**, 924-936.

Li SR and Batra RC. 2013, Relations between buckling loads of functionally graded Timoshenko and homogeneous Euler-Bernoulli beams, *Composite Structures*, **95**, 5-9.

Li ZH and Qiao P. 2015, Buckling and postbuckling behavior of shear deformable anisotropic laminated beams with initial geometric imperfections subjected to axial compression, *Engineering Structures*, **85**, 277-292.

Liu Y and Shu DW. 2014, Free vibration analysis of exponential functionally graded beams with a single delamination, *Composites: Part B*, **59**, 166-172.

Ma LS and Lee DW. 2011, A further discussion of nonlinear mechanical behavior for FGM beams under in-plane thermal loading, *Composite Structures*, **93**, 831-842.

Ma LS and Lee DW. 2012, Exact solutions for nonlinear static responses of a shear deformable FGM beam under an in-plane thermal loading, *European Journal of Mechanics A/Solids*, **31**, 13-20.

Maganti NVR and Nalluri MR. 2015, Flapwise bending vibration analysis of functionally graded rotating double-tapered beams, *International Journal of Mechanical and Materials Engineering*, **21**, 1-10.

Mori T. and Tanaka K. 1973, Average stress in matrix and average elastic energy of materials with misfitting inclusions, *Acta Metallurgica*, **2**, 1571–574.

MSRao P and Shu D. 2004, Buckling analysis of tri-layer beams with double delaminations, *Computational Materials Science*, **30**, 482–488.

MSRao P, Sylvain D, Shu D and Della CN. 2004, Buckling analysis of tri-layer beams with multiple separated Delaminations, *Composite Structures*, **66**, 53-60.

Murin J, Aminbaghai M, Kutis V and Hrabovsky J. 2013a, Modal analysis of the FGM beams with effect of axial force under longitudinal variable elastic Winkler foundation, *Engineering Structures*, **49**, 234-247.

Murin J, Aminbaghai M, Hrabovsky J, Kutis V and Kugler S. 2013b, Modal analysis of the FGM beams with effect of the shear correction function, *Composites: Part B*, **45**, 1575-1582.

Na KS and Kim JH. 2004, Three-dimensional thermal buckling analysis of functionally graded materials, *Composites: Part B*, **35**, 429-437.

Nateghi A and Salamat-talab M. 2013, Thermal effect on size dependent behavior of functionally graded microbeams based on modified couple stress theory, *Composite Structures*, **96**, 97-110.

Nguyen TK, Vo TP, and Thai HT. 2013, Static and free vibration of axially loaded functionally graded beams based on the first-order shear deformation theory, *Composites: Part B*, **55**, 147-157.

Nie GJ, Zhong Z and Chen S. 2013, Analytical solution for a functionally graded beam with arbitrary graded material properties, *Composites: Part B*, **44**, 274-282.

Niknam H, Fallah A and Aghdam MM. 2014, Nonlinear bending of functionally graded tapered beams subjected to thermal and mechanical loading, *International Journal of Non-Linear Mechanics*, **65**, 141-147.

Parlapalli MS and Shu D. 2004, Buckling analysis of two-layer beams with an asymmetric delamination, *Engineering Structures*, **26**, 651-658.

Pi YL, Bradford MA and Qu WL. 2011, Extremal thermoelastic buckling analysis of fixed slender beams, *Procedia Engineering*, **14**, 256-263.

Rahimi GH, Gazor MS , Hemmatnezhad M and Toorani H. 2013, On the postbuckling and free vibrations of FG Timoshenko beams, *Composite Structures*, **95**, 247-253.

Rajasekaran S and Tochaei EN. 2014, Free vibration analysis of axially functionally graded tapered Timoshenko beams using differential transformation element method and differential quadrature element method of lowest-order, *Meccanica*, **49**, 995-1009.

Rajasekaran S. 2013a, Differential transformation and differential quadrature methods for centrifugally stiffened axially functionally graded tapered beams, *International Journal of Mechanical Sciences*, **74**, 15-31.

Rajasekaran S. 2013b, Free vibration of centrifugally stiffened axially functionally graded tapered Timoshenko beams using differential transformation and quadrature methods, *Applied Mathematical Modelling*, **37**, 4440-4463.

Reddy JN and Chin CD. 1998, Thermomechanical analysis of functionally graded cylinders and plates, *Journal of Thermal Stresses*, **21**, 593-626.

Reddy JN. 2002, *Energy Principles and Variational Methods in Applied Mechanics*, John WIiley & Sons, Inc.

Sarkar K and Ganguli R. 2014, Closed-form solutions for axially functionally graded Timoshenko beams having uniform cross-section and fixed–fixed boundary condition, *Composites: Part B*, **58**, 361-370.

Shahba A and Rajasekaran S. 2012, Free vibration and stability of tapered Euler–Bernoulli beams made of axially functionally graded materials, *Applied Mathematical Modelling*, **36**, 3094-3111.

Shahba A, Attarnejad R, Marvi MT and Hajilar S. 2011, Free vibration and stability analysis of axially functionally graded tapered Timoshenko beams with classical and non-classical boundary conditions, *Composites: Part B*, **42**, 801-808.

Shames IH and Dym CL. 2009, *Energy and Finite Element Methods in Structural Mechanics*. Delhi: New Age International Publishers.

Shegokar NL and Lal A. 2013, Stochastic nonlinear bending response of piezoelectric functionally graded beam subjected to thermo-electromechanical loadings with random material properties, *Composite Structures*, **100**, 17-33.

Shen HS and Wang ZX. 2014, Nonlinear analysis of shear deformable FGM beams resting on elastic foundations in thermal environments, *International Journal of Mechanical Sciences*, **81**, 195-206.

Shen HS. 2009, *Functionally Graded Materials Nonlinear Analysis of Plates and Shells*. CRC Press, USA.

Shen HS. 2015a, Nonlinear analysis of functionally graded fiber reinforced composite laminated beams in hygrothermal environments, Part I: Theory and solutions, *Composite Structures*, **125**, 698-705.

Shen HS. 2015b, Non-linear analysis of functionally graded fiber reinforced composite laminated beams in hygro-thermal environments, Part II: Numerical results, *Composite Structures*, **125**, 706-712.

Şimşek M and Yurtcu HH. 2013, Analytical solutions for bending and buckling of functionally graded nano-beams based on the nonlocal Timoshenko beam theory, *Composite Structures*, **97**, 378–386.

Şimşek M, Kocaturk T and Akbas SD. 2013, Static bending of a functionally graded microscale Timoshenko beam based on the modified couple stress theory, *Composite* Structures, **95**, 740–747.

Sitar M, Kosel F and Brojan M. 2014, Large deflections of nonlinearly elastic functionally graded composite beams, *Archives of Civil and Mechanical Engineering*,**14**, 700-709.

Thai HT and Vo TP. 2012, Bending and free vibration of functionally graded beams using various higher-order shear deformation beam theories, *International Journal of Mechanical Sciences*, **62**, 57-66.

Touloukian YS. 1967, *Thermophysical Properties of High Temperature Solid Materials*, McMillan, New York.

Vangbo M. 1998, An analytical analysis of a compressed bistable buckled beam, *Sensors and Actuators A*, **69**, 212-216.

Vaz MA, Cyrino JCR and Neves AC. 2010, Initial thermo-mechanical post-buckling of beams with temperature-dependent physical properties, *International Journal of Non-Linear Mechanics*, **45**, 256-262.

Vo TP, Thai HT, NguyenTK, Inam F and Leed J. 2015, A quasi-3D theory for vibration and buckling of functionally graded sandwich beams, *Composite Structures*, **119**, 1-12.

Wattanasakulpong N, Prusty BG and Kelly DW. 2011, Thermal buckling and elastic vibration of third-order shear deformable functionally graded beams, *International Journal of Mechanical Sciences*, **53**, 734-743.

Wattanasakulpong N, Prusty BG, Kelly DW and Hoffman M. 2012, Free vibration analysis of layered functionally graded beams with experimental validation, *Materials and Design*, **36**, 182-190.

Xiao J, Liu Y and Shu D. 2014, Free Vibration of Exponential Functionally Graded Beams with Single Delamination, *Procedia Engineering*, **75**, 164–168.

Zhang B, He Y, Liu D, Gan Z and Shen L. 2014, Size-dependent functionally graded beam model based on an improved third-order shear deformation theory, *European Journal of Mechanics A/Solids*, **47**, 211-230.

Zhang DG. 2013, Nonlinear bending analysis of FGM beams based on physical neutral surface and high order shear deformation theory, *Composite. Structures*, **100**, 121-126.

Zhao F, Wang Z and Liu H. 2007, Thermal post-bunkling analyses of functionally graded material rod, *Applied Mathematics & Mechanics*, **28**, 59-67.

List of Publications

JOURNAL:

1. A. Majumdar and D. Das. A study on thermal buckling load of clamped functionally graded beams under linear and non-linear thermal gradient across thickness. *Proceedings of the Institution of Mechanical Engineers, Part L: Journal of Materials: Design and Applications*, (2016) (Accepted).

CONFERENCE:

1. D. Das and A. Majumdar. A study on thermal buckling load of FGM beams under temperature gradient across thickness. *Proceedings of 60th Congress of The Indian Society of Theoretical and Applied Mechanics (ISTAM)*, Jaipur (2015) Paper Code: 60-istam-sm-fp-27.

2. A. Majumdar and D. Das. Analysis of critical buckling load of uniformly tapered FGM beams. *Proceedings of National Conference on Mechanical Engineering – Ideas, Innovations & Initiatives (NCMEI3-2016)*, Aligarh (2016) 86-89.